FEBRUARY 2020
VOLUME 35 | NO. 2

Spectroscopy®

SOLUTIONS FOR MATERIALS ANALYSIS

CELEBRATING 35 YEARS

What do you need to digest today?

MARS 6™ can digest it all.

Environmental & Regulatory

Food, Plant & Animal Tissue

Pharmaceuticals

Inorganic Compounds

Oils & Plastics

Metallurgical

CEM We Simplify Science

Visit us at Pittcon booth 2219

MARS 6 is the world's best selling microwave digester.

With industry-leading technologies to make digestion easy and complete combined with round the clock service and application support, you will quickly see why CEM customers are customers for life. At CEM, your success is our goal and we continuously improve our systems to meet your current digestion challenges.

New Samples?

Over 100 years of digestion expertise is built into every MARS 6. Digest anything with hundreds of preprogrammed methods that guide you through sample weight, acid type and volume, and tips to achieve the best results.

Too many samples?

Why have we sold over 10,000 sets of MARSXpress vessels? Because they work! With their simple assembly and ability to digest 40 samples in under an hour MARSXpress continues to meet the demands of high throughput labs worldwide.

New operators?

Watch training videos right on your system. MARS 6 is simple and intuitive but if you need a refresher on vessel assembly or system features you can learn right on your system.

To much work, not enough time?

Work smarter with iLink remote system operation. Start, stop, and monitor multiple MARS 6 runs from the convenience of a tablet. Take iLink back to your desk so that you can work on other tasks all while you monitor your runs, review previous run data, and gain 24/7 access to CEM technical resources.

CEM understands the needs of busy testing labs and is here to support you along the way. Contact us today to see a MARS 6 digest YOUR samples in YOUR lab and learn why 10,000 CEM customers can't be wrong.

CEM We Simplify Science

cem.com/**MARS6**

FEBRUARY 2020
VOLUME 35 | NO. 2

Spectroscopy®

SOLUTIONS FOR MATERIALS ANALYSIS

CELEBRATING 35 YEARS 1985 • 2020

FLUORESCENCE

A Label- and Enzyme-Free Method to Detect Mercury in Cigarettes

RAMAN

Characterizing Extractables and Leachables with Raman Microscopy

ICP-OES

The Influence of Spectral Interferences on Data Reliability

PRACTICAL APPLICATIONS

Raman Spectroscopy of Graphene-Based Materials

LIBS

Advances in LIBS-Based Imaging

FUNDAMENTALS

Using CLS & PCA to Analyze Spectral Data

SPECTROSCOPYONLINE.com

World's Widest-range, MEMS-based NIR Device

NIR spectroscopy is now more accessible than ever.

NanoQuest is a rugged MEMS-based FT-IR spectrometer with best-of-its-kind 1350-2500 nm wavelength response in a single, compact instrument.

- Small enough to fit in the palm of your hand
- A fraction of the cost of traditional NIR instruments
- Ideal for product authentication and materials qualification

Ocean Insight

oceaninsight.com

State-of-the-Art XRF Solutions

•FAST SDD® •SDD •Si-PIN

In-house manufacturing = The highest performing detectors available

The best detector for optimal results

Amptek Detector Comparison: Si-PIN, Standard SDD, and FAST SDD®
^{55}Fe FWHM vs Peaking Time at 210 K

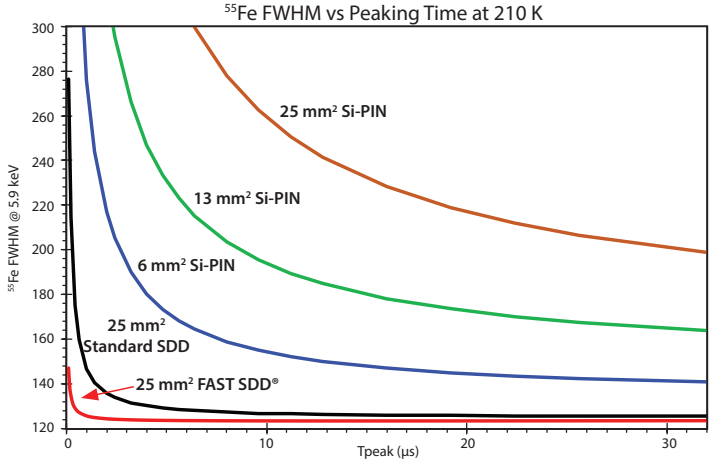

FAST SDD® Detector

>2,000,000 CPS and 122 eV FWHM Resolution

Options:

- 25 mm² collimated to 17 mm²
- 70 mm² collimated to 50 mm²
- Windows: Be (0.5 mil) 12.5 µm, or C Series (Si_3N_4)
- TO-8 package fits all Amptek configurations

Configurations to meet your needs

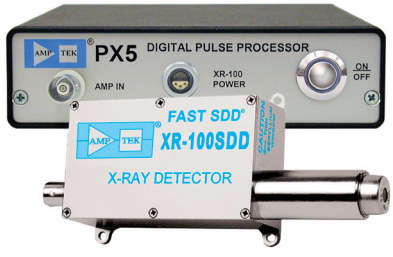

XR-100 and PX5 Digital Pulse Processor

X-123 Complete X-Ray Spectrometer

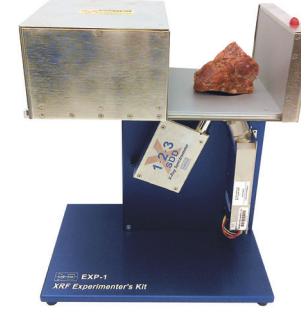

XRF Experimenters Kit

OEM Configurations

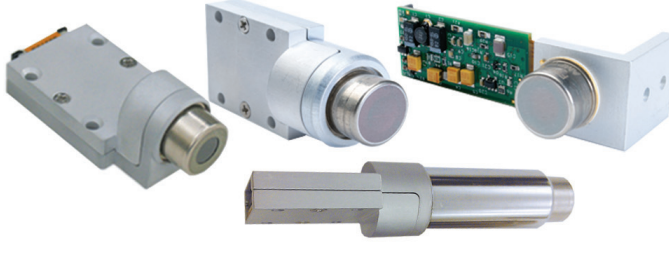

A sample of detectors with preamplifiers and heat sinks

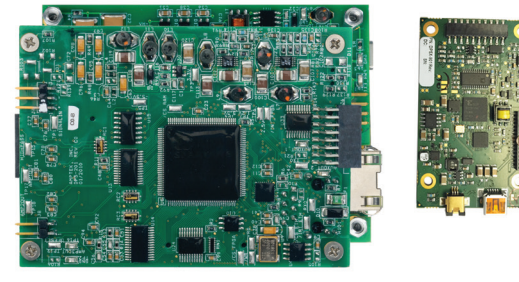

Digital Pulse Processors and Power Supplies

AMPTEK®

OEM's #1 Choice For XRF

amptek.com

AMETEK®
MATERIALS ANALYSIS DIVISION

Spectroscopy

MANUSCRIPTS: To discuss possible article topics or obtain manuscript preparation guidelines, contact the editorial director at: (732) 346-3020, e-mail: LBush@mmhgroup.com. Publishers assume no responsibility for safety of artwork, photographs, or manuscripts. Every caution is taken to ensure accuracy, but publishers cannot accept responsibility for the information supplied herein or for any opinion expressed.

SUBSCRIPTIONS: For subscription information: *Spectroscopy*, P.O. Box 457, Cranbury, NJ 08512-0457; email mmhinfo@mmhgroup.com. Delivery of *Spectroscopy* outside the U.S. is 3–14 days after printing.

CHANGE OF ADDRESS: Send change of address to *Spectroscopy*, P.O. Box 457, Cranbury, NJ 08512-0457; provide old mailing label as well as new address; include ZIP or postal code. Allow 4–6 weeks for change. Alternately, go to the following URL for address changes or subscription renewal: http://mmhpubs.mmhgroup.com/Welcome.aspx?pubid=SPEC

C.A.S.T. DATA AND LIST INFORMATION: Contact Melissa Stillwell, (218) 740-6831; e-mail: MStillwell@mmhgroup.com

Reprints: Contact Michael J. Tessalone, e-mail: MTessalone@mmhgroup.com

INTERNATIONAL LICENSING: Contact Kim Scaffidi, e-mail: KScaffidi@mjhassoc.com

CUSTOMER INQUIRIES: Customer inquiries can be forwarded directly to MJH Life Sciences, Attn: Subscriptions, 2 Clarke Drive, Suite 100, Cranbury, NJ 08512; e-mail: mmhinfo@mmhgroup.com

Alliance for Audited Media

50% Recycled Paper, 10-20% Post Consumer Waste

© 2020 MultiMedia Pharma Sciences, LLC. All rights reserved. No part of this publication may be reproduced or transmitted in any form or by any means, electronic or mechanical including by photocopy, recording, or information storage and retrieval without permission in writing from the publisher. Authorization to photocopy items for internal/educational or personal use, or the internal/educational or personal use of specific clients is granted by MultiMedia Pharma Sciences, LLC. for libraries and other users registered with the Copyright Clearance Center, 222 Rosewood Dr. Danvers, MA 01923, (978) 750-8400, fax (978) 646-8700, or visit http://www.copyright.com online. For uses beyond those listed above, please direct your written request to Permission Dept. email: ARockenstein@mmhgroup.com

MultiMedia Pharma Sciences, LLC. provides certain customer contact data (such as customer's name, addresses, phone numbers, and e-mail addresses) to third parties who wish to promote relevant products, services, and other opportunities that may be of interest to you. If you do not want MultiMedia Pharma Sciences, LLC. to make your contact information available to third parties for marketing purposes, simply email mmhinfo@mmhgroup.com and a customer service representative will assist you in removing your name from MultiMedia Pharma Sciences, LLC. lists.

Spectroscopy does not verify any claims or other information appearing in any of the advertisements contained in the publication, and cannot take responsibility for any losses or other damages incurred by readers in reliance of such content.

To subscribe, email mmhinfo@mmhgroup.com.

AN MJH life sciences™ BRAND

485F US Highway One South,
Suite 210
Iselin, NJ 08830
(732) 596-0276
Fax: (732) 647-1235

PUBLISHING/SALES

Vice President/Group Publisher
Michael J. Tessalone
MTessalone@mmhgroup.com

Publisher
Stephanie Shaffer
SShaffer@mmhgroup.com

Associate Publisher
Edward Fantuzzi
EFantuzzi@mmhgroup.com

Account Executive
Timothy Edson
TEdson@mjhassociates.com

Senior Director, Digital Media
Michael Kushner
MKushner@mmhgroup.com

EDITORIAL

Editorial Director
Laura Bush
LBush@mmhgroup.com

Managing Editor
John Chasse
JChasse@mmhgroup.com

Senior Technical Editor
Jerome Workman
JWorkman@mmhgroup.com

Associate Editor
Cindy Delonas
CDelonas@mmhgroup.com

Creative Director, Publishing
Ray Pelesko
rpelesko@mjhlifesciences.com

Senior Art Director
Gwendolyn Salas
gsalas@mjhlifesciences.com

Graphic Designer
Courtney Soden
csoden@mjhlifesciences.com

CONTENT MARKETING

Custom Content Writer
Allissa Marrapodi
AMarrapodi@mmhgroup.com

Webcast Operations Manager
Kristen Moore
KMoore@mmhgroup.com

Project Manager
Vania Oliveira
VOliveira@mmhgroup.com

Digital Production Manager
Sabina Advani
SAdvani@mmhgroup.com

Managing Editor, Special Projects
Kaylynn Chiarello-Ebner
KEbner@mmhgroup.com

MARKETING/OPERATIONS

Marketing Manager
Brianne Pangaro
BPangaro@mmhgroup.com

C.A.S.T. Data and List Information
Melissa Stillwell
MStillwell@mmhgroup.com

Reprints
Alexandra Rockenstein
ARockenstein@mmhgroup.com

Audience Development Manager
Jessica Stariha
JStariha@mmhgroup.com

CORPORATE

Chairman & Founder
Mike Hennessy Sr

Vice Chairman
Jack Lepping

President & CEO
Mike Hennessy Jr

Chief Financial Officer
Neil Glasser, CPA/CFE

Executive Vice President, Operations
Tom Tolvé

Senior Vice President, Content
Silas Inman

Senior Vice President, I.T. & Enterprise Systems
John Moricone

Senior Vice President, Audience Generation & Product Fulfillment
Joy Puzzo

Vice President, Human Resources & Administration
Shari Lundenberg

Vice President, Business Intelligence
Chris Hennessy

Vice President, Corporate Branding & B2B Marketing
Amy Erdman

Executive Creative Director, Creative Services
Jeff Brown

PIKE TECHNOLOGIES

SPECTROSCOPIC CREATIVITY

Accessories for UV/Vis, Near-IR and Mid-IR measurements.

PIKE Technologies is a primary source for spectroscopy accessories worldwide. Products include attenuated total reflection (ATR), diffuse and specular reflection, integrating spheres, polarizers, transmission sampling accessories and more.

LONG-PATH GAS CELL

High-performance gas cells for analysis of air contaminants, pure gases and gas mixtures in the ppm to ppb range. Pathlengths range from 1 to 30 meters. Temperature-controlled configurations, heating up to 200 °C are available.

XY AUTOSAMPLER

Speed up productivity with this automated NIR and MIR diffuse reflection/transmission accessory. Microtiter plates are customizable up to 96 wells. Visit our website or contact us for details.

THE IRIS DIAMOND ATR

With IRIS, you can expect high-quality spectra covering a wide range of samples, including powders, gels, liquids, solids. Ideal for research, QA/QC and sample identification.

608.274.2721 | info@piketech.com | www.piketech.com | 6125 Cottonwood Dr. Madison, WI 53719, USA

TABLE OF CONTENTS

Spectroscopy

February 2020
Volume 35 | Number 2

Cover image courtesy of *stock.adobe.com/k_yu*

COLUMNS

12 **Molecular Spectroscopy Workbench**
Use of Raman Microscopy to Characterize Extractables and Leachables
Fran Adar
Raman microscopy, combined with X-ray fluorescence, can provide detailed information about extractables and leachables from medically implantable devices.

16 **Chemometrics in Spectroscopy**
More About CLS, Part 2: Spectral Results (Not Needing Constituent Values) and CLS
Howard Mark and Jerome Workman, Jr.
A previous analysis of data is compared to the results achieved using classical least squares and principal component analysis. What did we learn?

SPECTROSCOPY SPOTLIGHT

26 **Raman Spectroscopy of Graphene-Based Materials**
Jerome Workman, Jr.
Ping-Heng Tan of the Chinese Academy of Sciences is advancing the use of Raman spectroscopy to characterize graphene-based materials.

30 **Advancing In Situ Applications of Spectroscopy in an Industrial Setting**
John Chasse
Xiaoyun (Shawn) Chen of Dow Chemical solves a range of analytical problems in R&D and production processes using in situ spectroscopy and chemometrics.

32 **New Spectroscopic Techniques Aid in Tissue Engineering**
Cynthia Delonas
Nancy Pleshko of Temple University is studying the use of FT-IR imaging and NIR spectroscopy to solve bioengineering problems related to human replacement tissue.

PEER-REVIEWED RESEARCH

34 **LIBS-Based Imaging: Recent Advances and Future Directions**
V. Motto-Ros, V. Gardette, L. Sancey, M. Leprince, D. Genty, S. Roux, B. Busser, and F. Pelascini
LIBS-based imaging has a broad range of applications. Here, we demonstrate those capabilities with examples from paleoclimate research and toxicology studies.

41 **A Label- and Enzyme-Free Fluorescent Method for the Rapid and Simple Detection of Hg^{2+} in Cigarettes Using G-Triplexes as the Signal Reporter**
Hui Zhao, Yang Zhao, Xiaoxi Si, Juan Li, Yuanxing Duan, Wei Jiang, Chunbo Liu, Junheng You, Zhenjie Li, and Qinpeng Shen
A novel method was developed for detecting Hg^{2+} in tobacco, with potential application to mercury detection in environmental water samples.

TUTORIAL

53 **Influence of Spectral Interferences on the Reliability of Data When Using Analyte Addition Techniques with ICP-OES**
Deborah K. Bradshaw
Contrary to popular belief, neither good "spike" recoveries nor the use of the method of standard additions (MSA) will guarantee accurate results in ICP-OES.

DEPARTMENTS

News Spectrum 10
Products and Resources 57
Short Courses 60
Calendar 62
Ad Index 64
Application Notebook 65

Like @SpectroscopyMagazine on Facebook

Follow @SpectroscopyMag on Twitter

Join the Group @SpecGroup on LinkedIn

Photo Credit: adobestock.com/prudkov

Spectroscopy (ISSN 0887-6703 [print], ISSN 1939-1900 [digital]) is published monthly by MultiMedia Healthcare, LLC., 230 W Superior Street, Ste 400, Duluth MN 55802. Spectroscopy is distributed free of charge to users and specifiers of spectroscopic equipment in the United States. Spectroscopy is available on a paid subscription basis to nonqualified readers at the rate of: U.S. and possessions: 1 year (12 issues), $83.95; 2 years (24 issues), $151.20. Canada/Mexico: 1 year, $107.10; 2 years, $168.53. International: 1 year (12 issues), $157.50; 2 years (24 issues), $281.40. Periodicals postage paid at Duluth, MN 55806 and at additional mailing offices. POSTMASTER: Send address changes to Spectroscopy, P.O. Box 457, Cranbury NJ 08512-0457. PUBLICATIONS MAIL AGREEMENT NO. 40612608, Return Undeliverable Canadian Addresses to: IMEX Global Solutions, P. O. Box 25542, London, ON N6C 6B2, CANADA. Canadian GST number: R-124213133RT001. Printed in the U.S.A.

50% reduction in cycle time

2X the throughput

50% lower labor costs

Visit us at PITTCON CONFERENCE & EXPO 2020 Booth #5031

Quantified microwave digestion excellence.

- Improved workflow
- Maximum throughput
- No batching required
- Lower operating costs

As the pioneer of Single Reaction Chamber (SRC) technology, Milestone has revolutionized the way industrial and research laboratories around the world prep samples for analysis. Our ultraWAVE transcends traditional closed and open vessel digestion, offering maximum throughput and lower cost of ownership.

High-performance stainless steel construction allows for higher pressures and temperatures and use of any combination of acids, while disposable vials eliminate the need to assemble, disassemble or clean between processing. Dissimilar samples can also be processed simultaneously, saving valuable time and resources.

The bottom line? The Milestone ultraWAVE is the superior solution to handle all your sample prep challenges.

Visit us at www.milestonesci.com/ultrawave to schedule an onsite demonstration.

powered by milestone connect

ETHOS UP

ultraWAVE

ultraCLAVE

MILESTONE

EDITORIAL ADVISORY BOARD

Fran Adar Horiba Scientific

Russ Algar University of British Columbia

Matthew J. Baker University of Strathclyde

Ramon M. Barnes University of Massachusetts

Matthieu Baudelet University of Central Florida

Rohit Bhargava University of Illinois at Urbana-Champaign

Paul N. Bourassa Blue Moon Inc.

Michael S. Bradley Thermo Fisher Scientific

Deborah Bradshaw Consultant

Lora L. Brehm The Dow Chemical Company

George Chan Lawrence Berkeley National Laboratory

John Cottle University of California Santa Barbara

David Lankin University of Illinois at Chicago, College of Pharmacy

Barbara S. Larsen DuPont Central Research and Development

Bernhard Lendl Vienna University of Technology (TU Wien)

Ian R. Lewis Kaiser Optical Systems

Howard Mark Mark Electronics

R.D. McDowall McDowall Consulting

Gary McGeorge Bristol-Myers Squibb

Francis M. Mirabella Jr. Mirabella Practical Consulting Solutions, Inc.

Ellen V. Miseo Illuminate

Michael L. Myrick University of South Carolina

John W. Olesik The Ohio State University

Steven Ray State University of New York at Buffalo

Jim Rydzak Specere Consulting

Jacob T. Shelley Rensselaer Polytechnic Institute

Jerome Workman Jr. Biotechnology Business Associates

Lu Yang National Research Council Canada

Spectroscopy's Editorial Advisory Board is a group of distinguished individuals assembled to help the publication fulfill its editorial mission to promote the effective use of spectroscopic technology as a practical research and measurement tool. With recognized expertise in a wide range of technique and application areas, board members perform a range of functions, such as reviewing manuscripts, suggesting authors and topics for coverage, and providing the editor with general direction and feedback. We are indebted to these scientists for their contributions to the publication and to the spectroscopy community as a whole.

Photo Credit: adobestock.com/prudkov

MilliporeSigma

NEW Milli-Q® IQ 7003/05/10/15

Ultrapure & Pure Water System

To find out more, visit **MilliporeSigma.com**

© 2019 Merck KGaA, Darmstadt, Germany and/or its affiliates. All Rights Reserved. MilliporeSigma, the vibrant M, and Milli-Q are trademarks of Merck KGaA, Darmstadt, Germany or its affiliates. All other trademarks are the property of their respective owners. Detailed information on trademarks is available via publicly accessible resources.

2019-21626 04/2019

The life science business of Merck KGaA, Darmstadt, Germany operates as MilliporeSigma in the U.S. and Canada.

Milli-Q®

Lab Water Solutions

Winter Conference Lifetime Achievement Award in Plasma Spectrochemistry Presented to Scott Tanner

Scott D. Tanner is the 2020 winner of the Lifetime Achievement Award in Plasma Spectrochemistry, sponsored by Thermo Fisher Scientific. The award was presented on January 13 at the 2020 Winter Conference on Plasma Spectrochemistry in Tucson, Arizona.

Tanner received his B.Sc. and PhD degrees from York University in Toronto, Ontario. He held positions at Sciex (Framingham, Massachusetts), the University of Toronto, and DVS Sciences (now part of Fluidigm). His contributions to the inductively coupled plasma–mass spectrometry (ICP–MS) community were substantial, focusing on the study of the fundamentals of ICP ion generation, dynamics, and transport, including prognostications on space charge and its implications for analyses; the development of the dynamic reaction cell for removing polyatomic ion interferences; and the development of ICP time-of-flight instrumentation for single-cell cytometry and subcellular imaging.

Spectroscopist Eileen Skelly Frame Dies

Eileen M. Skelly Frame, PhD, a spectroscopist, chemistry professor, and industrial chemist, died at the age of 66 on Monday, January 13, 2020, following a year-long battle with cancer.

Frame served as Medical Service Corps officer in the U.S. Army from 1975 to 1986, rising to the rank of captain. For the first five years of her military career, Skelly Frame was stationed at the 10th Medical Laboratory at the U.S. Army Hospital in Landstuhl, Germany. Then she was selected to attend a three-year PhD program in chemistry at Louisiana State University (LSU). She received her doctorate in 1982 and became the first female chemistry professor at the U.S. Military Academy at West Point, in New York. Following her military service, Skelly Frame joined General Electric (GE) Corporation and supervised the atomic spectroscopy laboratory at GE's Research and Development Center in Niskyuna, New York. She analyzed practically every stable element in the periodic table in support of all company programs. She also held positions as Clinical and Adjunct Professor of Chemistry at Union College, in Schenectady, and at Rensselaer Polytechnic Institute, in Troy. She was a 45-year member of the American Chemical Society and served one year as the local section chair. She was the co-author, with her husband, George M. Frame II, of a 1200-page textbook, *Undergraduate Instrumental Analysis*. She delivered the draft of a new edition weeks before her death.

Market Profile: Near Infrared (NIR) Spectroscopy

Near infrared (NIR) spectroscopy can probe material and specimens requiring deep sample penetration without substantial preparation. NIR is based on the absorption of photons at wavelengths in the range 780–2500 nm and is used to measure molecular overtone and combination vibrations within these ranges. As in most spectrometers, light is passed through diffraction grating to separate it into individual wavelengths through a sample to the detector. The results are a spectrum of transmittance at NIR wavelengths.

At first, NIR instruments were add-ons to UV-vis spectrophotometers before becoming stand-alone systems focused on chemical analysis. Now, monochromators and fiber optics have allowed NIR analyzers to be used in medical and physiological diagnostics, and in research in kinesiology, rehabilitation, and neurology. Industries have also made use of NIR analyzers for bioenergy, forestry, building materials, textiles, and quality assurance. A large portion of NIR instruments are used for food to analyze crops, meat, dairy, beverages to ascertain finished product profiles of density, moisture, protein, oils, and carbohydrates.

The total market for NIR was measured at about $470 million in 2019 and is expected to reach over $570 million by 2024. The fastest growth within this segment is from portable/handheld NIR analyzers, which is expected to top $100 million in demand by 2024. Scanning & Diode array NIR analyzers account for the largest segment. Environmental and food industries make up over a third of demand by application in 2019 and will continue to be the fastest growing segment due to increased adoption in agriculture. Leading suppliers of NIR instruments are Bruker, Foss, and Thermo Scientific.

Market size and growth estimates were adopted from TDA's *Industry Data*, a database of technology market profiles and benchmarks covering laboratory and process analytical instrumentation that are updated quarterly. It also includes data from the *2020 Instrument Industry Outlook* report from independent market research firm TDA. For more information, contact Glenn Cudiamat, president & CEO, at (310) 871-3768 or glenn.cudiamat@tdaresearch.com.

2019 NIR market demand by industry

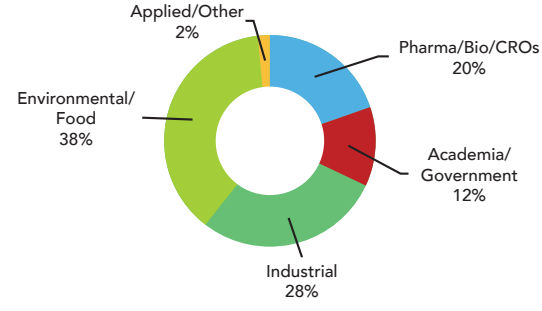

Photo Credit: adobestock.com/selensergen

SHIMADZU
Excellence in Science

Outstanding UV-Vis Performance Across a Broad Spectrum of Applications

Shimadzu's UV-2600i and UV-2700i double-beam spectrophotometers are true research-grade instruments for a wide variety of applications. The high-absorbance measurement capability and sub-nanometer bandwidths make them perfect for both advanced materials characterization and any routine work expected of a UV-Vis spectrophotometer.

Key features include:

- Selectable bandwidths to comply with requirements of regulated laboratories and high-end research
- Measurements up to 8 abs
- Wavelength region expandable to the near-IR
- Multiple measurement modes and accessories
- Supports database management, user authority management and data audit trails

Learn more about Shimadzu's UV-2600i/2700i. Visit us online at **www.ssi.shimadzu.com**

Order consumables and accessories on-line at http://store.shimadzu.com Shimadzu Scientific Instruments Inc., 7102 Riverwood Dr., Columbia, MD 21046, USA

Use of Raman Microscopy to Characterize Extractables and Leachables

Fran Adar

Any product used for medical purposes has to follow the adage "do no harm." In the current work, we assess if and how Raman microscopy, in combination with X-ray fluorescence (XRF), can aid in the characterization of material leached from several implantable devices. The results show both the presence of metal oxides and organic compounds. In one case, two crystalline forms of an identical oxide existed simultaneously, and we suggest that such information may be useful in characterizing the oxidation of the metal. One of the samples was tinged pink, and its spectrum was consistent with a resonance Raman (RR) spectrum of a pigment. Because information on the source of these samples was not known, it is not possible to perform a complete characterization, but we can suggest ways that these results can be used in the future when a more complete study can be done.

Any product that comes in contact with the human body or with a product that is subsequently ingested, injected, or inserted into a human body has the potential to carry harmful products. If a polymer is part of an implant, it can release low molecular weight oligomers or additives that are present to engineer the polymer's properties. If a drug product is contained in a polymer bag or vessel, especially if the drug is liquid, similar problems are possible. An implant is often composed of metallic parts that have the potential to oxidize, even if chipping is not likely. Metallic oxidation products from an implant can either chip away or be dissolved in fluids and carried from the site of the implant, or material from a metallic container can be ingested, injected, or inserted into a human body.

Pharmaceutical companies are constantly testing their products for extractables and leachables, both before FDA release and during the life of the product. *Leachables* are products that can be released by a product under normal ambient conditions. *Extractables* are products that are released under conditions designed to indicate worse case scenarios. For example, an implant can be immersed in a solution meant to mimic biological fluids, and then subjected to elevated temperatures to determine what can be forced out of that part; this would be called a *leachable*. Exposure to non-physiological solvents would produce extractables.

We will show here the results of a study of material leached from two implants, and indicate how this information can be of use to the biomedical community.

Description of the Samples

Two saline solutions of material leached from two different implants were examined. To aid in the interpretation of the Raman spectroscopy results, X-ray fluorescence (XRF) was also measured. Figure 1a shows the vials of solutions as received. Figure 1b shows some of these materials deposited on a stainless steel microscope slide.

Elemental analysis performed on an XG7200 (Horiba Scientific) showed that the elements in the green deposit were dominated by titanium, with some silicon, calcium, nickel, and sodium. The pink sample

Photo Credit: adobestock.com/selensergen

contains a lot of iron, aluminum, and sulfur, with some copper, chromium, manganese, and silicon, and small amounts of zinc and nickel.

Raman Analysis

As readers of this column are aware, Raman spectroscopy provides information on both organic and inorganic materials. In fact, the original concept of the Raman microscope (1) was to provide molecular identification of organic molecules, especially manufacturing contaminants that could not be analyzed by the standard microprobes in use at the time. Today, there are extensive Raman spectral libraries that can assist in the identification of unknowns, and even if a library does not provide a match, there are tools to aid in the assignment of functional groups (2).

The Raman spectrum of organic materials is separated into several characteristic regions. The region below 1500 cm^{-1} is called the *fingerprint region,* because the motions of all the atoms are coupled together, so it is not possible to assign a particular band in the spectrum to the motion of one or a few atoms. Between 1500 and 1800 cm^{-1}, there are bands that can be assigned to the >C=C< and >C=O stretches (~1650 and ~1730 cm^{-1}, respectively). Between 2000 and 2400 cm^{-1} are triple bonds, and close to 2500 cm^{-1} is the –SH stretch. Then there are CH stretches (2700–3100 cm^{-1}), the NH stretch (~3350 cm^{-1}), and the OH stretches (anywhere between 3100 and 3600 cm^{-1}, depending on H-bonding).

Most of the bands of the Raman spectrum of inorganic materials fall below 1400 cm^{-1} but if there are hydroxyl groups, they will appear above 3000 cm^{-1}, and the position and width of the bands will also depend on H-bonding.

In both cases, there are shifts and splittings of bands in the crystal phases, and it is important to point out that there is a significant number of inorganic materials in which there are not identifiable vibrating functional groups, so when these materials crystallize in different forms, the spectra are totally different. Examples are TiO_2, ZrO_2, and carbon (diamond vs. graphite). One of the examples that is shown below in one of the deposits illustrates this in the spectra of two phases of $Al(OH)_3$.

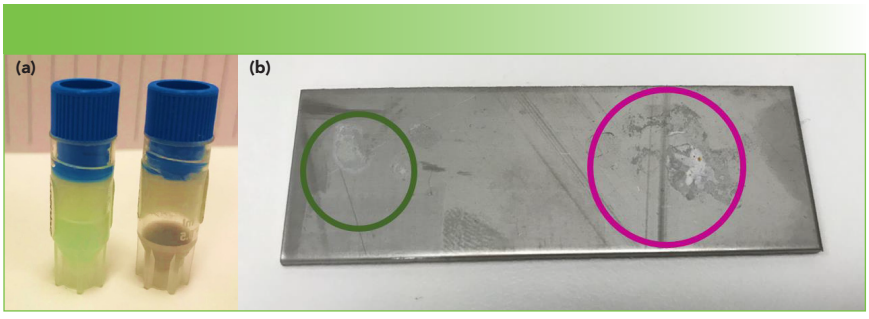

FIGURE 1: (a) Vials with material extracted from two implants, and (b) deposit on a stainless steel slide.

Raman Analysis

Because the sample deposits did not have any good morphology on which to focus, I recorded maps in order to acquire a good sampling of representative spectra. Spectra were isolated from the maps using either classical least squares (CLS) or multiple curve resolution (MCR).

Pink Sample

The top of Figure 2 shows both bright field and dark field micrographs of the region that was studied by Raman microscopy. While the sample in the vial had a weak pinkish color, that color is not seen in the micrographs. In bright field, one is essentially seeing the re-

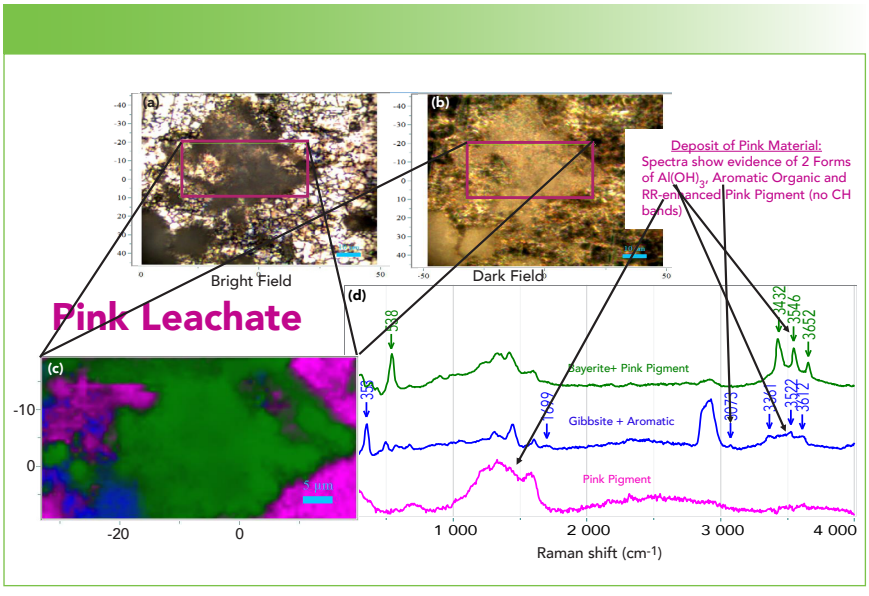

FIGURE 2: Analysis of pink leachate. (a) Bright field, and (b) dark field micrographs of an area of the pink leachate deposit. (d) Raman spectra derived from the mapped file showing the presence of two forms of $Al(OH)_3$ (green and blue), organic material with both saturated and unsaturated functionality (blue) and a resonance Raman (RR) enhanced organic (pink). (c) The Raman map is color-coded to be consistent with the spectral display colors.

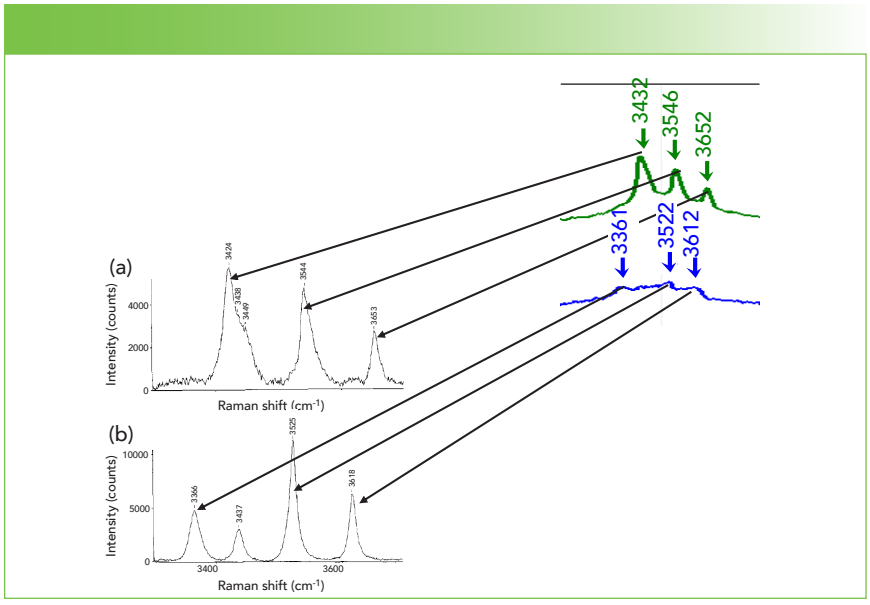

FIGURE 3: The spectra of $Al(OH)_3$ extracted from our map, and the spectra of the identified phases of $Al(OH)_3$ reproduced from reference (3); (a) is bayerite, and (b) is gibbsite.

flectivity of the sample, so it is not unusual so see bright areas where the sample is reflective and areas of different tones of gray from less reflective material; sometimes one can see color here if it is intense. In dark field, we are seeing light scattered from the periphery through the sample, and then up the bright field objective. The pink box in the micrograph is the region from which we collected spectra.

Figure 2 also shows the extracted spectra on the right and the rendered map on the left, using the spectral colors on the right; the spectra and map are color-coded, so that it is clear which spectrum corresponds to which region on the map. The OH bands in the green and blue spectra are good matches to the spectra of bayerite (blue) and gibbsite (green), two crystallographic forms of $Al(OH)_3$.(3), and the fingerprint bands between 300 and 600 cm^{-1} are good matches as well. In the blue spectrum, there is a strong CH band below 3000 cm^{-1} indicating saturated organic material, and a small band at 3073 cm^{-1} indicating the presence of an aromatic. There are (unlabeled) bands in the blue spectrum near 1450 and 1600 cm^{-1}, also consistent with these assignments of saturated organic and aromatic species. The spectrum in pink at the bottom of the figure is consistent with an aromatic, but because the CH region is weak and the strongest bands are between 1000 and 1700 cm^{-1}, it is believed that this represents the resonance-enhanced spectrum of the pink pigment. Examination of the green spectrum indicates the presence of similar bands.

Figure 3 shows the $Al(OH)_3$ bands from Figure 2 compared to the spectra in the cited publication, illustrating a remarkable match in spectral features.

Figure 3 shows our spectra that we assign to the two phases of $Al(OH)_3$, bayerite in green, and gibbsite in blue.

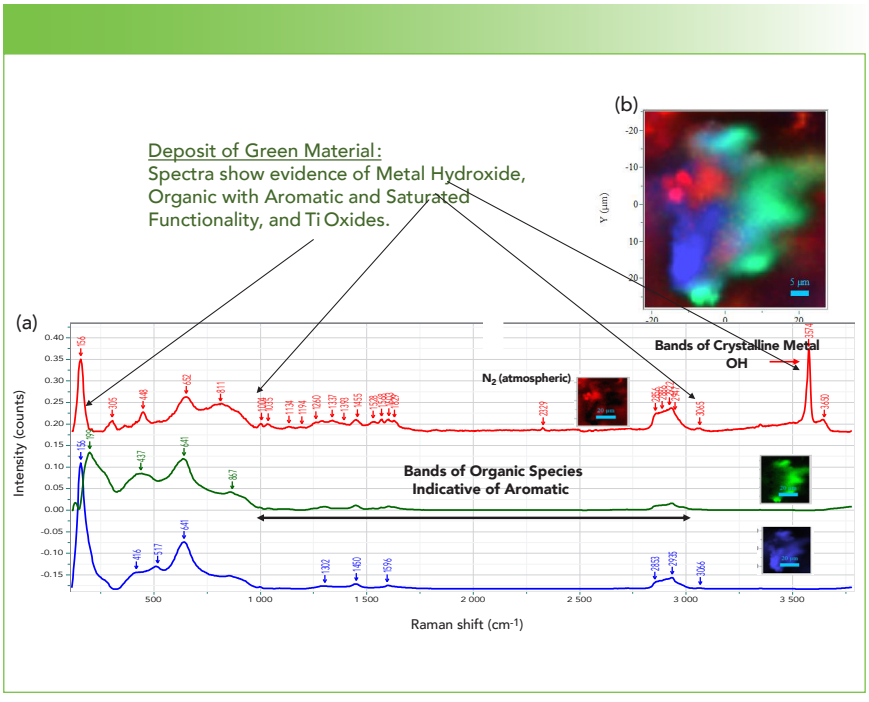

FIGURE 4: Analysis of green leachate. (a) shows the three spectra isolated from the map file; (b) shows the Raman rendition with colors matched to the colors of the spectra.

Green Sample

The map of this sample was treated in a manner similar to that of the pink sample. Three spectra were isolated and used to produce the Raman rendition shown in the upper right side of the figure. In this sample, there is also evidence

for organic material with aromatic functional groups. (The band close to 2330 cm^{-1} is atmospheric nitrogen which is often seen in our spectra.). This sample also shows surprising behavior in the hydroxide region; there is a sharp band at 3574 cm^{-1}, with a much weaker but fairly sharp band at slightly higher frequency. This sample was known to have a high content of titanium, and the low frequency region is consistent with an oxide of this metal, although not an exact match to any of the common phases. I made a considerable effort to assign the OH band, but was unsuccessful. However, in searching, I did find a very old article on the OH band in a series of metal hydroxides that occur in this region of the spectrum (± 50 cm^{-1}) (4).

Discussion

There are several issues about this report that may be unsettling to analysts who need detailed answers to solve problems. At this point, I am unable to make firm assignments to neither the organic species nor the inorganic species. But because I really have no information on the implants from which these samples came, it seems gratifying that I can make any assignments at all. If I knew the composition of the implants (that is, the type of organic or polymeric material present), I would be in a better situation to identify these materials. What, for me, is surprising is that I am seeing hydroxides of the metals. The real question for the analyst is whether the identity of the hydroxides in these extracted samples is meaningful, or is just an artifact of the preparation of the slurries that we deposited on a slide. The use of a saline solution is, for sure, meant to mimic physiological conditions. The question is whether these species are coming off the implants in the states that we are observing, or are they flaking off in a different form and then changing in solution or during precipitation. Again, we need more information on the original implants, and then need to consult with a physical chemist who would understand the possible chemical and phase changes that are possible under what conditions.

Conclusion and Summary

I chose to do this pilot study on extractables and leachables because I am getting multiple meeting announcements per month on this topic, and the topic just spoke to me about the potential of Raman microscopy to be helpful. What is surprising is that vibrational spectroscopy doesn't seem to be exploited in this field for its potential. Maybe some of my readers can tell me I am wrong, or tell me why it is not being used.

References

(1) M Delhaye and P Dhamelincourt, *J Raman Spectrosc.* **3,** 33–43 (1975). This is the first publication describing the concept of the Raman microscope, with its potential for analytical work implicit in the publication.

(2) Bio-Rad KnowItAll Software. https://www.bio-rad.com/en-us/product/knowitall-software-analytical-edition?ID=N19OQWKSY

(3) H.D. Ruan, R.L. Frost, and J.T. Kloprogge, *J. Raman Spectrosc.* **32,** 745–750 (2001).

(4) D. Krishnamurti, *The Raman and Infra-red Spectra of Some Solid Hydroxides Part II. Correlation with Crystal Structure*, Memoir No. 119 from the Raman Research Institute, Bangalore, India.

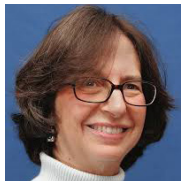

Fran Adar is the Principal Raman Applications Scientist for Horiba Scientific in Edison, New Jersey. Direct correspondence to: SpectroscopyEdit@mmhgroup.com. ●

SPEX SamplePrep

THE COMPLETE SOLUTION FOR ICP SAMPLE PREPARATION

Grind samples to micron level particle sizes or prepare fused beads for fast and effective acid digestion.

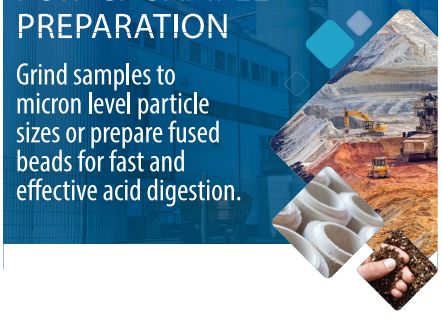

GRIND YOUR SAMPLE WITH THE MIXER/MILL®

SPEX Mixer/Mills® are renowned for their simplicity and durability. These high energy ball mills are capable of grinding hard samples to analytical fineness in minutes. Single and dual vial clamp mills are available. Can't grind a sample? Try the Freezer/Mill®, the ultimate cryogenic grinder.

PREPARE FUSED BEADS USING THE X-FLUXER®

Our range of Katanax X-Fluxers® are the next generation of electric fusion fluxers. They combine speed, simplicity and a robust design to produce fused beads or direct dissolution in acid for difficult to dissolve samples.

www.spexsampleprep.com
learnmore@spex.com • 1-855-GET-SPEX

More About CLS, Part 2: Spectral Results (Not Needing Constituent Values) and CLS

Howard Mark and Jerome Workman, Jr.

In our previous column, we introduced a set of data suitable for more extensive examination than was permitted in our previous discussion of the classical least squares (CLS) algorithm. In this column, we start to analyze the data using two methods (CLS and principal component analysis [PCA]) that do not involve the concentrations of the components of the mixtures. We begin our expansion of the analysis by examining the data from the 70-sample data set the same way we did for the previous 15-sample data set. First, we examine the spectral results, and then apply the CLS algorithm to verify the previous findings. Neither of these types of analysis requires the use of external constituent information. We then further expand the analysis by calculating principal components.

Although the goal of this column is to examine the effects of using volume fractions vs. weight fractions as the constituent concentrations for principal component regression (PCR) and partial least squares (PLS) calibrations, there is much to be learned from the spectroscopic data itself, without reference to any constituent compositions. Therefore, our initial inspection of the data parallels the initial examination of the smaller, 15-sample set of mixtures, to verify that those computed values did not require concentration values, or involve the application of advanced chemometric calibration algorithms. Instead, our initial foray into looking at the results from the statistical experimental design described in the previous column (1) was to examine the behavior of the spectral data alone, without involving the use of chemometrics. The application of chemometrics to the data will be described later, and for reasons that will become clear, may not be described fully here. The advantage of analyzing the spectral data without bringing in the constituent values is that the expectations of their behavior are better known, and more easily described. This allows us to compare our results with the theoretical expectations, so that when we introduce the constituent values, we will have some foreknowledge of how we might expect the data to behave. Some of these behaviors have already been listed qualitatively in Tables I and II (see the previous column [1]), where we compared current near-infrared (NIR) spectroscopy practice to theoretical expectations.

While we have spectra of the pure materials that comprise the mixtures, they were not taken as part of the calibration set. Therefore, for comparison and demonstration purposes, we use the five mixtures containing each of those materials at 60% (the maximum value they can attain in these samples) with each of the other mixture components at their lowest value (10%) as surrogates for the pure materials. The plots in Figure 1 present these spectra, for reference.

CLS Results

In keeping with our desire for initial analysis to not use the reference values, our next activity is to present the results of performing classical least squares (CLS) analysis on the mixture data. One aspect of CLS

Photo Credit: adobestock.com/selensergen

Email: sales@specac.com

Specac

www.specac.com

The Quest

- Interchangeable pucks
- All-reflective optics and monolithic crystals
- Pressure tower for sampling of solids and powders
- Optional liquid puck format
- Coming soon: Arrow™ silicon ATR slides

Manual Press

- Robust and reliable hydraulic press for low-volume sample preparation
- Manual load application using hand pump
- Quick pressure release
- Analog pressure gauge
- Loads up to 25 Tons

The Pearl

- The easiest to use FTIR liquid sampling system available
- Faster, more accurate and more repeatable than traditional liquid cells
- Wedged option to eliminate troublesome fringing completely

PITTCON 2020 CONFERENCE & EXPO

3rd-5th March (stand 2824)

Visit our booths

In march you can catch us at both Pittcon and ACS shows, let us know you're attending on sales@specac.com

ACS Chemistry for Life®

22nd-26th March (stand 1024)

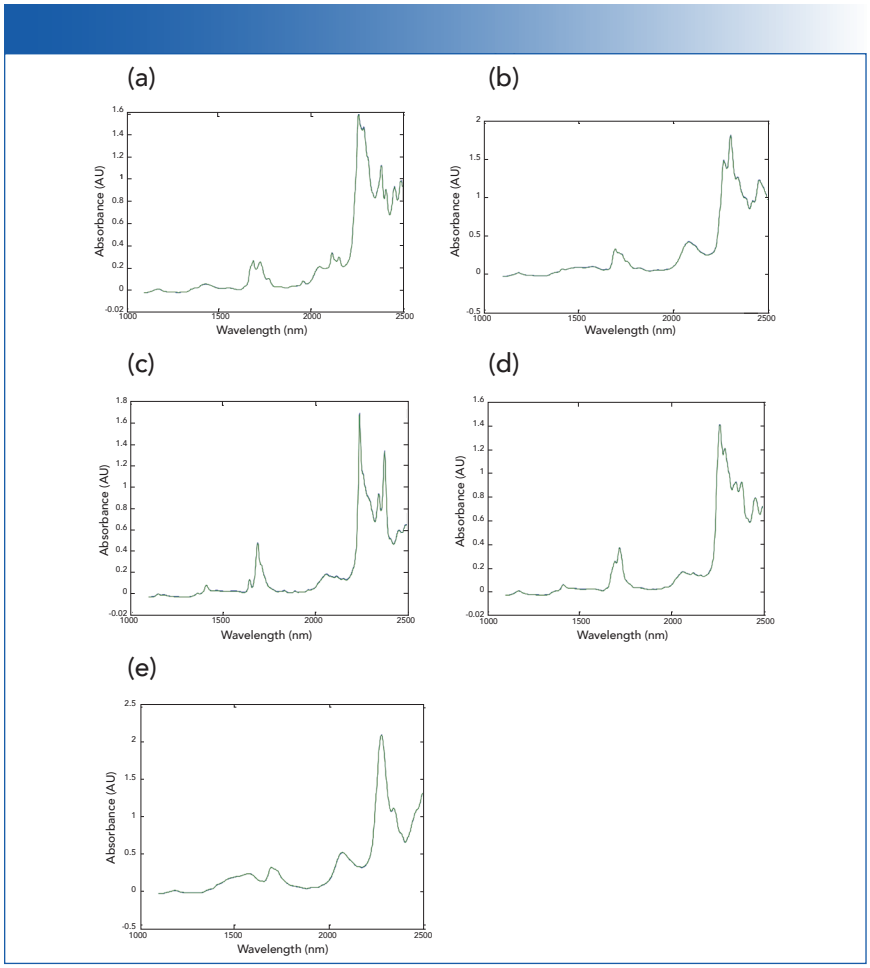

FIGURE 1: Spectra of selected mixtures. Each of the spectra represents one of the mixtures, which contains the maximum concentration (60%) of the component corresponding to the label for that spectrum: (a) acetone, (b) butanol, (c) dichloromethane, (d) dichloropropane, and (e) methanol. Each of the other four components present in that mixture are at their minimum concentrations (10%). The pair of measured spectra from each mixture are plotted on the same axes; it is clear that all these pairs of spectra exactly overlap, showing only the second plotted spectrum in each case.

gives us the ability to reconstruct the spectrum of a sample from the spectra of the pure components. Thus the validity of the data analysis, as well as the quality of the data, can be captured by CLS analysis by the agreement between a pure-component spectrum computed from the mixture spectra and the measured spectrum of that chemical component. These plots are shown in Figure 2, for the mixtures containing the maximum amount (60 wt%) of each of the ingredients respectively, and for each mixture the minimum amount (10 wt%) of all the other ingredients. It is clear that the agreement between the theoretical reconstructed spectrum and the actual spectrum of each ingredient is almost, although not quite, as good as the agreement between duplicate spectra of the same material. This an important observation, since later on we will be comparing spectra to each other, and knowing the amount of deviation expected between actual measurements and computed approximations will be important in evaluating the computed results.

In Figure 3, we have plotted, for each of the five ingredients, the values of the CLS-calculated concentrations vs. the known weight percent and volume percent of the ingredients. Not surprisingly, we note the following characteristics of the plots in Figure 3:

- For the plots where the abscissa variable represents the weight fraction, the points corresponding to a given weight fraction of the ingredient lies on a vertical line. The explanation is simple—the samples were made up gravimetrically to prescribed values, thus the actual and the nominal values of weight fraction are all the same (within experimental error) for a given fraction of the specified ingredient. The spectral values plotted on the ordinate direction varied due to the actual changing composition, reflected in the spectral response, hence the data points corresponding to samples of the nominal composition are spread out in only the *Y*-direction.
- For the plots where the abscissa variable represents the volume fraction, the points corresponding to a given volume fraction of the ingredient lie along a line essentially parallel to the direction of the line through all the samples of varying composition. This reflects the improvement of the performance attainable through the use of volume fractions. As we've seen previously with the more limited sample set (2), when volume fractions are used as the measure of concentration, the change in value of the constituent concentration is mirrored by an equivalent change in the value of the concentration as determined by the CLS algorithm (2). The calculated values of the concentration measure within each group of data points then follows the trend of the data very nicely, instead of them all lying vertically as in the weight percent values of Figure 3.

The difference between the two cases is that when weight fraction is used for the constituent concen-

Kaiser Raman

The Powerhouse of Industrial Raman Spectroscopy

For all your lab-to-process needs

Bioprocessing

Cell culture and fermentation

Measure and control multiple parameters *in situ* and in real-time with one probe

Pharmaceutical

PAT during product lifecycle

Understand your API from synthesis to crystallization to drug product release

Food & Beverage

Real-time inline product quality

Ensure product quality while reducing operational costs

Chemical

Process efficiency

Control product quality for efficient operations

Oil & Gas

In-process analysis 24/7/365

Optimize process and product quality with no consumables

Stay Connected with us!

www.kosi.com

https://www.linkedin.com/company/kaiser-optical-systems

KAISER OPTICAL SYSTEMS, INC.

An Endress+Hauser Company

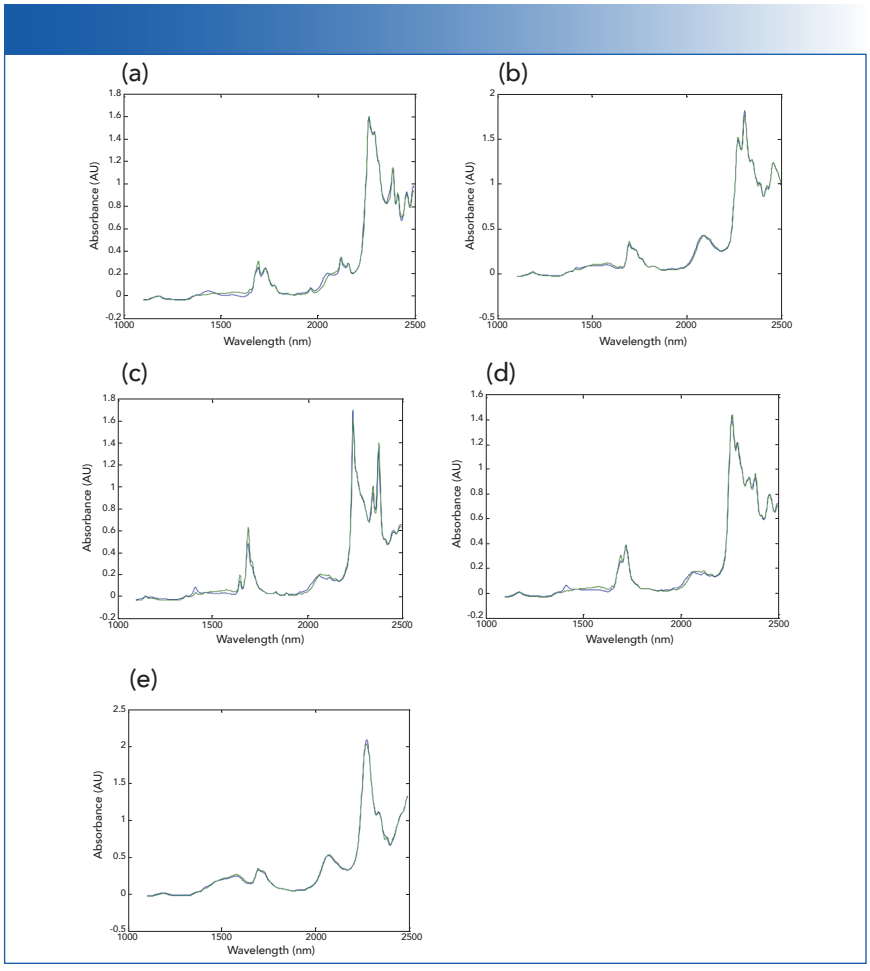

FIGURE 2: Comparisons between the actual measured spectra of the five mixtures containing the maximum amount (60 wt%) of each mixture component, and the reconstruction of that spectrum using the CLS algorithm. In all cases. blue = measured spectrum, green = reconstructed spectrum using CLS algorithm. Spectra shown include: (a) acetone, (b) butanol, (c) dichloromethane, (d) dichloropropane, and (e) methanol.

tration, the value used to represent concentration of the sample is constant, because the samples were made up that way—to contain a prespecified amount of the ingredient. In this case, only the spectroscopically calculated value changes (due to the variations in the other components), and therefore the resulting data points fall on a vertical line. When the volume fraction is used as the constituent value, then both the spectroscopically calculated value and known reference value change, and change concurrently, so that the data points for each sample lie on a sloping line that reflects the corresponding changes in the two values.

Another characteristic of the data can also be seen in some (although not all) of the plots in Figure 3. Some of the clusters of data points for the plots of spectral values versus volume fractions show an additional effect. This effect is the spreading of the data points away from the line defining the main direction of the points in each cluster, in this case perpendicular to the line. In some cases (and this is particularly noteworthy for the butanol plots, methanol plots, and to a lesser extent, for dichloropropane plots), the clusters of points are not randomly spaced away from the line defining the direction of the data, but form a pattern. Albeit imperfect, the pattern shows lines of data points within the cluster, each line containing a different number of data points: first one isolated point, then two on a line, then three, then four. The net effect is that for each cluster, the points appear to be contained in a triangular envelope, mimicking, to some extent, the experimental design from which the plots were created.

The cause of this phenomenon is not entirely clear at this time, although suspicion falls on the potential residual interactions between the various chemical components of the samples. The possibility of hydrogen bonding between the two alcohols and the highly polar -C-Cl bonds in the chlorine-containing molecules also seem likely sources of this sort of interaction.

Expanding Beyond CLS: Introducing PCA

CLS is not the only type of data analysis that can be applied to the spectral data without needing constituent values. Principal component analysis (PCA) is a data analysis method that can be applied to the spectra alone, without needing auxiliary constituent information. We have shown in earlier columns (3–8) that a principal component is a least-square estimator of the underlying data, and that, at each stage, it accounts for the maximum amount of variance remaining in the data after all previous components have been used to explain their respective contributions to the measured data values.

This being the case, if the theoretical assumptions underlying the data are valid, it should not be necessary to compute more principal components than there are independent sources of variation affecting the data set being examined. This is effectively the same as saying this reflects the number of degrees of freedom in the data, ignoring the in-

Are you compliant with the latest USP Chapter <857>?

Can you ensure your data integrity?

SEE US AT
PITTCON
Booth 3816

Starna Certified Reference Materials provide an essential tool to achieving data integrity and compliance!

Wide range of available materials to cover all AIQ requirements:

Wavelength accuracy: From Deep UV to the Near Infra-red

Absorbance accuracy & Photometric Linearity: Absorbance & Linearity checks up to 3.5 A

Stray Light

Instrument Resolution

UKAS Accreditation as a:

Reference Material Producer - ISO 17034:2016

Calibration Laboratory - ISO/IEC 17025

NIST Traceable

Lifetime Guarantee

Fast re-calibration service

Starna your first choice for:

Certified Reference Materials
Spectrophotometer & fluorometer cells
Optics for industry and science

Starna

Starna Cells Inc. (800) 228-4482
sales@starnacells.com www.starna.com

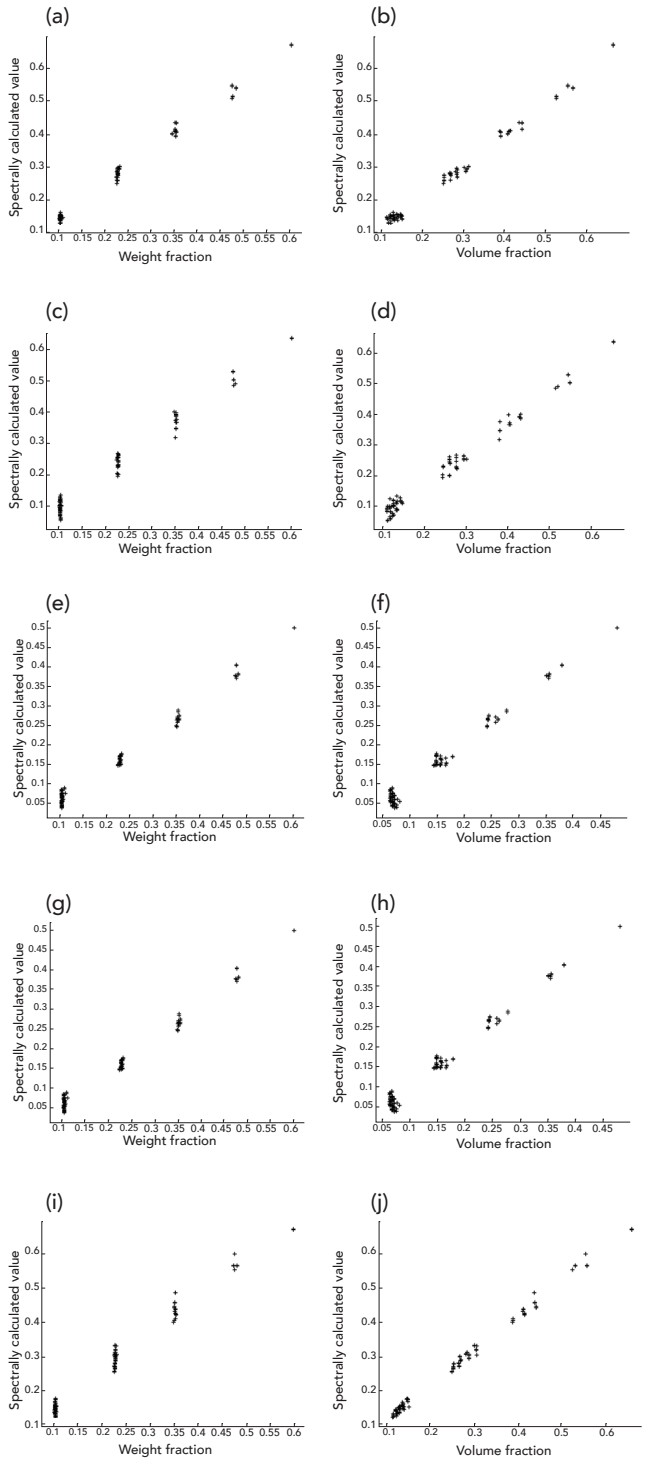

FIGURE 3: Spectrally calculated values versus reference weight fraction and volume fraction, for the five components in the mixtures. In all plots, the ordinate is the spectrally calculated value, and the abscissa is the weight or volume fraction value, as marked. Figure plots are for the following compounds: (a,b) acetone, (c,d) butanol, (e,f) dichloromethane, (g,h) dichloropropane, and (i,j) methanol.

numerable degrees of freedom that represent the noise content of the spectroscopic data.

In the case of five-component mixtures such as we are dealing with here, you might think that there would be five degrees of freedom in the spectral data. However, since the mixture components must add up to 100% (called *closure* of the dataset), the concentration of any four components determines the concentration of the fifth; therefore it is not "free" to vary independently. The restriction that the mixture ingredients must add up to 100% removes a degree of freedom from the data. Therefore the spectral data should contain 5 - 1 = 4 degrees of freedom. Ideally, therefore, a five-component mixture should be completely represented by four principal components, ignoring the noise. What we should observe then, upon performing PCA, is that the variance remaining in the spectral data should decrease as each new principal component is computed and the effect of that component is removed from the data set. Furthermore, the early components will account for more variance than later components; the first principal component that is calculated will account for the most variance of the data, while each of the later components will remove less and less. The effect is cumulative, and successive components will remove more and more variance from the data until the first four components are found, at which point the remaining variance should represent the random noise remaining in the data, and that noise should not change by any appreciable amount if more principal components are computed. The remaining variance will then remain almost constant as successive principal components are calculated. Plotting this residual variance as a function of the number of components should therefore approach a very small almost-constant value, once all the non-noise variations of the data

PlasmaQuant

Engineered for Excellence.

ICP-MS Tailored to Your Requirements

The PlasmaQuant MS series

With the PlasmaQuant MS, Analytik Jena offers ICP-MS instruments perfectly adapted to your application. Individual instrument configurations, upgrade options and accessories make the PlasmaQuant MS your analytical tool of choice for highly efficient work.

Benefit from superior ICP-MS technology:

- Best analytical performance with 10 times more sensitivity
- Highest throughput with 50% more samples per hour
- Most efficient operation saving 50% of the plasma running costs
- True wide range multielement analysis with 11 orders analytical range in pulse-counting mode only
- Exceptional application efficiency with outstanding mass separation and lowest abundance sensitivity in ICP-MS

For more information, contact us:

info@us.analytik-jena.com
www.analytik-jena.us

30 years analytikjena
An Endress+Hauser Company

Emerald Conference | San Diego, CA **| Booth 509**
Pittcon | Chicago, IL **| Booth 2248**
STLE | Chicago, IL **| Booth TBD**

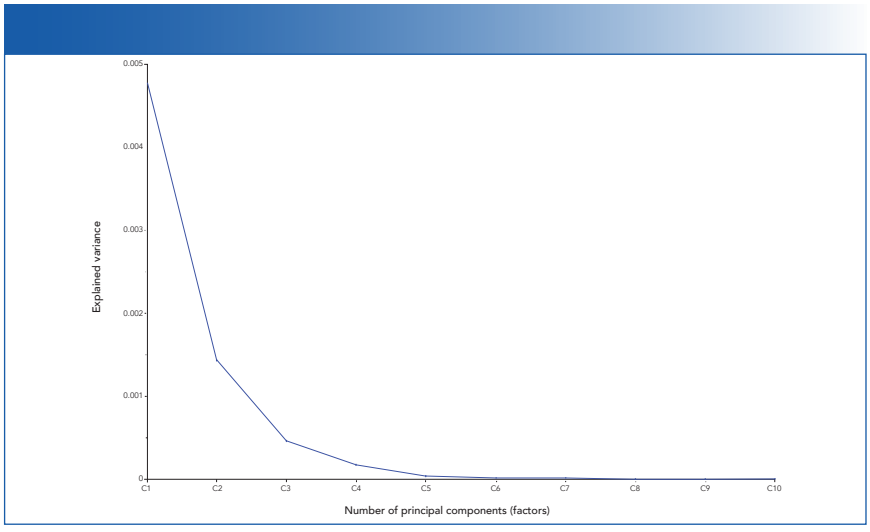

FIGURE 4: Variance remaining in the set of mixture spectra, as successive principal components are applied to the set of spectral data. Theory tells us that four principal components should be sufficient for all constituents.

are removed by this process. The actual behavior of this data set is shown in Figure 4.

What we actually find in Figure 4, distinct from the theoretical expectation, however, is that there is a continual drop-off of the remaining variance in the data up to at least the sixth principal component. In conformance with theory, the earlier principal components do indeed account for more variance than later ones. Nevertheless, the number of principal components needed to account for or "explain" the spectral data is more than the four degrees of freedom, due to the five individual chemical components that we know are present in the data set (while accounting for the closure of the dataset). The reason for this is also not entirely clear, although it is consistent with the finding, from the examination of the CLS results, of possible interactions between some of the ingredients in the mixtures.

Conclusions (From This and the Previous Column)

CLS analysis of this new data set, which is appreciably larger than the previous data set we were able to use, confirms the results we obtained from the previous data set. The CLS algorithm enabled the reconstruction of the spectra of mixtures from the spectra of the components of each mixture. For several of the constituents (methanol is a good example here), the plot of calculated vs. measured concentration is a straight line when the measured concentration is expressed as volume fraction, but exhibits visible curvature when the concentration is expressed as weight fraction.

Principal component analysis shows that, contrary to theoretical expectation, it requires the calculation and use of more (>6) principal components to account for all the variance in the spectra than theoretical evaluations (four principal components) of the data would suggest (see Figure 4 for the actual amounts of variance explained). Initial explanations for this behavior, based on previous understanding, cast suspicion on more of the "usual suspects"—mainly interactions between ingredients in the mixtures list.

Further, and closer, examination of the results revealed that, while interactions cannot be completely exonerated as a cause of the observed behavior, another unexpected phenomenon showed up, which changes our understanding of how apportionment of variance among several competing effects influences the final results obtained. This phenomenon will be described in a subsequent column.

References

(1) H. Mark and J. Workman, *Spectroscopy* **34**(6), 16–24 (2019).
(2) H. Mark, R. Rubinovitz, D. Heaps, P. Gemperline, D. Dahm, and K. Dahm, *Appl. Spectrosc.* **64**(9), 995–1006 (2010).
(3) H. Mark and J. Workman, *Spectroscopy* **22**(9), 20–29 (2007).
(4) H. Mark and J. Workman, *Spectroscopy* **23**(2), 30–37 (2008).
(5) H. Mark and J. Workman, *Spectroscopy* **23**(5), 14–17 (2008).
(6) H. Mark and J. Workman, *Spectroscopy* **23**(6), 22–24 (2008).
(7) H. Mark and J. Workman, *Spectroscopy* **23**(10), 24–29 (2008).
(8) H. Mark and J. Workman, *Spectroscopy* **24**(5), 14–15 (2009).

Jerome Workman Jr. serves on the Editorial Advisory Board of *Spectroscopy* and is the Senior Technical Editor for *LCGC* and *Spectroscopy*. He is also a Certified Core Adjunct Professor at U.S. National University in La Jolla, California. He was formerly the Executive Vice President of Research and Engineering for Unity Scientific and Process Sensors Corporation.

Howard Mark serves on the Editorial Advisory Board of *Spectroscopy*, and runs a consulting service, Mark Electronics, in Suffern, New York. Direct correspondence to: SpectroscopyEdit@mmhgroup.com ●

COMPLETE SOLUTIONS

Handheld

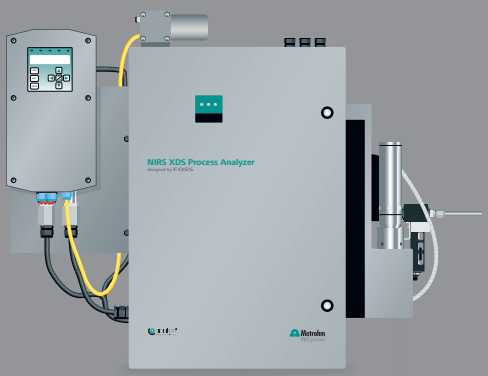

Process

Laboratory

Going Beyond Spectrometers to Build Complete Solutions

At Metrohm, we understand that you aren't looking for a spectrometer, you need answers that provide a complete solution.

Our team works with you from feasibility, to installation and beyond to deliver an application that works from the start. This coupled with our rugged handheld spectrometers, easy to use benchtop instruments, or powerful process analyzers turns instruments into solutions for:

- Raw materials inspection
- Quality assurance
- Process control
- And more

Find out more at www.metrohm.com/spectroscopy

Metrohm USA Inc.

NIRS A1.1009-SPE © 2018 Metrohm USA, Inc. Metrohm and design® is a registered trademark of Metrohm Ltd.

Raman Spectroscopy of Graphene-Based Materials

Jerome Workman, Jr.

Raman spectroscopy is a versatile tool to identify and characterize the chemical and physical properties of graphene-based materials (1–4), providing information on graphene structures for fundamental research and for practical device fabrication, as well as demonstrating the first- and second-order modes in intrinsic graphene, as well as the shear, layer-breathing, and the G and 2D modes of multilayer graphene. Professor Ping-Heng Tan from the State Key Laboratory of Superlattices and Microstructures at the Institute of Semiconductors at the Chinese Academy of Sciences is carrying out new research to advance the use of Raman analysis of these materials. We recently interviewed Tan about this work.

You have described Raman techniques to determine the number of graphene layers, to probe resonance Raman spectra of monolayer and multilayer graphenes, and to obtain Raman images of graphene-based materials. What are the greatest benefits of applying Raman spectroscopy to investigate graphenes? How does Raman compare to other methods for this application?

Raman spectroscopy is a fast, nondestructive, and versatile tool for the characterization of the lattice structure and the electronic, optical, and phonon properties of graphene-based materials. Raman spectra of all graphene-based materials show a few prominent features (D, G and 2D modes), regardless of the final structure. However, the positions, line shapes, and intensities of these peaks give abundant useful information for the investigation of the structures and electronic properties of graphene-based materials. In comparison to other methods, Raman spectroscopy can give more information without the additional treatments or damage to the sample, and with much less time and cost.

Would you briefly explain the theory behind how Raman measurements provide detailed information for investigation of the fundamental properties of graphene, including the states, effects, and mechanisms of graphene?

The first-order Raman scattering in a crystal is a three-step process, including the generation of the photo-excited electron and hole, scattering of the excited electron or hole by the phonon phenomena, and the recombination of the electron and hole. The phonons involved reflect the corresponding fundamental properties. For example, the single-axis strain of graphene can be revealing by the splitting of the E_{2g} phonon (G mode), and the frequency of the interlayer shear (C) mode, giving information on the number of graphene layers as well as the interlayer coupling strength. Moreover, it's obvious that the intensities of the Raman modes are related to the optical properties of graphene. By obtaining the resonance Raman spectra, the optical transition probability of graphene-based materials can be obtained. For example, the twisted bilayer graphene has a twist-angle dependent Van Hove singularity in the joint density of state, which leads to twist-angle dependent optical transition energies, and can be inves-

Photo Credit: adobestock.com/selensergen

tigated by multi-wavelength Raman spectroscopy. Moreover, due to the unique linear band structure, the second-order Raman scattering (involving two phonons, represented by the 2D mode) is easily observed in graphene-based materials, which is enhanced by a double resonance Raman scattering process. This excitation-wavelength dependent mode allows one to detect the phonon dispersion, electron-phonon coupling, and band structure of graphene-based materials.

Why are graphene-based materials important?

Graphene is a truly two-dimensional system, consisting of sp^2 carbon hexagonal networks with strong covalent bonds. Multilayer graphene can be stacked layer by layer in a Bernal or rhombohedral way through van der Waals coupling. High-quality monolayer graphene and multilayer graphene can be produced by several methods, such as micromechanical exfoliation, chemical vapor deposition, and epitaxial growth from the silicon carbide (SiC) surface. Other artificial fabrication routes for production, such as the reduction of a graphene oxide solution and organic synthesis, tend to introduce defects into the graphene, such as vacancies and dislocations, as well as exposing the graphene to oxidation, hydrogenation, fluorination, and other chemical functionalization. Graphene can also be decomposed into one-dimensional and zero-dimensional forms, such as graphene nanoribbons and nanographene. All these materials with various dimensions are derived from graphene, and can be termed *graphene-based materials*.

The remarkable properties of graphene and graphene-based materials, including their high carrier mobility (near ballistic transport), high thermal conductivity, unique optical and mechanical properties, and high specific surface area, make them promising materials for high-frequency nanoelectronics, micro- and nanomechanical systems, thin-film transistors, transparent and conductive composites and electrodes, batteries and supercapacitors with high charging speeds, highly sensitive chemical sensors, flexible and printable optoelectronics, and photonics.

In addition, recent research studies have advanced to investigate vertical van der Waals heterostructures because they can be formed by vertically stacking various two-dimensional materials by van der Waals forces but without any constraints of lattice matching and fabrication compatibility, offering huge opportunities for the design of new functionalities. Graphene and multilayer graphene are the essential

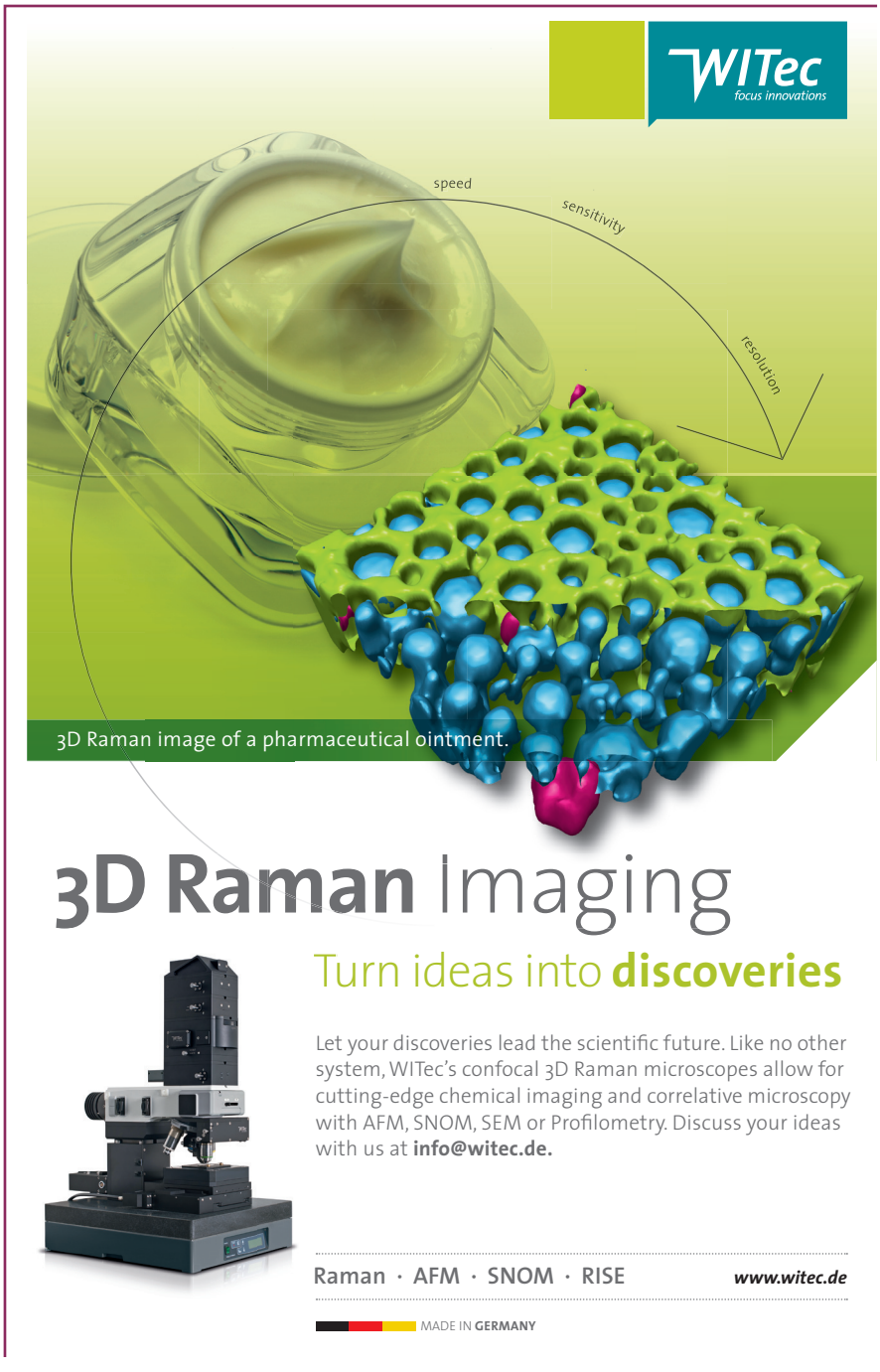

building blocks for van der Waals heterostructures as electrodes in various high-performance devices, such as field-effect tunneling transistors, logic transistors, photovoltaics, and memory devices.

What is the potential for Raman spectroscopy to be used routinely for characterizing graphene materials in a manufacturing or production environment?

For the large-scale characterization of graphene materials in industry, Raman spectroscopy has several advantages, including short measurement time, low cost, lower training requirements compared to other techniques, and, very importantly, the nondestructive nature of the technique. The relatively simple features of the Raman spectra in graphene-based materials make them quite easy to interpret by an engineer with some limited training. The cost of the Raman measurement is becoming lower and lower with the development of Raman instrumentation, including portable systems. It just takes a few minutes to obtain a state-of-art Raman spectrum of graphene-based materials. And the Raman measurement would not affect the quality of the materials after measurement by gently controlling the incident laser power.

What recent advances in Raman instrumentation, software, or sampling methods have you been most active in over the recent past?

Recently, I have been active in pushing the detection limit of the low frequency Raman modes in a single-monochromator Raman system. Our target is to probe the Raman modes with the frequency as low as possible. As we know, a well-aligned triple grating spectrometer can give a low frequency limit down to 5 cm^{-1}, but with a low detection efficiency. In our previous work, we obtained a frequency limit down to 2.0 cm^{-1} by a single-monochromator Raman system coupled with volume-Bragg-grating-based notch filters (5), and achieved a frequency limit down to 10 cm^{-1} by a single-monochromator Raman system with long pass edge filters (6). Those filter-based techniques to detect low frequency Raman modes are much higher in efficiency than a triple grating spectrometer. We have also developed a tunable single-monochromator Raman system based on the supercontinuum laser and tunable filters, showing its potential application for resonant Raman profile measurements (7). We also devote ourselves to updating a single grating spectrometer with our homemade micro-Raman module into a high-throughput confocal Raman system. The homemade micro-Raman module can connect two single grating spectrometers to obtain a very broad photoluminescence spectrum in a single capture and a Raman spectrum with high spectral resolution. You can see a demonstration of this on the website http://www.fergiespec.com/case-study/ping-heng-tan/.

What have been your greatest challenges in scientific discovery over your career? What is your general approach to problem solving in your scientific work?

As a physicist studying Raman spectroscopy, the greatest challenge in scientific discovery is always how to obtain the intrinsic Raman spectra and how to understand them properly. That challenge arises frequently when you are exploring the fundamental properties of new materials by Raman spectroscopy. Fortunately, with the development of theoretical approaches, it's becoming easier to understand the measured Raman results quickly and accurately. As an experimental physicist, I always benefit a lot by collaborating with many theoretical scientists.

What are some major gaps in knowledge for Raman technology that you would like to see more research and development time devoted to?

I have been working on Raman spectroscopy for over 20 years. At the beginning, Raman technology was used as a tool by a few Raman experts in physics and chemistry to investigate the lattice and molecular dynamics of molecules and their other related properties. The Raman technique has developed exponentially in past 15 years, leading to many non-experts wishing to enter this field. Now, Raman spectroscopy has become a standard and routine technique to identify and characterize many materials, both at the laboratory and mass-production scale. However, some users may just know how to measure Raman spectra simply by using a commercial Raman system, but do not know the real physical meaning behind the spectra they measure. Thus, as a physicist of Raman spectroscopy, I would like to appeal to and help more researchers to put their sights on the depths of this area, which will be helpful for the development of this field.

What do you anticipate is your next major area of research or application in this field?

We are really interested in characterizing the two-dimensional materials (especially graphene-based materials) and related van der Waals heterostructures in an operating device in situ. It would be helpful for us to understand the working mechanism of the device, and to reveal new physical phenomena of various materials and related devices.

For those having greater interest in this topic, what reference papers or books would you recommend they obtain to read or study?

In the past decade, the attention to this field keeps growing. The following review papers or books can be recommended for non-experts wishing to enter the field:

- L.M. Malard, M.A.A. Pimenta, G. Dresselhaus, and M.S. Dresselhaus, "Raman Spectroscopy in Graphene," *Physics Reports* **473**(5–6), 51–87 (2009).
- A. Jorio, M.S. Dresselhaus, S. Riichiro, G. Dresselhaus, *Raman Spectroscopy in Graphene Related Systems* (Wiley-VCH, 2011).
- A.C. Ferrari and D.M. Basko, "Raman Spectroscopy as a Versatile Tool for Studying the Properties of Graphene,"*Nature Nanotechnology* **8**(4), 235 (2013).
- J.B. Wu, M.L. Lin, X. Cong, H.N. Liu, and P.H. Tan, "Raman Spectroscopy of Graphene-Based Materials and its Applications in Related Devices," *Chemical Society Reviews* **47**(5), 1822–1873 (2018).
- P.-H. Tan, Ed., *Raman Spectroscopy of Two-Dimensional Materials* (Springer Nature Singapore Pte Ltd., 2019). DOI: 10.1007/978-981-13-1828-3.

The first three suggestions present the fundamental understanding of the use of Raman spectroscopy in graphene materials, and the last two give a more complete understanding and updates on newer progress in the analysis of graphene-based materials and other two-dimensional materials.

References

(1) J.B. Wu, M.L. Lin, X. Cong, H.N. Liu, and P.H. Tan, *Chem. Soc. Rev.* **47**(5), 1822–1873 (2018).

(2) P.-H. Tan, Ed., *Raman Spectroscopy of Two-Dimensional Materials* (Springer Nature Singapore Pte Ltd., 2019). DOI: 10.1007/978-981-13-1828-3.

(3) M.L. Lin and P.H. Tan, *Ultralow-Frequency Raman Spectroscopy of Two-dimensional Materials. In Raman Spectroscopy of Two-Dimensional Materials* (Springer, Singapore, 2019), pp. 203–230.

(4) J.B. Wu, M.L. Lin, and P.H. Tan, "Raman Spectroscopy of Monolayer and Multilayer Graphenes," in *Raman Spectroscopy of Two-Dimensional Materials* (Springer, Singapore, 2019), pp. 1–27.

(5) X.L. Liu, P. H. Tan et. al., *Rev. Sci. Instrum.* **88**(5), 053110 (2017).

(6) M.L. Lin, P.H. Tan et. al., *Rev. Sci. Instrum.***87**(5), 053122 (2016).

(7) X. L. Liu, H.-N. Liu, and P.-H. Tan, *Rev. Sci. Instrum.* **88**(8), 083114 (2017). ●

For more information on this topic, please visit our homepage at:
www.spectroscopyonline.com

LightMachinery
Excellence in Lasers and Optics

Hyperfine Spectrometer

A sub-picometer resolution spectrometer in a compact package.

For Brillouin spectroscopy and laser diagnostics.

For sample spectra, visit www.lightmachinery.com
See us at SPIE Photonics West, Booth 5363

Advancing In Situ Applications of Spectroscopy in an Industrial Setting

John Chasse

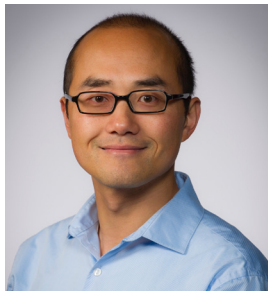

The Clara Craver Award, awarded annually by the Coblentz Society, was named after Craver in recognition of her pioneering efforts in promoting the practice of infrared vibrational spectroscopy, and recognizes the efforts and contributions of young professional spectroscopists in applied analytical vibrational spectroscopy. The 2019 recipient, Xiaoyun (Shawn) Chen, a senior research scientist working in the Core R&D Analytical Sciences department of the Dow Chemical Company,has been leading Dow's global optical spectroscopy technology network since 2013, and also the molecular structure capability since 2016, solving a broad range of problems and improving many different types of R&D and production processes, introducing many colleagues to the benefits of spectroscopy for their applications. Chen recently spoke to *Spectroscopy* about his work.

You have over a decade of experience in spectroscopic and chemometric method development for industrial research and development (R&D) and manufacturing projects, focusing on in situ reaction monitoring. What motivated you to focus on this area??

Let me begin with how I got started. It was probably around my third year at Dow, and I was working on whatever projects that happened to come my way, when my mentor, Anne Leugers, handed me two attenuated total reflectance (ATR) dipper probes, which were no longer needed by another group, and told me to explore whether I could make use of them. By chance, several colleagues in our engineering and process science group reached out to us to monitor a low-temperature reaction that they could not seem to grasp with conventional off-line methods such as gas chromatography (GC), liquid chromatography (LC), or nuclear magnetic resonance (NMR) spectroscopy. We borrowed another Fourier-transform infrared (FT-IR) instrument from our process analytical group, so that we could use the ATR dipper probe to monitor that reaction. In situ monitoring immediately helped us to detect and prove the existence of a highly labile intermediate, which explained why earlier off-line analysis failed. The focus of the project then shifted to characterizing the reaction kinetics for process optimization, and, as a result, we needed to find a way to quantify the concentration of all reaction species. I was very fortunate that Randy Pell, a world-renowned chemometrician, became my mentor in chemometrics, and together we were able to apply several chemometric tools such as classical least squares (CLS) and partial least squares (PLS) to quantify all the reaction species within the complex mixture. This work was later published externally (1)

So, that was how I got started—as a confluence of instrument and probe availability and project need. I was truly amazed by how useful and enabling in situ spectroscopy turned out to be. The results from in situ infrared (IR) substantially impacted the direction of that particular project and the work of multiple PhD-level process chemists and engineers. As encouraged by my mentors and my leaders, I started to make an intentional effort to further explore and identify similar opportunities. Very quickly, it became apparent to me that the in situ spectroscopy project was not a lucky one-off, but

Photo Credit: adobestock.com/selensergen

that there were actually many projects that would benefit. Even though people might not know how they could benefit from in situ spectroscopy, I took it upon myself to champion the application of in situ spectroscopy throughout Dow, and even outside. Since then, I just became naturally drawn to that method, and often had to force myself not to be solely focused on in situ spectroscopy. I truly believe that in situ spectroscopy can be a revolutionary tool for process monitoring.

How broad is the range of projects that you work on? Are the projects very similar to each other, or diverse?

Extremely broad. Let me start with types of projects. Currently, I have several projects dealing with silicone, a few dealing with catalysts ranging from zeolites to MOF, one related to radical polymerization, one related to polyurethane foaming, several related to ethylene polymerization, and several related to customer applications, such as paper coating and airbag coating, among others. In terms of commercialization stages of these projects, they may range from early stage concept-shaping, to process development, to customer applications. There is never a dull moment as far as projects are concerned. The only common theme among them all is that they all can benefit from the use of optical spectroscopy.

What are the biggest challenges you tend to encounter in your work?

Time management, motivating others, and delegation. There are many things you need to do well as an industrial analytical scientist. First, you need to make sure that you are working on important and relevant research topics. In my current role, I also need to make sure that we keep abreast of the latest analytical instrument development, so that we can solve the toughest analytical problems with the newest tools. We also need to deliver on existing projects, look out for new projects, document past projects, and mentor new people. Whether you can manage your time well among all the above-mentioned tasks is critical in determining how fulfilled, productive, and successful you can be. I forgot to mention that additionally you may also need to maintain an external presence, and I do that by serving as the newsletter editor for the Society for Applied Spectroscopy (SAS), and on the board of the Coblentz Society, and by continuing to publish in peer-reviewed journals. Motivating others and delegation are things that aren't necessarily taught at graduate school, but become increasingly important as you progress through your career. They are often easier said than done, and I am fortunate to have several great leaders and mentors who have been coaching me throughout this process. I don't feel I am an expert in them yet, but am trying very hard to be better at them.

You recently published a study about monitoring polyimide production using a combination of in situ infrared and Raman spectroscopy (2). Why did you use both techniques in the study? What was different about what the two techniques enabled you to see? Can the results of that study guide your choice for IR or Raman spectroscopy for future studies?

The short answer to your first question is "because we can." I routinely take an IR, Raman, and near-infrared (NIR) spectrometer with me when I visit my colleagues at their labs. Sometimes there's a clear winner regarding which type of spectroscopy will be the best fit, and we'll just use that. Just as often, we cannot really predict which technique will work best, and then we try all of them. Which technique is the most appropriate also depends on the focus of the project, which may continue to shift as we make progress. Often optical spectroscopy may not be the right tool, and then we'll bring in other analytical tools as well, though that's probably outside the scope for this interview. You'll have to read that paper to see our exact findings. For this particular study, I would say both techniques would eventually lead to similar findings, though your perspective into the reaction progress would be very different, due to the different selection rules. Another advantage of using such a broad range of techniques lies in the insights potentially offered by them. There have also been numerous times when we originally set out to solve one problem, but discovered something totally unexpected, which led the whole project to take on a new direction.

What do you consider to be the most satisfying aspects of mentoring junior spectroscopists, as well as introducing those unfamiliar with spectroscopy to the techniques?

As I am starting my 12th year with Dow, I am also starting to take on new roles, and one of the most important ones is to mentor young people coming to our group. I feel very lucky that I have the chance to interact with the brightest minds coming out of graduate school, and I feel especially privileged to see that such bright young people actually take on my advice as they start to navigate their first "real world" job. Seeing their maturing into driven and motivated researcher is the most satisfying part. As for introducing spectroscopy to those outside the field of spectroscopy (which is the case for ~98% of the colleagues I interact with), that's almost an infinite source of joy for me. I can still vividly remember the first time when my friend Doug Bland told me that he didn't believe my in situ IR results, because they didn't line up with the earlier GC results he had been getting for two years, and his subsequent "conversion" and full embracement of in situ spectroscopy. Changing people's minds and attitudes is often the most challenging part, but definitely the most rewarding part when you manage to do so. I now have many colleagues who no longer treat in situ spectroscopy as the last resort after they cannot use GC or LC, but rather first try to monitor their reactions with IR or

• Continued on Page 33

New Spectroscopic Techniques Aid in Tissue Engineering

Cynthia Delonas

Advanced techniques in tissue engineering hold promise to those who suffer from damage to or degeneration of joint cartilage. But some challenges exist for tissue engineers to gain a better understanding of the development of these constructs and their mechanical properties. Nancy Pleshko, a professor of Bioengineering at Temple University, in Philadelphia, Pennsylvania, has been studying the use of Fourier-transform–infrared imaging spectroscopy (FT-IRIS) as well as near-infrared (NIR) spectroscopy to explore the ways in which these techniques can aid in the development of replacement tissue. We spoke to her about her research and findings.

In a recent paper about tissue engineering and its ability to repair defects in articular cartilage (1) you discussed the use of FT-IRIS to study the distribution of water and extracellular matrix produced in engineered constructs such as those that are created for cartilage repair. Why is this an important study, and how might it help patients with osteoarthritis?

Tissue engineering strategies are being investigated for repair of tissues that are challenging to regenerate naturally, such as articular cartilage. Osteoarthritis is a disease that results in degeneration of joint (articular) cartilage, resulting in pain and mobility loss for millions. Development of engineered constructs could be a solution for tissue repair, but the compositional properties of the native cartilage should ideally be duplicated in the engineered tissues. The primary tissue components are extracellular matrix, including collagen and proteoglycans, and water. Thus, we need to know the relative amount and distribution of these components in both native tissue and engineered constructs.

What are the advantages of using FT-IRIS over more traditional techniques that allow a visual comparison between native cartilage and engineered cartilage? You reported spatial resolution of 25 mm to permit visualization of matrix and water throughout the tissue. What would be the ideal spatial resolution for this work?

There are several advantages of using this technique. First, FT–IRIS permits quantification of compositional information without the addition of external contrast agents. Different protein components, or mineral, if present, and water, can be evaluated in one unstained tissue section. This saves a significant amount of tissue preparation time and preserves the rest of the tissue for additional studies. Further, many other techniques can't be used to visualize water distribution, so this is certainly an advantage of this modality. The ideal spatial resolution would vary, depending on the question of interest. In cartilage, for example, spatial resolution in the 10–25 mm range is acceptable, as this can be related to variations in different zones of cartilage.

Photo Credit: adobestock.com/selensergen

However, it could be desirable to have better spatial resolution if there is a question of what specifically a cell is producing. Then one may want to investigate this at a better resolution, which could theoretically be done with attenuated total reflection (ATR) spectral imaging.

What challenges did you face in developing this method? Did you encounter problems with sample preparation and cryosectioning 80-mm sections of native and engineered cartilage?

The primary challenge was optimizing the sample thickness to enable collection of data from the same sample in both the mid-IR and NIR spectral regions. The sample had to be thick enough to obtain a reasonable NIR signal, but not so thick that the mid-IR absorbances were off scale. Investigation of mid-IR absorbances related to collagen and proteoglycan that have small absorptivity coefficients enabled us to achieve this goal. But, protein absorbances that are typically investigated in the mid-IR, such as the amide I absorbance, would not be feasible in an 80-mm tissue section.

Another recent paper of yours describes how NIR spectroscopy may be an alternative to destructive biochemical and mechanical methods for the evaluation of hyaluronic acid (HA) (2). What makes NIR a good technique for evaluating HA?

In that study, we used an NIR fiber optic to investigate hyaluronic acid–based developing engineered cartilage tissues. Typically, engineered tissues have to be harvested for implantation at an optimal timepoint, and determination of that timepoint is challenging. In particular, if, for example, you're growing six constructs, you may harvest one, and perform a biochemical analysis to assess the composition, and whether or not the construct is ready to implant. However, the variation in composition among constructs can be high, even if grown in the exact same conditions. So, relying on the outcome from one construct to reflect the composition of another in the same batch isn't always accurate. Thus, collection of NIR fiber optic data that reflect compositional data of an individual construct is an ideal solution.

What results have you achieved so far, and what differences, if any, can you observe between native and engineered cartilage using FT-IR imaging and NIR?

So far, we have successfully developed multivariate models based on NIR fiber optic data to predict compositional properties of developing engineered cartilage. We have also used FT-IR imaging data to help us understand how the fiber optic data change based on distribution of various components in the tissues, and how sensitive the fiber optic data are to these variations. The combination of the two different sampling modalities enables us to more fully understand the tissue development, and how to optimize our data collection and processing.

What are your next steps in this work?

The next steps for us are going to be very exciting! We will grow engineered cartilage in the laboratory, identify optimal constructs based on our NIR fiber optic data, and then harvest them to implant in a preclinical model. Further, we will use the same fiber optic sampling to assess how the engineered construct composition changes once it is implanted in vivo. If these experiments are successful, it will be a major step towards improved ability to select ideal constructs for tissue repair.

References

(1) J.P. Karchner, W. Querido, S. Kandel, and N. Pleshko, *Ann. NY Acad. Sci.* **442**(1), 104–117 (2019). doi:10.1111/nyas.13934

(2) F. Yousefi, M. Kim, S.Y. Nahri, R. L. Mauck, and N. Pleshko, *Tissue Eng. Regen. Med.* **24**(1,2) (2018). doi:10.1089/ten.tea.2017.0035 ●

• Continued from Page 31

Raman, and only move on to GC or LC when IR and Raman don't work sufficiently well (which does happen from time to time). I'm very proud of this.

What do you think are the aspect of working in industry that scientists in academia don't understand or appreciate?

I am not sure whether it is true that academic scientists don't understand or appreciate industrial scientists. Everyone has his or her own focus and perspective. Even within my own group, I don't think I always understand or appreciate the importance of another fellow spectroscopist's work. For example, I have fellow spectroscopists who spend all their time in QC labs or QC method development, and colleagues who devote themselves to process analytical, and still others whose focus was on the data management side, such as library, data communication, and chemometrics. I think we all need to put ourselves into others' shoes to really appreciate each other more. Along the same lines, maybe it's really the diverse type of work we do in industry that may be something not fully understood or appreciated by outsiders. We also face very different types of pressure in industry. While we usually do not get stressed out by funding or teaching, there are many other things that you have to keep abreast of to do your job well, such as keeping up with the latest technology development, ensuring a robust project pipeline, creating a roadmap to ensure that we have the most relevant capabilities matching the company's direction, and last, but not the least, meeting the ever-changing customer and market needs.

References

(1) R.J.Pell and X. Chen, J. Chemom. 28(5), 319—489 (2014) DOI: 10.1002/cem.2507

(2) X. Chen, Q.M. Wang, and L. Bu, Appl. Spectrosc. 71(9), 1—8, (2017) DOI: 10.1177/0003702817700427 ●

PEER-REVIEWED RESEARCH
Spectroscopy papers have undergone a double-blind peer review process and are available on our open-access website.

LIBS-Based Imaging: Recent Advances and Future Directions

V. Motto-Ros, V. Gardette, L. Sancey, M. Leprince, D. Genty, S. Roux, B. Busser, and F. Pelascini

Laser-induced breakdown spectroscopy (LIBS)–based imaging is becoming a promising technique in the panel of spatially resolved elemental approaches. This method has outstanding advantages, such as all-optical instrumentation, fast acquisition speed, operation at ambient atmosphere, and detection limits at the ppm scale for most elements. LIBS-based imaging has an extensive range of applications, including biology, medicine, industry, and geology. In this paper, we report on recent advances in LIBS imaging, focusing on instrumentation, performance, and applicability. Two examples are shown: first, a speleothem with application to paleoclimate studies, and second, a biological organ with implications for toxicology of new drugs based on nanoparticles. Finally, some future directions are discussed.

In the past few years, the application of laser-induced breakdown spectroscopy (LIBS) to microscopic elemental imaging has seen significant developments, in terms of both instrumentation and applications (1–4). In LIBS imaging, a series of laser-induced plasma is generated at different positions on the sample surface with a predefined sequence covering the region of interest. Such plasma sources allow specific optical responses resulting from the electronic relaxation of atoms and ions excited by the high plasma temperature to be elicited from the elements constituting the sample. The light emitted by the plasma is collected and analyzed using an optical spectrometer. The elemental "signal" (atomic and ionic emissions) is then extracted from the recorded spectra, and elemental maps can be obtained in a pixel-by-pixel manner (Figure 1) (5,6).

The main advantage of LIBS certainly lies in its simple implementation. This simplicity is because a single laser pulse simultaneously samples the material by laser ablation, atomizes, and then excites the vaporized mass by heating the plasma plume. This simplicity endows this technique with a series of advantages, including an all-optical design compatible with conventional optical microscopy, operation in ambient atmosphere, and fast operating speed up to kHz. In addition to its tabletop instrumentation, this technique has multielement capabilities, no restrictions in the detection of light elements, detection limits in the range of ppm for most elements, and microscopic-scale resolution (2). It also has quantitative capabilities through the use of standards with known concentrations or an external calibration using different strategies (6–9). All of these advantages make LIBS imaging highly promising, with the potential to become a reference technique in the area of spatially resolved elemental techniques as a complement to gold standard methods, such as laser ablation inductively coupled plasma mass spectrometry (LA-ICP-MS), synchrotron radiation microanalysis, or electron probe microanalysis (EPMA) (10–13).

Recently, the LIBS community demonstrated the value of this technique for a range of applications, covering geological, industrial, and biomedical domains. For example, the capability of LIBS imaging to characterize complex samples was explored with the analysis of a multiphase hydrothermal ore sample (14). More than 30 elements were identified, with the concentration

ranges extending from major to trace elements. In an application to paleoclimate studies, large-scale speleothems and coral samples (>10 cm^2) were analyzed, with the aim of revealing the laminar structures related to vegetation or climatic variations (5). Several studies of industrial materials have also been conducted on crystals (7,9) or heterogeneous catalysts (8,15). The possibility of obtaining elemental images of biological tissues was also demonstrated in different biomedical situations (16–18). In this paper, we illustrate recent advances in LIBS imaging in terms of instrumentation and applicability. Two different examples are shown to illustrate the specificities and the current performance of this technique.

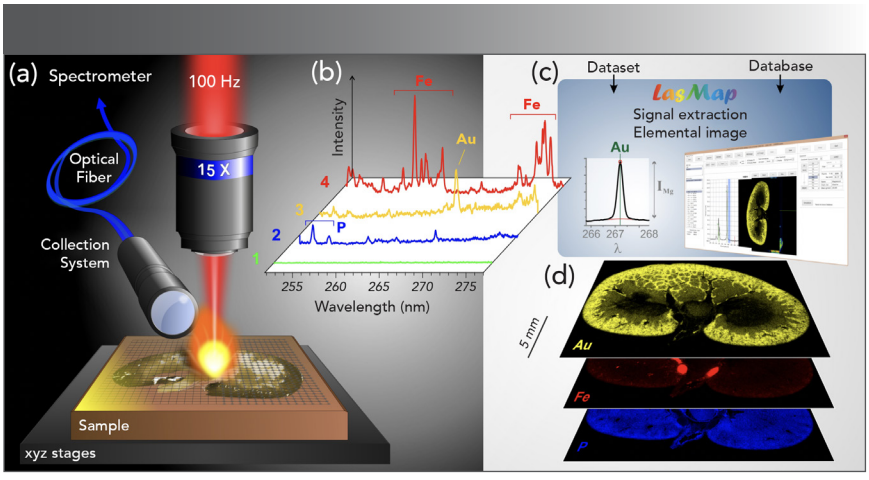

FIGURE 1: The principle of LIBS-based imaging. (a) Schematic view of the micro-LIBS setup showing the 15x microscope objective used to focus the laser pulse, the motorized platform supporting the sample and an optical detection system connected to the optical spectrometer via an optical fiber. (b) Example of single-shot emission spectra recorded in four different regions of the sample (a rat kidney sampled 1 h after gold nanoparticle administration) with the characteristic emission lines of iron (Fe), phosphorous (P), and gold (Au). (c) Principle of data extraction using LasMap Software. (d) Example of relative-abundance images of Au (yellow), Fe (red), and P (blue).

Experimental

The micro-LIBS system developed in our group is based on a custom microscope (Figure 2). The optomechanical structure has been designed with the use of cage and tube systems commercialized by

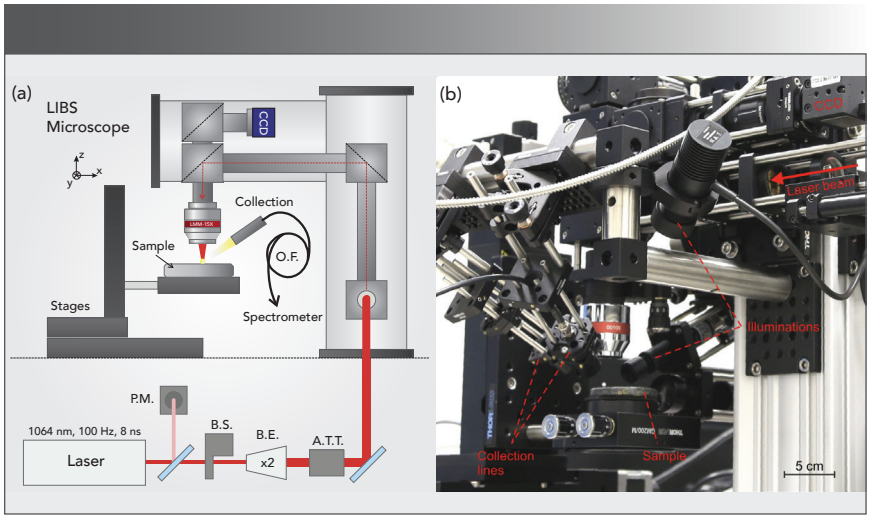

FIGURE 2: LIBS imaging setup. (a) Schematic view of the LIBS setup: P.M. (power meter), B.S. (beam shutter), B.E. (beam expander), A.T.T. (attenuator), and O.F. (optical fiber). (b) Photo of the LIBS imaging instrument.

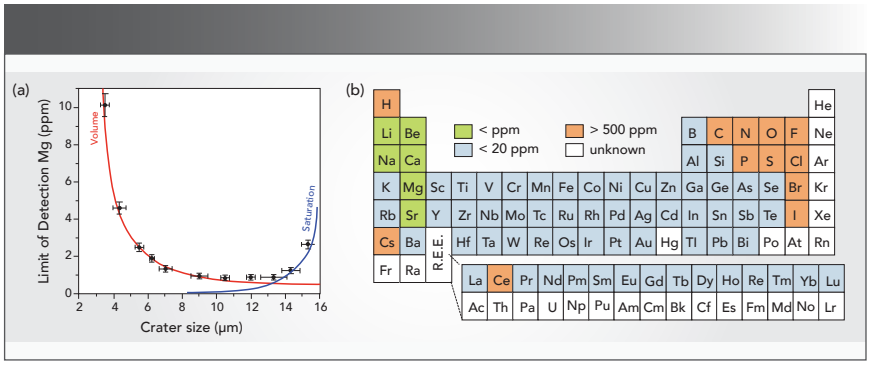

FIGURE 3: (a) Evolution of the Mg limit of detection (LOD) with increasing crater size. (b) Estimated values of relative detection limits obtained in single pulse configuration.

Thorlabs. The device includes a laser injection line, monitoring cameras (sample surface, plasma), and illuminators (white light, laser pointer), as well as up to three collection lines connected to spectrometers with optical fibers (19). The device is also equipped with a Raman system operating at 735 nm, and allowing punctual analysis to be performed. The laser used is a nanosecond Nd:YAG laser working at the fundamental wavelength (1064 nm) with a frequency rate of 100 Hz (Centurion, Quantel). The typical pulse energy is in the range of 1 mJ for most applications. The laser energy is stabilized throughout the experiment by using a servo control loop consisting of a power meter and a computer-controlled attenuator (Figure 2a). The system is equipped with several Czerny-Turner spectrometers (Shamrock 303 and Shamrock 500, Andor technology) coupled to ICCD cameras (Istar, Andor Technology) as well as compact spectrometers (MayaPro and HR2000+ from Ocean Optics), which can be operated simultaneously. In our instrument, the laser beam is focused using a 15x magnification objective (LMM-15X-P01, Thorlabs). The typical crater size is in the range of 7 µm. For all imaging experiments, a laser-induced plasma is generated continuously while scanning the sample surface. The scanning is performed line by line, continuously, in a raster scan mode with the use of motorized x–y–z stages. The operating speed is equivalent to the laser frequency (100 Hz), and a 1-megapixel image is typically obtained in less than 3 h (5). In addition, the measurements are performed at room temperature under ambient pressure in air or in an argon atmosphere. Finally, in-house developed software written in the LabVIEW environment is used to control the entire imaging setup, thereby allowing automatic scanning sequences in any selected region of interest of a given sample with a preset laser pulse energy and spatial resolution.

For processing the spectral dataset, our group has developed a custom LabVIEW software, named "LasMap." This software allows the relevant intensities to be extracted from the spectra before building the corresponding elemental images. We generally use the average spectrum (computed with the whole spectral dataset) to obtain an overview of the spectral structure of the sample, allowing the selection of the lines of interest free of interference. Algorithms then extract the net intensity of the lines by taking into account the baseline level to generate a 2D matrix (relative abundance image) (20). This procedure is relatively fast for a single matrix sample, with a megapixel dataset typically processed in less than a few minutes.

Results and Discussion

Imaging "Performance"

In LIBS-based imaging, the achievable performance (for example, spatial resolution and detection limits) is strongly related to the laser ablation process. To guarantee the best shot-to-shot repeatability, it is important to set up the experiment to avoid any overlap between consecutive laser shots. The lateral resolution is then ultimately governed by

the laser-induced damage and the limits of detection (LOD) depend both on the mass of vaporized material (such as the crater volume) as well as the excitation capability of the laser pulse. Therefore, there is a compromise between these parameters. As an example, the evolution of the detection limit of magnesium (Mg) as a function of the crater diameter is shown in Figure 3a. This result was obtained on a reference glass by modifying the laser pulse energy. The LOD shows significant deterioration when reducing the crater size due to the reduction of the ablated mass (plasma density). With larger crater sizes, there is also an increase of the LOD due to the saturation of the detector, that was optimized for detecting weak signals. To give priority to the detection limits, we preferentially use crater sizes in the range of 6 to 10 µm. It is important to mention that laser ablation is a violent process. It is accompanied by different mechanisms, including shock wave formation and thermal diffusion through the sample, that might cause more sample deterioration than the ablation itself. The resolution will then be dependent on the material properties, particularly the hardness. However, resolution <15 µm can easily be obtained for the large majority of materials.

Figure 3b shows the typical accessible range of LODs, expressed in weight %, obtained in this configuration for most of the elements. Sub-ppm LODs are generally achieved for alkali and alkali-earth metals. The sensitivity remains attractive for other metals, with LODs better than 20 ppm, but strongly deteriorates for organic and halogen elements. It is important to emphasize that such relative LODs are obtained in a single pulse configuration and from an ablated mass in the range of 0.1 nanogram (typical ablated mass from a single laser pulse). Expressed in absolute detection limits (for example, the smallest mass quantity that can be detected), values typically lower than the femtogram can be achieved.

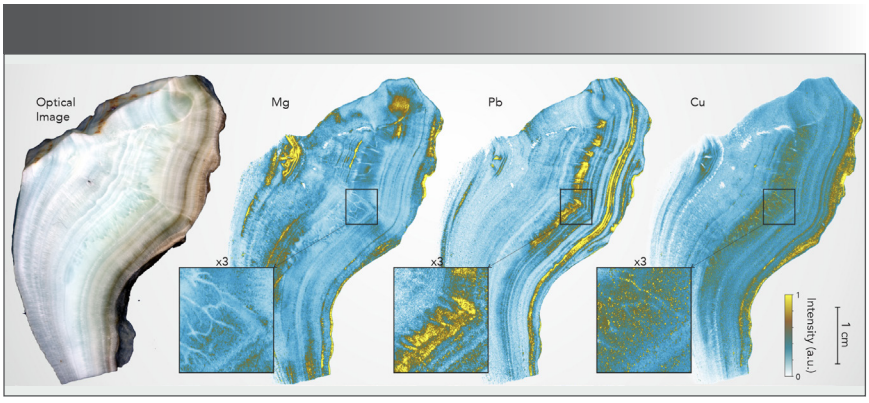

FIGURE 4: Example of elemental images obtained from a speleothem section recovered from the Gallo-Roman copper ore mine located close to the "*Grotte Bleue*" in Aude, France. Images shown are (from left to right): an optical image, and highlighted composition images for magnesium (Mg), lead (Pb), and copper (Cu).

Paleoclimate Application

Thanks to the 100 Hz scanning speed, and because there is no constraint on the size of the sample (such as, for example, no need for an ablation cell), large surfaces can be easily analyzed. Such features may be valuable with geological samples, particularly for the characterization of speleothems. Stalagmites, stalactites, or columns precipitate from

Orbis Micro-XRF Analysis System

- Non-destructive X-ray elemental analysis from Na to Bk
- Excitation geometry perpendicular to sample for accurate sample targeting
- High-intensity analysis for micro to millimeter areas
- Increased sensitivity with filters as standard
- Fastest analytical speed with state of the art detectors

For more information, please visit:
https://www.edax.com/micro-xrf

AMETEK® MATERIALS ANALYSIS DIVISION

edax.com

EDAX® Smart Insight

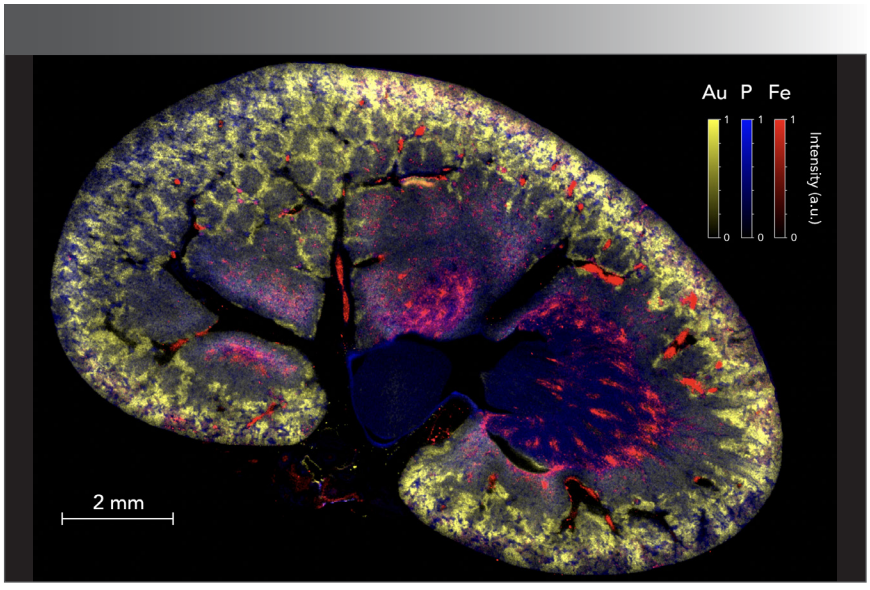

FIGURE 5: Multielemental image of a rat kidney after intravenous injection of gold (Au) nanoparticles. Merged image composed of the combination of three false color elemental images for Au (yellow), P (blue) and Fe (red). These animal experiments were approved by the local ethics committee under agreement A21231016EA.

seepage waters in caves, and usually consist of calcium carbonate, with calcite being the most common mineral phase. Climate proxies, such as Mg, Sr, or Ba, can be retrieved from these materials, and may indicate changes in climate or environmental conditions that occurred during the growth periods and provide information on past temperature, precipitation, and vegetation changes over the last hundreds of thousands of years (21). For recording paleoclimate proxies, it is interesting to analyze several centimeters, or even more, of a sample while maintaining resolution on the scale of the annual speleothem growth (typical rates of 0.01 to 2 mm per year) (22).

An example is shown in Figure 4 for a speleothem extracted from a Gallo-Roman copper ore mine situated close to the "Grotte Bleue" in Aude, France (courtesy of D. Genty and P. Cabrol of Les directions régionales de l'Environnement, de l'Aménagement et du Logement [DREAL], in Toulouse, France). At the collection site, there is a strong abundance of copper, which gives a particular blue color to this mineral. This site is also known to be rich in iron, lead, and arsenic. Amphoras discovered on the site suggested Roman use of the cave from the 1st century BC, but it is suspected that the site was also occupied in the Bronze Age (23). In the example shown in Figure 4, a mapping sequence of 2300 x 1600 pixels was performed with a step size of 24 µm, which corresponds to a surface of analysis of more than 20 cm². The optical image of the sample and elemental images of Mg and Pb are shown. These results illustrate that the resolution capabilities of the LIBS imaging method and annual growth layers can be observed. It is worth mentioning that other elements, such as Cu, Ag, Sr, Ba, Al, and Si, were also detected. The interpretation of their results is currently being explored by specialists.

Imaging Biological Specimens

LIBS-imaging can also be applied on soft biological tissues. Our first work in this area was conducted on a mouse kidney to image the biodistribution of NPs before administration to animals (6,24,25). These studies were followed by several articles reporting biological studies conducted on murine animals, where LIBS was used as a complement to more conventional techniques such as transmission electron microscopy (TEM) or fluorescence microscopy (17,18,26). More recently, studies were also conducted with human specimens of medical interest (16,27). In health infrastructures, the possibility of coupling LIBS imaging with conventional histopathology could be highly valuable for making some medical diagnoses. Because LIBS imaging is compatible with the light microscopy used in pathology laboratories, it may provide important support for uncovering the elemental composition of tissues, particularly in the case of numerous pathologies relating to exposure to metals (such as respiratory diseases, dermatological diseases, and cancers).

As an example, Figure 5 shows an image obtained for a rat kidney section. The organ was sampled 1 h after intravenous administration of gold nanoparticles (NPs). This experiment was performed with a resolution of 10 µm, and represents 2 million individual pixels. Three elements are represented with a false color scale: Au in yellow, P in blue (the P distribution reflects the histological structure of the tissue), and Fe in red (in this case, the threshold allows for visualizing Fe from hemoglobin, and by extent, blood vessels). As observed in several previous work (6,26), small NPs are mainly eliminated by the renal route with partial retention in the cortex region of the organ (peripheral region), indicating a normal elimination process. More generally, the possibility of imaging NP distribution at the entire organ scale and without any labeling is highly relevant for studies involving the development of new drugs based on metals.

Status and Future Directions

LIBS-based imaging is a mature technique for various classes of

REVEAL THE UNREVEALED

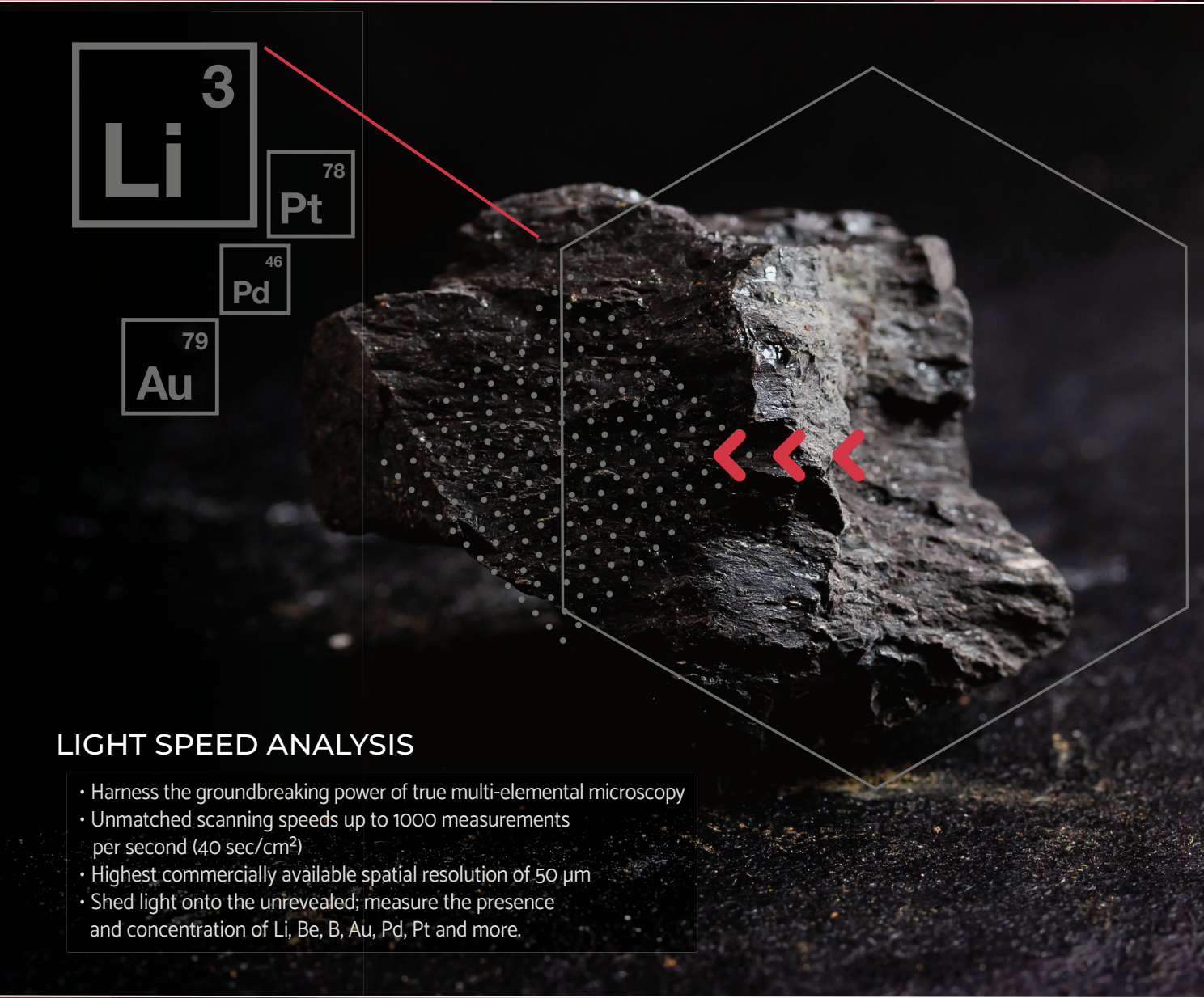

LIGHT SPEED ANALYSIS

- Harness the groundbreaking power of true multi-elemental microscopy
- Unmatched scanning speeds up to 1000 measurements per second (40 sec/cm^2)
- Highest commercially available spatial resolution of 50 µm
- Shed light onto the unrevealed; measure the presence and concentration of Li, Be, B, Au, Pd, Pt and more.

ELEMISSION

LIBS TECHNOLOGY

elemission.ca

materials. These materials consist of a homogeneous matrix in which it is desired to observe the possible heterogeneity of minor or trace elements (both examples shown above in Figures 4 and 5). The advantage of such a simple material is that matrix effects can be avoided, greatly facilitating the calibration of raw intensities. In addition, since we are interested in minor or trace elements, line saturation phenomena (such as self-absorption and detector saturation) are nonexistent, and the intensity of the measured lines is linearly dependent on the concentration.

However, difficulties arise when considering complex materials with multiple matrices. These difficulties are inherent to all elemental imaging methods. Regardless of the analytical technique, the interaction between the primary beam and the material will always depend on the sample properties. The recorded signal will then be dependent on the material (nature, hardness, composition, and so on), so it is difficult to generate a quantitative analysis on such complex material, regardless of the technique used. Currently, the classical way to calibrate the intensities is to use reference samples for each phase of the material, knowing that in practice these standards do not always exist. An interesting possibility for the future is to implement a calibration-free approach. Such a method does not require external references because it only relies on the physical analysis of the spectra. By considering a given plasma model and measuring its parameters (such as temperature or electronic density, for example), it is possible to extract the concentrations of the various detected elements, regardless the type of the matrix. Such a method could be highly promising for the development of the technique, and several groups are currently working on its implementation.

An additional difficulty related to emission spectroscopy comes from the possible complexity of the signal. Some elements, such as transition metals, have a large number of emission lines from the ultraviolet (UV) to near infrared (NIR) range. This is the case in particular for iron or titanium. If one or more of these elements are a matrix constituent, the observed spectra will be spectrally dense, and the desired lines (generally from minor or trace elements) will likely be masked. In this case, the performance in terms of sensitivity will deteriorate.

Managing the processing of data obtained on complex samples also represents a challenge and limits the fields of possible exploration of the technique. It must be kept in mind that the data to be processed are very large (up to several tens of gigabytes), and the software used cannot be supervised. It is indeed impractical to interpret spectra one by one for a megapixel analysis. A promising possibility that is currently being explored is the use of statistical analysis methods (such as chemometrics). In general, these methods allow the dimensionality of a series of data to be reduced by looking for correlations among the different variables, thus making the information less redundant and easier to handle. We recently published an article detailing the implementation of principal component analysis (28), and several groups in the LIBS community are currently exploring other methods, such as the possibility of using machine learning approaches.

Conclusion

LIBS imaging is currently experiencing significant development, with an increase in the number of published papers during the last three years. Due to the feasibility studies conducted in laboratories, this approach is becoming increasingly mature, and is currently a good candidate to become a reference approach for spatially resolved elemental characterization in the near future. LIBS has unique specificities, such as the possibility of reaching micrometer-scale resolution with limits of detection down to ppm, operation at ambient conditions with tabletop, and all optical instrumentation. Regarding the acquisition rate, recent work has demonstrated the possibility of access to kHz acquisition rates (29), and higher operating speeds should be achieved very soon.

The future will tell if LIBS-based imaging can be generalized and used outside academic laboratories. What is certain is that, at some point, its development will have to be supported by large industrial groups. In the meantime, researchers still have some work to explore. In particular, the analysis of complex materials (those composed of several matrices) appears challenging, both for quantification and data processing. Further studies dedicated to these issues need to be conducted, and the use of calibration-free LIBS and advanced chemometric tools represent interesting opportunities.

Acknowledgments

This work was partially supported by the French region Rhônes Alpes Auvergne (Optolyse, CPER2016) and the French ANR (projects MediLIBS ANR-17-CE18-0028-04 and Imazinc ANR-16-CE29-0024). In addition, we gratefully acknowledge Florian Trichard from Ablatom S.A. S, Nicolo Omenetto from the University of Florida, Ludovic Duponchel from the University of Lille, and Christophe Dujardin from ILM for fruitful discussions.

References

(1) M.P. Mateo and G. Nicolas, *App. Spectrosc. Rev.* **48,** 357–383 (2013).
(2) L. Jolivet, M. Leprince, S. Moncayo, L. Sorbier, C.P. Lienemann, and V. Motto-Ros, *Spectrochim. Acta Part B* **151,** 41–53 (2019).

• Continued on Page 64

PEER-REVIEWED RESEARCH
Spectroscopy papers have undergone a double-blind peer review process and are available on our open-access website.

A Label- and Enzyme-Free Fluorescent Method for the Rapid and Simple Detection of Hg^{2+} in Cigarettes Using G-Triplexes as the Signal Reporter

Hui Zhao, Yang Zhao, Xiaoxi Si, Juan Li, Yuanxing Duan, Wei Jiang, Chunbo Liu, Junheng You, Zhenjie Li, and Qinpeng Shen

Knowledge about the quantity of Hg^{2+} in tobacco is important for the health of smokers. Thus, a novel G-triplex-based label- and enzyme-free fluorescent method was developed for detecting Hg^{2+} in tobacco. In this system, the target Hg^{2+} ions associate with the DNA complex that serves as a probe through formation of specific thymine-Hg^{2+}-thymine (T-Hg^{2+}-T) base pairing, which results in the release of the P2-containing G-triplexes. Subsequently, fluorescence enhancement is achieved by producing G-triplexes, which bind with thioflavine T (ThT). A detection limit of 0.2 nM was achieved within 40 min. The method has been successfully applied to the detection of mercury in tobacco. At this time, the application for detecting Hg^{2+} in tap and river water samples also indicates that further applications are anticipated.

In recent years, the development of non-ferrous metal minerals, coal-fired flue gas, and solid waste incineration have increased the production of heavy metals and toxic substances in the environment, resulting in increased risk of excessive levels of mercury in tobacco (1–4). This can impart a sizable health risk to smokers when too much mercury, present as Hg^{2+}, is deposited in tobacco (5–7). Therefore, it is important to be able to provide rapid and simple detection of the quantities of Hg^{2+} in tobacco.

Conventional trace Hg^{2+} detection methodologies include the use of atomic fluorescence spectrometry (AFS), atomic absorption spectroscopy (AAS), and inductively coupled plasma–atomic emission spectrometry (ICP-AES), but the instrumentation required for such approaches is expensive, and the process is complicated, which limits the application into a broader range of areas. At the same time, colorimetric sensor technology (8–10), electrochemical sensors (11–14), and fluorescence sensors (15–18) have also been developed for the detection of mercury ions. For example, Zhu and associates developed a strategy to detect Hg^{2+} using a highly sensitive colorimetric sensor based on the aggregation of gold nanoparticles driven by cationic polymers (9). The method has the advantages of high efficiency and speed, but requires additional capital investment and more time. Bao and colleagues developed an electrochemical aptamer sensor for Hg^{2+} detection, which makes use of an exonuclease to achieve cycling and amplification, but the enzyme was found to be difficult to store and was easily inactivated (13). To solve the above problems, a fluorescence method (19–25), which has advantages such as stability, simplicity, and rapid detection, has been successfully used for profiling low levels of Hg^{2+}. For example, Wang and colleagues de-

A Robust, High-Performance, Revolutionary Demountable ICP Torch

An Inductively Coupled Plasma (ICP) torch can be a costly consumable item requiring regular maintenance and replacement, particularly with aggressive sample matrices, such as hydrofluoric acid (HF), organic solvents and high total dissolved solids (TDS).

The patented D-Torch is a revolutionary demountable torch from Glass Expansion, the world's leader in the design of sample introduction systems for ICP. A single, precision-engineered D-Torch can lower running costs and provide the flexibility to run any sample matrix by simply interchanging the injector. There's no need to have different torches for samples with organics, HF or best detection limits. The Glass Expansion D-Torch (shown below) for the Agilent 5100 and 5110 is also fully compatible with Agilent's 5800 and 5900 instruments.

D-Torch Body Assembly | Outer Tube Options (Quartz or Ceramic) | Injector Options (Various Materials & IDs) | Injector Adaptor Assembly

Agilent 5100/5110 & 5800/5900 D-Torch

Compared to other conventional torches, the D-Torch offers:

- Better analytical precision with the unique tapered injector design
- A choice of quartz, alumina, sapphire and platinum injectors in a range of diameters for aqueous, organic, high salt, fusions or HF-containing samples
- Optional ceramic outer tube that produces a hotter, more robust plasma that is virtually indestructible
- Lower running costs as only the outer tube is replaced when it wears-not the whole the torch
- Easier cleaning without O-rings that get brittle and stick to the outer tube

GLASS EXPANSION
Quality By Design

Head office
6 Central Boulevard,
Port Melbourne Vic 3207,
Australia
+61 3 9320 1111
enquiries@geicp.com

Americas
31 Jonathan Bourne Drive,
Unit 7 Pocasset, MA 02559,
USA
508 563 1800
geusa@geicp.com

Europe
Friedenbachstrasse 9,
35781 Weilburg,
Germany
+49 6471 3778517
europe@geicp.com

Comparative torch ownership costs versus the D-Torch

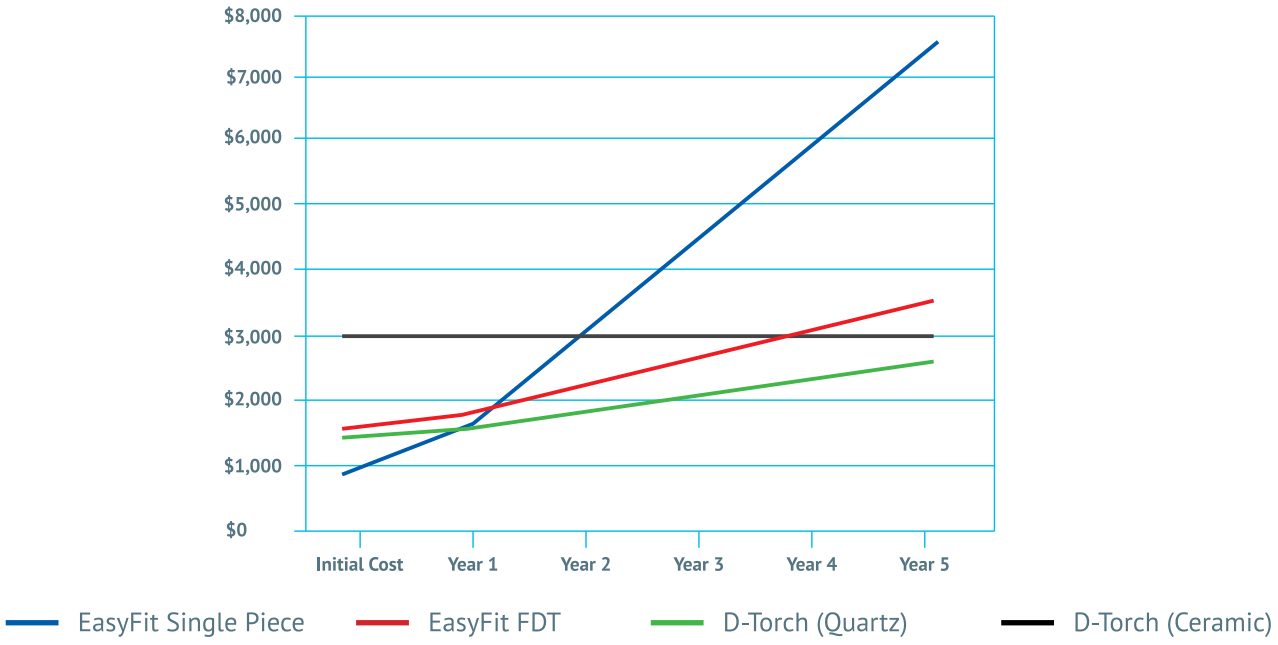

Virtually Indestructible Ceramic Outer Tube

Glass Expansion pioneered the design of ceramic torches more than 20 years ago. Since then, we have provided ceramic versions of our D-Torch for dozens of different ICP models.

Using a ceramic outer tube on your ICP torch produces a hotter, more robust plasma, which reduces matrix effects and improves detection limits. Compared to a quartz outer tube, the ceramic outer tube has a much longer lifetime, greatly reducing maintenance, cleaning and downtime due to torch failure. In some sample matrices, quartz outer tubes can degrade in hours while the ceramic outer tube will last years under the same conditions.

The ceramic outer tube is ideal for:

- Analyses at the detection limit as the hotter plasma increases sensitivity
- Monitoring of wear metals in engine oils, as quartz outer tubes often suffer cracking and shortened lifetimes due to thermal shock
- Analysis of fusion samples where the lithium salts rapidly attack quartz
- Measuring high TDS samples that will quickly devitrify the quartz outer tube

Six hours of running 10% NaCl

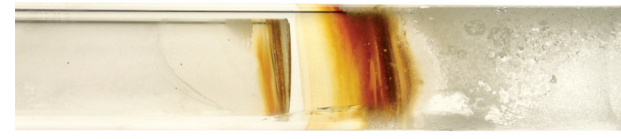

Quartz outer tube

Ceramic outer tube

A combination of high temperature and salt deposit causes a quartz torch to devitrify. Higher concentrations of salt in the samples lead to more rapid devitrification. The quartz torch in the photo was run for only 6 hours with samples containing 10% NaCl and is already badly degraded. By contrast, the ceramic material does not devitrify and is not affected by salt deposits.

The ceramic D-Torch in the photo was run for the same period and with the same samples as the quartz torch but shows no degradation at all.

Learn more at: www.geicp.com/D-Torch

TABLE I: A comparison of methods for detecting Hg^{2+}

Detection Method	Target	Linear Range	Detection Limit	Reference
Colorimetric	Hg^{2+}	0.25–500 nM	0.15 nM	(9)
Electrochemical	Hg^{2+}	0.5 nM–5 μM	0.14 nM	(11)
Electrochemical	Hg^{2+}	0.2 pM–35 nM	0.12 pM	(13)
Flourescence	Hg^{2+}	50 pM–20 nM	10 pM	(19)
Flourescence	Hg^{2+}	0.1–100 nM	65 pM	(27)
Flourescence	Hg^{2+}	18.4–14.7 nM	1.2 nM	(28)
Flourescence	Hg^{2+}	1–100 nM	0.2 nM	This work

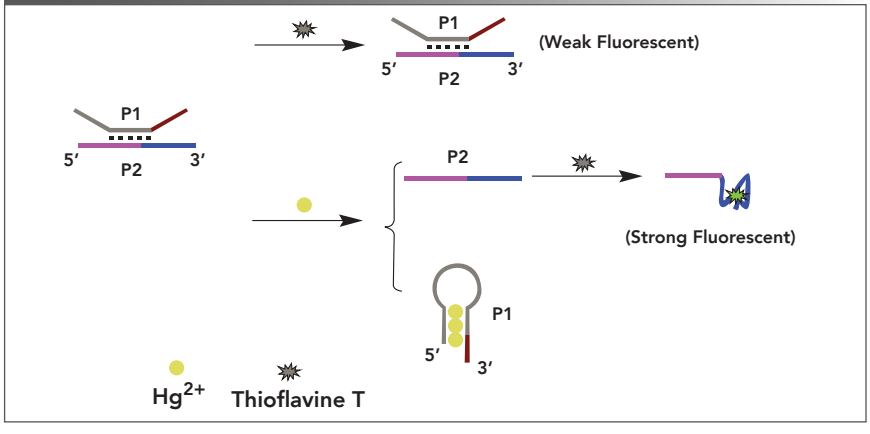

SCHEME 1: Diagram of the probe-based G-triplet for detecting Hg^{2+}

TABLE II: The experimental results for six cigarette shreds analyzed by this method

Sample	Hg^{2+} Concentration (μg/L)	Hg^{2+} Content (μg/Kg)
1	0.5392	26.96
2	0.7158	35.65
3	0.7530	37.65
4	0.6507	32.54
5	0.9110	45.55
6	0.7995	39.98

veloped a DNA-fueled molecular machine for fluorescent detection of Hg^{2+} (19), Chen and associates reported a gold nanorods-based FRET assay for ultrasensitive detection of Hg^{2+} (24). However, the cumbersome fluorophore labeling contributes to making the experimental process more complicated. Therefore, it was imperative to develop an enzyme-free and label-free fluorescence method for the detection Hg^{2+}.

In the present study, a simplified approach that makes use of a fluorescence probe based on the G-triplex structure to detect Hg^{2+} with high sensitivity is reported. The P1 chain is composed of a large number of T bases, which are bound by Hg^{2+} to form a stable hairpin structure, ThT. The terminal end of the P2 strand was packed with abundant G sequences, which combine to produce enhanced fluorescence in the presence of ThT. Thus, a label- and enzyme-free strategy was implemented for simple and rapid detection of Hg^{2+}, avoiding a cumbersome labeling process and avoiding the use of G-triplex enzymes. Moreover, the method has been successfully applied to the detection of mercury in both tobacco and water samples, which indicates that broader applications of this method are anticipated.

Materials and Methods

Materials

The polyacrylamide gel electrophoresis (PAGE)-purified P1, d(CATTCA ATACTTTGGGTACTTCATCATCAC TTCCCATTGTATTGAATTAGATCTT CGTA), and the polyacrylamide gel electrophoresis (PAGE)-purified P2, d(CCACATACATCATATTCTCTCAT TCAATACAATGGGTAGGGCGGG), were obtained from Sangon Biotechnology Co., Ltd., the P1 and P2 were designed according to previous literature (19). The documentation pertaining to the indicated amino acid sequences is available on the supplier website. The salts used to prepare the ionic solutions, including KCl and Hg $(NO_3)_2$, and trishydroxymethylaminomethane hydrochloride (Tris-HCl) were purchased from Comio Chemical Reagent Co., Ltd. ThT was supplied by J&K Scientific Co., Ltd.

Instrumentation

DNA fluorescence intensity was measured at the excitation band of 420 nm using a spectrofluorophotometer (RF-5301pc, Shimadzu), in which the slits were set to 5.0 and 5.0 nm for excitation and emission, respectively. The method was evaluated at the fluorescence intensity of 490 nm, which has been demonstrated to be the maximum emission intensity. Absorbance spectral measurements were obtained on a UV-2450 spectrophotometer (Shimadzu Co.).

The accurate results are growing. The microbes aren't.

SPECIALLY FORMULATED TO PREVENT THE GROWTH OF MICROBIALS.

Inorganic Ventures' colored pH buffers and conductivity certified reference materials (CRMs) are NIST-traceable and manufactured according to stringent Quality Assurance guidelines. For highly regulated and accredited industries like biomedical, pharmaceutical, life sciences and nutraceutical, these CRMs deliver confidence, control, and support from the recognized industry leader.

The savings and our service and support will grow on you. Microbes won't.

Visit us in Chicago at Pittcon Booth 1620!

BENEFITS:

- **No microbial growth**
- **Certified at multiple temperatures**
- **Custom capability**
- **Scientific expertise to refine formulations to address your specific needs**

INORGANIC™ VENTURES

inorganicventures.com

REGISTERED ISO 9001 QSR-1034 BY QSR

ACCREDITED ISO 17025 0883.01 BY A2LA

ACCREDITED ISO 17034 0883.02 BY A2LA

300 Technology Dr | Christiansburg, VA 24073 USA
P: 800.669.6799/540.585.3030 | F: 540.585.3012

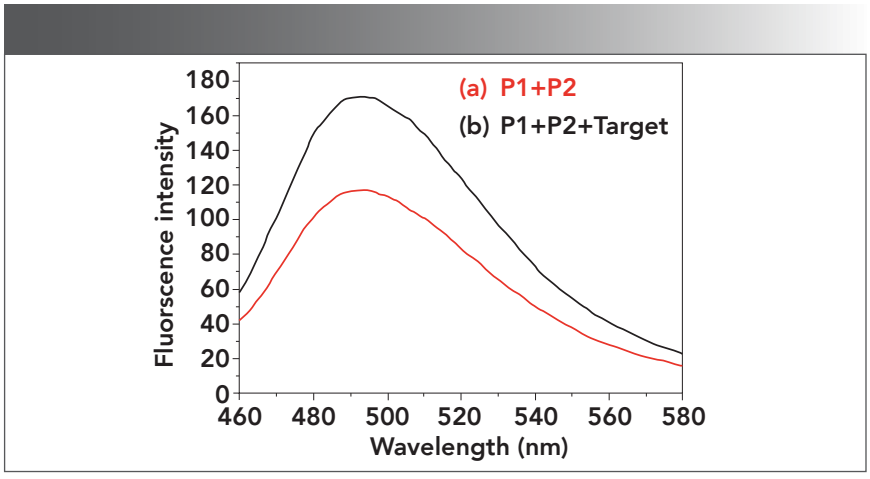

FIGURE 1: Fluorescence intensity of samples under different conditions. From bottom to top: (a) P1 + P2 (red), and (b) P1+P2+Target (black). The concentrations of P1 and P2 were both 100 nM. All the above solutions were incubated in Tris-HCl buffer at 35 °C for 40 min followed by fluorescence measurement.

Fluorescence Measurements

P1 and P2 were diluted in Tris-HCl buffer, heated to 95 °C for 5 min. and then cooled slowly to room temperature for 1 h. Then 250 µL reaction samples containing P1 and P2 with different concentrations of Hg^{2+} were prepared in Tris-HCl buffer followed by incubation at 35 °C for 40 min. The fluorescence intensity of ThT was measured in the spectral region 460–580 nm, where the maximum emission was at 490 nm.

Real Sample Analysis

Initially, 0.2000 g of dried tobacco samples and 5.0 mL of concentrated nitric acid and 1.5 mL of hydrogen peroxide were combined in polytetrafluoroethylene (PTFE) high-pressure digestion tanks, and were digested in a microwave digestion apparatus. A graphite furnace electrothermal acid meter was used to catch acid at 120 °C. After 30 min, the sample was centrifuged (10000 r/min) and filtered through a 0.22 µm microporous membrane to eliminate possible interference factors, and the volume was adjusted to 100 mL with an appropriate amount of distilled water. A volume of 100 µL of the above-mentioned shredded tobacco digestion solution was taken, and mixed with 100 µL of probe

Enhance the Performance

of your X-ray Analytical Instruments for XRF and XRD Analysis

XOS is a leading manufacturer of polycapillary and DCC X-ray optics and source solutions.

Our industry experts work closely with customers to optimize their instrument design and performance for a variety of challenging and pioneering applications.

Visit xos.com/oem-solutions to learn more.

Set up a meeting to discuss your custom optic solution at Pittcon with our OEM & X-ray Optics Director, Dr. Ning Gao by emailing **info@xos.com**.

XOS®

Visit XOS and Lazar Scientific at Pittcon – **booth #2915**!
Check out Petra MAX Autosampler & Clora 2XP.

Lazar Scientific, Inc. | XOS®

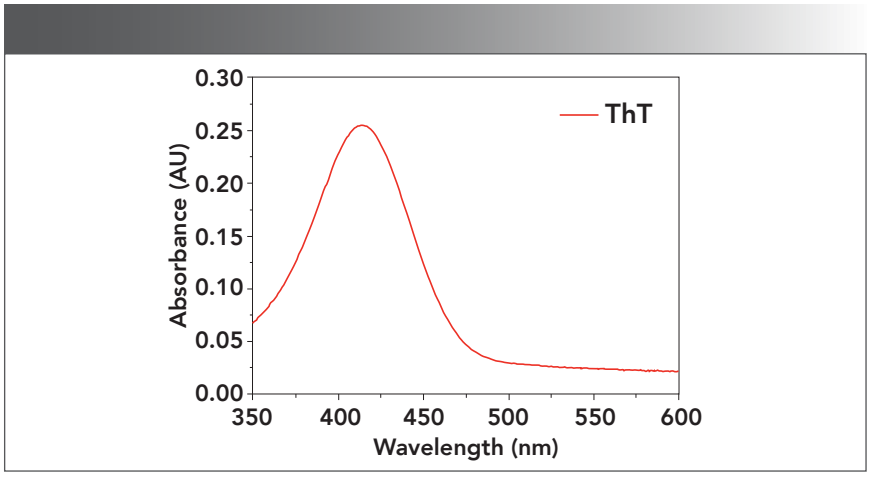

FIGURE 2: UV-vis absorbance spectrum of ThT. The molar concentration of ThT is 5 µM, which is obtained by ultrapure water dilution.

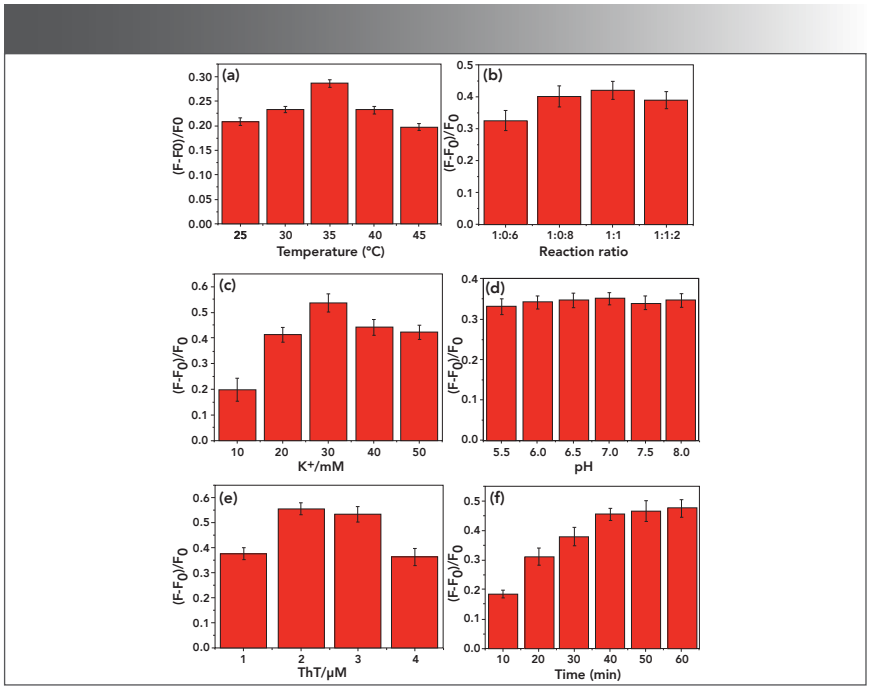

FIGURE 3: Optimization of the experimental conditions: (a) the hybridization temperature, (b) the reaction ratio, (c) the concentrations of K^+, (d) pH, (e) the concentrations of ThT, and (f) the reaction time. The error bar represents the standard deviation of three measurements. All the above solutions were incubated in Tris-HCl buffer followed by fluorescence measurement.

solution, 200 µL of Tris-HCl buffer solution (pH 7.0), and to that added an appropriate volume of distilled water to a final volume of 1 mL. After being allowed to stand for 10 min, the sample was transferred to a quartz cuvette and the absorbance spectrum measured.

Under optimal conditions, it was necessary to filter the river samples to avoid insoluble impurities. In the recovery tests, aliquots of tap and river water samples together with the fluorescent probe with different concentrations (10, 20, 30 nM) of Hg^{2+} were added to the probe solutions and incubated for 40 min. All other reaction conditions were the same as in the above procedures.

Results and Discussion

Fluorescence Detection of Hg^{2+} Design Mechanisms

Scheme 1 illustrates the operating principle of the proposed method for rapid label- and enzyme-free Hg^{2+} detection. The P1 chain is composed of a large number of T bases, which are bound by Hg^{2+} to form a stable hairpin structure ThT. The terminal end of the P2 strand was packed with abundant G sequences, which combine to enhance the fluorescence intensity in the presence of ThT. Thus, when there was no target, a weak fluorescence intensity was be observed. However, when the target was added, the fluorescence intensity was enhanced significantly.

To demonstrate the method, Hg^{2+} was detected by assessing the changes in fluorescence intensity before and after adding Hg^{2+}. As shown in Figure 1, when there was no target, a weak fluorescence intensity was observed. When the target was added, the fluorescence intensity was enhanced significantly. At the same time, to further verify feasibility of the experiment, the absorption spectrum of ThT, in which the maximum absorption peak was 420 nm, was verified as shown in Figure 2.

Optimization of the Experimental Conditions

For measurement of the enhanced fluorescence intensity, the reaction temperature was found to be a key factor affecting the fluorescence intensity. As shown in Figure 3a, the fluorescence intensity is strongest at 35 °C. Thus, 35 °C should be used as the optimum reaction temperature for subsequent experiments. At the same time, as seen in Figure 3b, an optimal reaction ratio between P1 and P2 can be considered to be 1:1. In addition, we also tested the effect of K^+ concentration and pH and ThT concentration on fluorescence intensity. As shown in

Figures 3c, 3d, and 3e, the fluorescence intensity reached a maximum at a K^+ concentration of 30 mM, and an optimum at pH = 7, and 2 µM can be considered as the optimum concentration of ThT. At the same time, the reaction (incubation) time was also optimized and extended from 10 min to 60 min, as shown in Figure 3f, where the fluorescence intensity gradually increased up to 40 min. The fluorescence intensity plateaued after 40 min and thus was selected as the optimum time for incubation.

Assay Performance of the System

To understand the sensitivity of this strategy, the change in fluorescence intensity of Hg^{2+} at 420 nm was used to quantitatively detect the Hg^{2+} concentration. From Figure 4, the fluorescence intensity is enhanced with addition of increasing Hg^{2+} concentration. When the Hg^{2+} concentration was increased incrementally from 1 nM to 100 nM, the intensity increased linearly, with a linear regression equation of Y = 0.573C + 118.937 (R^2 = 0.989), where Y and C represent fluorescence intensity and Hg^{2+} concentration, respectively. The detection limit for Hg^{2+} was calculated to be 0.2 nM (3 δ/k) and the results of from methods previously reported for Hg^{2+} detection were compared, as listed in Table I.

TABLE III: Recovery experiments for Hg^{2+} in tap and river water samples

Sample	Added (nM)	Found (nM)	Recovery (%)
Tap water 1	0	Not found	NA
Tap water 2	10	11.1 ± 0.2	111
Tap water 3	20	19.5 ± 1.6	97.5
Tap water 4	30	28.3 ± 2.2	94.3
River water 1	0	Not found	NA
River water 2	10	11 ± 1.3	110
River water 3	20	21 ± 1.4	105
River water 4	30	34 ± 2.2	113

Selectivity of Hg^{2+} Detection

Selective detection represents a critical performance characteristic to verify this strategy. To selectively distinguish between Hg^{2+} and other interfering metal ions (Cd^{2+}, Cu^{2+}, Fe^{2+}, Mg^{2+}, Ca^{2+}, Mn^{2+}, Na^+), we conducted a series of control experiments and the results are summarized in Figure 5. These represent a good illustration of the selectivity for Hg^{2+} and further

Spectrometers – See the difference

Stability without the bulky cooling

Vertically integrated, Hamamatsu offers not just sensors, but also superior spectrometers. Thanks to our high-quality transmission grating and optical design, our spectrometers provide excellent stability and better absorption readings, at lower cost, so you can accurately control pharmaceutical and semiconductor processes.

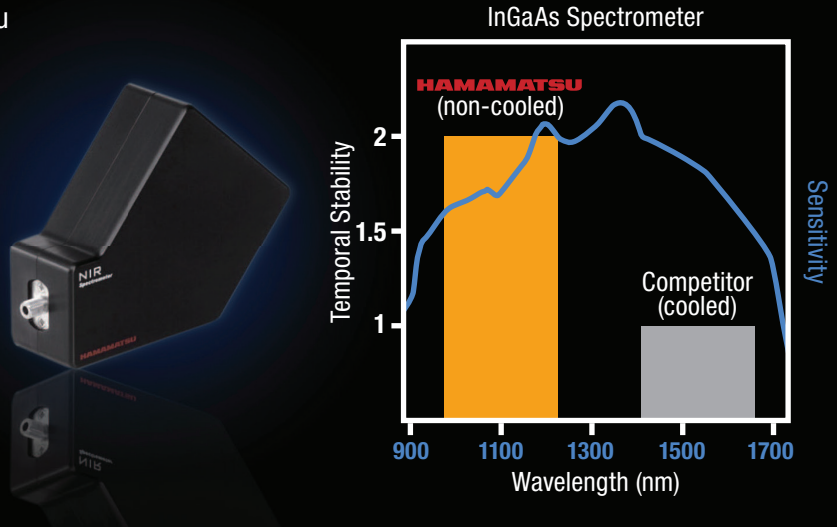

HAMAMATSU
PHOTON IS OUR BUSINESS

For more info visit www.hamamatsu.com or email us at photonics@hamamatsu.com

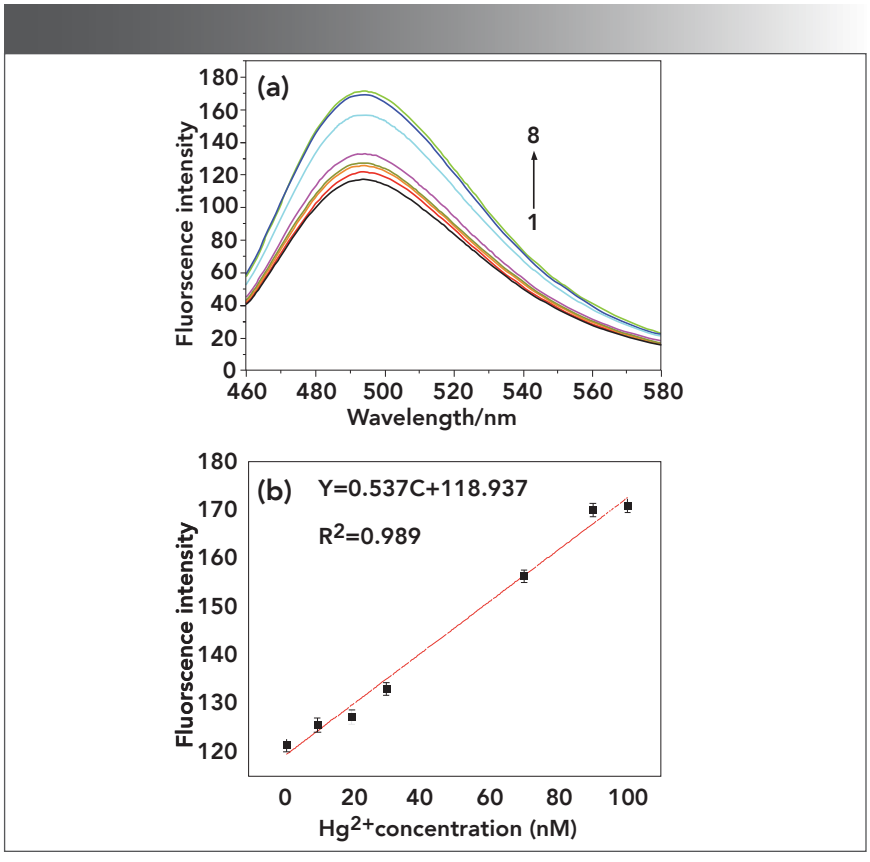

FIGURE 4: (a): The fluorescence intensity variation for the assay of Hg^{2+} at different concentrations (0 nM, 1 nM, 10 nM, 20 nM, 30 nM, 70 nM, 90 nM, and 100 nM from 1 to 8). (b): The resulting calibration curve for fluorescence intensity. The error bar represents the standard deviation of three measurements. The concentrations of P1, P2 were both 100 nm. All of the above solutions were incubated in Tris-HCl buffer at 35 °C for 40 min followed by fluorescence measurement.

demonstrates the feasibility of the present strategy.

Analysis of Real World Samples

To examine the feasibility of the developed fluorescence probe, we analyzed real samples. Six cigarette shreds on the market were measured by this method. As summarized in Table II, the average content of Hg was found to be 36.41 µg/kg in the tested tobacco, which indicates considerable exposure to the smoker if smoking cigarettes for a long time.

In addition, two real samples of tap and river water were also analyzed to assess the feasibility of the strategy. Various concentrations of Hg^{2+} (10, 20, and 30 nM) were added to tap and river water, and the results are shown in Table III. Appreciable recovery was detected, indicating that the method based on G-triplex can be successfully applied to real samples.

Conclusion

A G-triplex-based fluorescence strategy for the detection of Hg^{2+} is reported, that avoids cumbersome labeling procedures and unstable enzymes. At the same time, the probe also demonstrates good sensitivity and selectivity for the detection of Hg^{2+}. The limit of detection was found to be 0.2 nM with a wide linear range from 1 nM to 100 nM (R^2 = 0.989). We believe that this strategy provides support for ion detection based on G-triplex probes.

Acknowledgment

This work was supported by the Basic Research Foundation of Yunnan Province (Nos. 2016CP021, 2017FD236), the Project Foundation of Yunnan Key Laboratory of Tobacco Chemistry (KCFZ-2017-1096) and the Basic Research Foundation of China Tobacco Yunnan Industrial Co., Ltd. (No. 2019XY01, 2018JC04).

References

(1) S. Haque, M. Zeyaullah, G. Nabi, P.S. Srivastava, and A. Ali, *J. Microbiol. Biotech.* **20,** 917–924 (2010).

(2) E.M. Suszcynsky and J.R. Shann, *Environ. Toxicol. Chem.* **14,** *61–67 (1995).*

(3) J.Z. Wang, S. Y. Ren, G.F. Zhu, L. Xi, Y.G. Han, Y. Luo, and L.F. Du, *J. Mol. Struct.* **1052,** 85–92 (2013).

(4) J.-j. Deng, Y. Zhang, J.-w. Hu, Y. Yi, X.-k. Su, X.-f. Huang, and F.-x. Qin, *Hubei Agr. Sci.* **48,** 1171–1175 (2009).

(5) Y. Xu, X. Niu, H. Zhang, L. Xu, S. Zhao, H. Chen, and X. Chen, J. Agr. *Food Chem.* **63,** 1747–1755 (2015).

(6) X. Hu, W. Wang, and Y. Huang, *Talanta* **154,** 409–415 (2016).

(7) Y. Liu, O. Q, H. Li, M. Chen. Z. Zhang, and Q. Chen, *J. Agr. Food Chem.* **66,** 6188–6195 (2018).

(8) W. Feng, X. Xue, and X. Liu, *J. Am. Chem Soc.* **130,** 3244–3245 (2008).

(9) Y. Zhu, Y. Cai, Y. Zhu, L. Zheng, J. Ding, Y. Quan, L. Wang, and B. Qi, *Biosens. Bioelectron.* **69,** 174–178 (2015).

(10) W. Ren, Y. Zhang, W. T. Huang, N. B. Li, and H. Q. Luo, *Biosens. Bioelectron.* **68,** 266–271 (2015).

(11) Y. Lv, L. Yang, X. Mao, M. Lu, J. Zhao, and Y. Yin, Biosens. *Bioelectron.* **85,** 664–668 (2016).

(12) F. Tan, L. Cong, N. M. Saucedo, J. Gao, X. Li, and A. Mulchan-

HARRICK Scientific Products

© 2015 HARRICK SCIENTIFIC PRODUCTS, INC. ALL RIGHTS RESERVED. ILLUSTRATION: © ISTOCK.COM/MAIRGIOLD88

the NEXT GENERATION

ConcentratIR2™

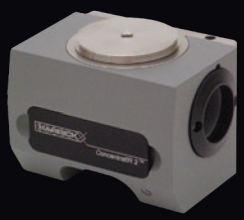

A high-precision multiple reflection ATR accessory measuring only 18.5 cubic inches. Designed for microliter sampling. Compact enough to fit any spectrometer.

Choice of diamond or silicon ATR crystals.
Flow and heated options available.

>>>>>>>> **harrickscI.com/ConcentratIR2**

See us at ACS-#1115

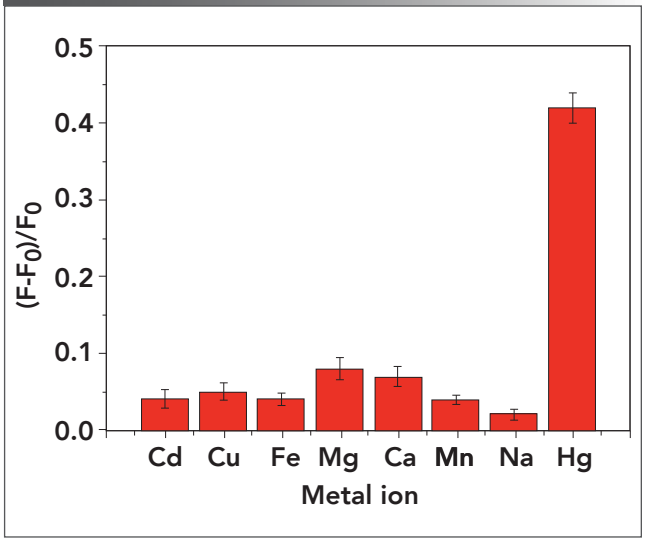

FIGURE 5: Selectivity of the assay for Hg^{2+}. The concentrations of Hg^{2+} sequence and other interfering metal ions are both 100 nM. The error bar represents the standard deviation of three measurements. The concentrations of P1 and P2 were both 100 nM. All the above solutions were incubated in Tris-HCl buffer at 35 °C for 40 min followed by fluorescence measurement.

danib, *J. Hazard. Mater.* **320,** 226–233 (2016).
(13) T. Bao, W. Wen, X. Zhang, Q. Xia, and S. Wang, *Biosens. Bioelectron.* **70,** 318–323 (2015).
(14) A. Shirzadmehr, A. Afkhami, and T. Madrakian, *J. Mol. Liq.* **204,** 227–235 (2015).
(15) W. Yun, W. Xiong, H. Wu, M. Fu, Y. Huang, X. Liu, and L. Yang, *Sensor. Actuat. B-Chem.* **249,** 493–498 (2017).
(16) M.D.L. Cruz-Guzman, A. Aguilar-Aguilar, L. Hernandezad-Ame, A. Bañuelos-Frias, F.J. Medellín-Rodríguez, and G. Palestino, *Nanoscale Res Lett.* **9,** 431 (2014).
(17) H. Dai, Y. Shi, Y. Wang, Y. Sun, J. Hua, P. Ni,and Z. Li, *Biosens. Bioelectron.* **53,** 76–81 (2014).
(18) Q. Fang, Q. Liu, and X. Song, *Luminescence* **30,** 1280–1284 (2016).
(19) S. Wang, X. Li, J. Xie, B. Jiang, R. Yuan, and Y. Xiang, *Sensor. Actuat. B- Chem.* **295,** 730–735 (2018).
(20) B. Adhikarl and A. Banerjee, *Chem. Mater.* **22,** 4364–4371 (2010).
(21) Y. Cai, L. Yan, G. Liu, H. Yuan, and D. Xiao, *Biosens. Bioelectron.* **41,** 875–879 (2013).
(22) X. M. Li, R. R. Zhao, Y. L. Wei, D, Yang, Z.J. Zhou, J.F. Zhang, and Y. Zhou, *Chinese Chem. Lett.* **27,** 813–816 (2016).
(23) G. K. Wang, Q. L. Mi, L. Y. Zhao, J. J. Hu, L. E. Guo, X. J. Zou, B. L. Xiao, and P. Y. Zhou, *Chem.–Asian J.* **9,** 744–748 (2014).
(24) G. Chen, Y. Jin, L. Wang, J. Deng, and C. Zhang, *Chem. Comm.* **47,** 12500–12502 (2011).
(25) P.I. Girginova, A.L. Daniel-da-Silva, C.B. Lopes, P. Figueira, M. Oteroa, V.S. Amaral, E. Pereiraa, and T. Trindadea, *J. Colloid Interf. Sci.* **345,** 234–240 (2010).
(26) T. Yu, T.T. Zhang, W. Zhao, J.J. Xu, and H.Y. Chen, *Talanta* **165,** 570–576 (2017).
(27) A. Han, X. Liu, G.D. Prestwich, and L. Zang, *Sensor. Actuat. B-Chem.* **133,** 274–277 (2014).
(28) S. Wang, B. Lin, L. Chen, N. Li, J. Xu, J. Wang, Y. Yang, Y. Qi, Y. She, X. Shen, X. Xiao, *Anal. Chem.* **90,** 11764–11769 (2018).

Hui Zhao and **Yang Zhao** are with the Key Laboratory of Tobacco Chemistry of Yunnan Province, at the Yunnan Academy of Tobacco Science, in Kunming, in the People's Republic of China. **Xiaoxi Si, Juan Li, Yuanxing Duan, Wei Jiang, Chunbo Liu, Junheng You, Zhenjie Li,** and **Qinpeng Shen** are with Tobacco Yunnan Industrial Co., in Kunming, in the People's Republic of China. Direct correspondence to: ashb345@126.com ●

Influence of Spectral Interferences on the Reliability of Data When Using Analyte Addition Techniques with ICP-OES

Deborah K. Bradshaw

A common misconception among users of inductively coupled plasma optical emission spectrometry (ICP–OES) is that good "spike" recoveries automatically indicate that the original sample results are accurate. Another common misconception is that the use of method of standard additions (MSA) as a means of calibration to correct for interferences will also always produce accurate results. This tutorial shows that neither of these techniques will produce accurate results if the interference is from spectral overlaps that have not been corrected by other appropriate means.

When using any atomic spectroscopy technique for elemental analysis, it is easy to obtain results. Validating that the results are accurate is not always so easy. There are many practices used to help validate that results are accurate. The analysis of calibration verification solutions, reference materials, interference check solutions, samples prepared in duplicate, and analyte addition techniques are some ways used to verify the data is accurate.

There are two types of analyte addition techniques commonly used in atomic spectroscopy. The first is to fortify a portion of a sample with a known additional concentration of analyte, or what is termed to "spike" the sample. There are also times when, instead of using simple calibration standards and reading the analyte concentration from the calibration curve, a technique of method of standard additions (MSA) is used. In this scenario, the calibration curve is achieved in the presence of the sample matrix.

There are three basic types of interferences that can be experienced using this inductively coupled plasma optical emission spectrometry (ICP-OES): 1) physical interferences that have to do with how much sample is transported into the plasma with each solution analyzed; 2) interferences from the sample matrix having an effect on the population of excited atoms and ions within the plasma; and 3) spectral interferences where something other than the analyte of interest produces spectra different from the plasma at the measured wavelength. Acceptable spike recoveries (typically 85% to 115% in a real sample matrix) is a good indicator of physical and matrix interferences. Using MSA can help alleviate both of these problems. What neither of the techniques properly addresses are spectral interferences.

Unfortunately, a common mistake is believing that achieving good "spike" recovery or obtaining results using MSA is a guarantee for reporting accurate results. While obtaining poor spike recoveries is an indicator of results that are probably not accurate, good recoveries do not guarantee compensation

TABLE I: Results for the sample and fortified sample using simple calibration and for sample using MSA calibration

	Simple Calibration			MSA Calibration	
P Wavelength	Sample Conc. (mg/L)	Fortified Sample Conc. (mg/L)	% Spike Recovery	Sample Conc. (mg/L)	% Recovery
P 213.617	21.2	32.2	110	24.9	249
P 214.914	13.5	23.3	98	17.3	173
P 177.427	15.0	24.7	97	14.2	142
P 178.221	10.5	20.1	96	9.7	97

for all types of interferences. While using MSA rather than simple calibration can compensate for some types of interferences, it does not compensate for all interferences for the same reason. Neither of these techniques will indicate or compensate for spectral interferences.

Experimental

To show the problem, the determination of phosphorus in the presence of a high concentration of Cu is used as an example. Two very commonly used phosphorus wavelengths, 213.617 and 214.914, both suffer from overlaps from nearby copper wavelengths, 213.597 (and 213.599) and 214.898, respectively. A third wavelength, 177.434, also will show overlap from Cu 177.427. The P 178.221 wavelength does not suffer from this same problem. In this study, the P 178 wavelength is used as a control.

A method was set up for the determination of P at the four wavelengths cited above. Calibration was achieved using standards prepared in 1% HNO_3 at 5, 10, and 20 mg/L P. All calibration curves had correlation coefficient of 0.998 or 0.999 with linear regression type curve. A solution containing 10 mg/L P and 200 mg/L Cu was analyzed. A portion of this sample was then spiked with an extra 10 mg/L P, and analyzed.

MSA was then used for sample analysis. Four portions of the sample were spiked with the calibration blank and the three standards, 5, 10, and 20 mg/L, to achieve calibration. Correla-

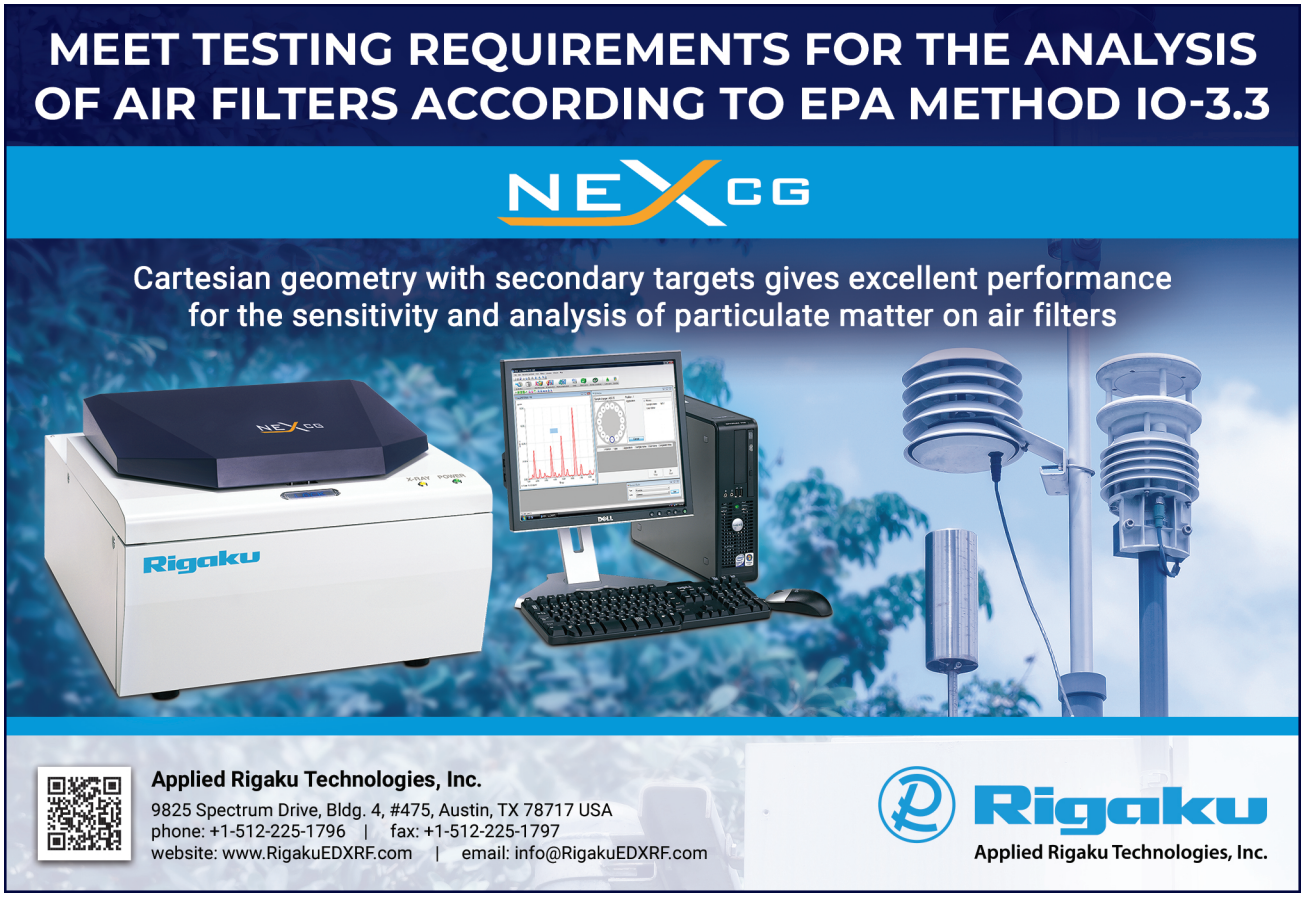

The 2020 Powder Diffraction File™

Diffraction Data You Can Trust

- Standardized Data
- More Coverage
- All Data Sets Evaluated for Quality
- Reviewed, Edited and Corrected Prior to Publication
- Targeted for Material Identification and Characterization

ICDD databases are the only crystallographic databases in the world with quality marks and quality review processes that are ISO certified.

ICDD® International Centre for Diffraction Data

MDI Materials Data™

www.icdd.com | marketing@icdd.com

ICDD, the ICDD logo, PDF and JADE are registered in the U.S. Patent and Trademark Office, Powder Diffraction File, Materials Data, Materials Data-JADE logo, and Denver X-ray Conference logo are trademarks of the JCPDS-International Centre for Diffraction Data. ©2020 JCPDS-International Centre for Diffraction Data. – 1/22/20

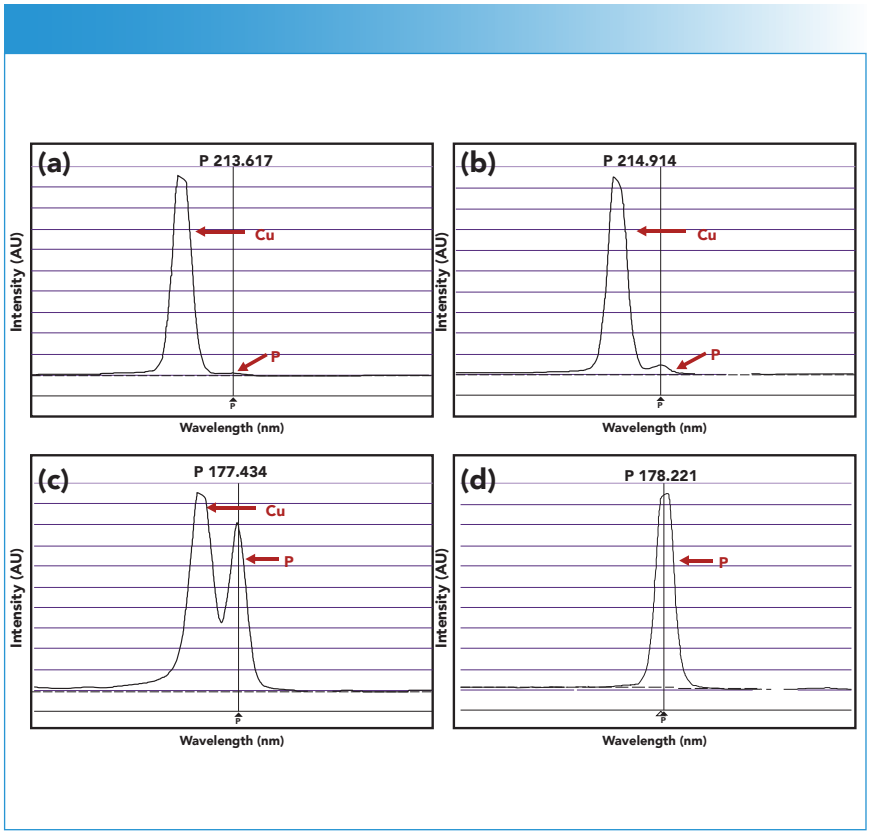

FIGURE 1: Spectra for the sample containing 10 mg/L P and 200 mg/L Cu for the four wavelengths used for this study: (a) P 213.617, (b) 214.914, (c) P 177.434, and (d) P 178.221.

TABLE II: Results for the sample and fortified sample using simple calibration after spectral interferences have been corrected using interelement corrections (IEC)

P Wavelength	Sample Conc. (mg/L)	Fortified Sample Conc. (mg/L)	% Spike Recovery
P 213.617	10.7	21.6	109
P 214.914	10.1	19.9	98
P 177.427	9.95	19.5	96

tion coefficients were again 0.998 and 0.999 for the wavelengths used.

Results

Generally, acceptable "spike recoveries" are considered to be within 15%. When the sample and its spike were analyzed, the recoveries were calculated. The results are shown in Table I. Calculated spike recoveries for all the wavelengths fall within acceptable (15%) criteria. However, the only wavelength to show correct results for the known concentration of 10 mg/L is P 178.221. The results for the sample when using MSA are also shown in this table. When using MSA, that is also the only wavelength to show correct results.

The problem is that Cu provides a spectral interference on all wavelengths except the P 178, contributing to the P concentration, and this has not been compensated. Figure 1 shows examples of the spectral peaks for the unknown at the four wavelengths. Only P 178.221 is free from the spectral overlap.

To correct for the spectral overlaps, interelement correction was applied for the P 213, P 214, and P 177 wavelengths. Simple calibration was once again used and not MSA. Table II shows the corrected data for these wavelengths. Now all wavelengths are in concentration agreement of the known value of 10 mg/L, as well as good recoveries of the fortified portion of the sample.

Conclusion

It is important for the analyst to use all quality control tools when analyzing sample with complex matrices. Good spike recoveries and using MSA alone may end up in the reporting of inaccurate data. Analyte addition techniques are helpful for compensation of physical and matrix issues, but are not sufficient for correcting for spectral interferences. Viewing the spectral data is a good troubleshooting tool to determine if these problems exist and need further correction for the wavelengths chosen.

Deborah Bradshaw is an analytical chemist who has been working the field of atomic spectroscopy for over 35 years. For the past 20 years, she has been working as a consultant in the field of atomic spectroscopy, conducting training classes and giving technical support for atomic absorption (AA) spectroscopy, inductively coupled plasma-optical emission spectroscopy (ICP-OES), and inductively coupled plasma-mass spectrometry (ICP-MS). Direct correspondence to: bradshawdk@cs.com ●

For more information on this topic, please visit our homepage at:
www.spectroscopyonline.com

Portable Raman spectrometer

The STRam, part of B&W Tek's i-Raman series, is designed to unite a high throughput spectrometer, specialized sampling optics, and advanced algorithms in a portable Raman system. According to the company, the spectrometer provides material identification through a variety of barrier layers and packaging previously impenetrable with Raman, including clear or semi-transparent containers, white and red plastics, pill coatings, and more.

B&W Tek,
Newark, DE.
www.bwtek.com

Raman probe

The TR-PROBE Raman probe from Coherent is designed as a plug-and-play upgrade to existing spectrometers with multiple-sample interface accessory options. According to the company, the probe offers a user-friendly option for simultaneously collecting both chemical and structural information from the sample in a range of environments, and is suitable for monitoring reactions and measuring degree of crystallinity.

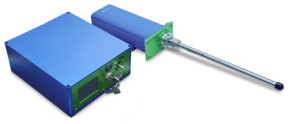

Coherent,
Santa Clara, CA.
https://go.coherent.com/pittcon20

Automated muiti-elemental microscope

Elemission's Coriosity analyzer is designed to scan surfaces using LIBS technology at a speed of 1000 measures per s and down to 50 µm spatial resolution. According to the company, the microscope enables analysts of all experiment levels to observe, measure, and analyze micro or macro samples for lithium batteries, electrical/electronics, forensics, geosciences, element segregation, studying sample homogeneities, and more.

Elemission, Inc.,
Montreal, QC, Canada.
www.elemission.ca

Demountable torch

Glass Expansion's D-Torch is designed as a fully-demountable torch. According to the company, the torch can provide lower running costs, chemical inertness, and configurable injector geometry without compromising usability, performance, or durability, and it is available for many of the most popular ICP models, including Agilent's 5100, 5800, and 5900 ICO-OES models.

Glass Expansion, Pocasset, MA. www.geicp.com/D-Torch

Diamond ATR accessory

Harrick's DiaMaxATR is designed to fit most FT-IR spectrometers. According to the company, the accessory can be used with a variety of sample types, including challenging samples such as extremely hard solids, abrasive powders, and highly corrosive liquids. Optional headed and flow cells are available, along with a force sensor with digital read-out.

Harrick Scientific Products, Inc.,
Pleasantville, NY.
www.harrricksci.com

Raman analyzer

The Raman Rxn2 analyzer from Kaiser Optical Systems is designed to provide high-resolution, research-grade Raman spectra on a portable platform for process development monitoring and control. According to the company, a single analyzer can collect Raman data from four channels, addressable by fiber-optic probes, and is capable of direct in situ measurements with the need for custom sampling devices.

Kaiser Optical Systems, Inc., Ann Arbor, MI. www.kosi.com

MEMS-based NIR spectral sensor

Ocean Insight's NanoQuest spectral sensor is designed for qualification and quantification of materials from 1350 to 2500 nm (7400 to 400 cm^{-1}). According to the company, the micro-electro-mechanical systems (MEMS)-based sensor includes an optical fiber and operating software, and can be coupled to its various light sources and accessories to configure systems for absorbance and transmission or reflectance measurements.

Ocean Insight, Largo, FL. www.oceanInsight.com

Raman analyzer

The Virsa Raman analyzer from Renishaw is designed for reliable and detailed remote analysis. According to the company, the analyzer enables the expansion of applications of Raman spectroscopy to a new range of samples and environments beyond the confines of a laboratory Raman instrument, and the system includes a spectrometer with one or two internal lasers.

Renishaw, West Dundee, IL.
www.renishaw.com

Photo Credit: adobestock.com/selensergen

PITTCON PRODUCT SHOWCASE

UV-vis spectrophotometers

The UV-i group of UV-vis spectrophotometers from Shimadzu are designed to provide improved quality control productivity, data analysis and management, and operating efficiency. According to the company, the series includes six models, all of which include an automatic pass/fail determination and are equipped standard with a spectral evaluation function in the software that automatically determines whether data satisfies the specified criteria.

Shimadzu Scientific Instruments, Columbia, MD. www.ssi.shimadzu.com

Raman spectrometer

A Raman spectrometer from Wasatch photonics is designed with an integrated 250 mW multimode laser with fiber-coupled output and power control via software. According to the company, units are available in 785 nm and 830 nm models, covering the fingerprint region with ~6 cm^{-1} resolution (uncooled, TEC-regulated, or cooled detector).

Wasatch Photonics, Durham, NC. www.wasatchphotonics.com

Microparticle analysis tool

ParticleScout from WITec is designed as an analysis tool for the alpha300 Raman microscope series that surveys, categorizes, analyzes, quantifies, and identifies particles over large sample areas. According to the company, automated routines sort particles and acquire their Raman spectra, generating a report that provides a detailed overview of the sample.

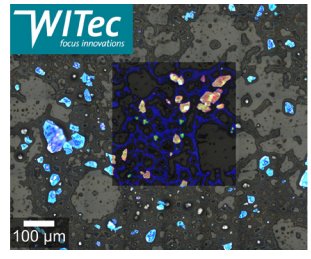

WITec GmbH, Ulm, Germany. www.witec.de

In-situ reaction monitoring analyzer

ABB's MB-Rx in-situ reaction monitoring analyzer is designed to provide plug-and-play analyses for research laboratories and pilot plants. According to the company, the analyzer offers chemists direct access to real-time experiment data via an insertion probe and an intuitive software interface.

ABB Measurements & Analytics, Quebec, Canada. www.abb.com/analytical

Electron backscatter diffraction camera

The Velocity EBSD camera from EDAX is designed for high-speed electron backscatter diffraction mapping. According to the company, the camera combines indexing speeds greater than 3000 indexed points per s, with indexing success rates of 99% or better, and image resolution that provides orientation precision values of less than 0.1°.

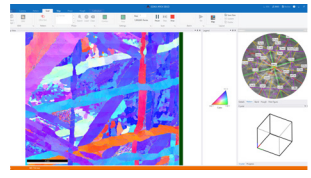

EDAX, Inc., Mahwah, NJ. www.edax.com

Spectrofluorometer

The FS5 integrated fluorescence spectrometer from Edinburgh Instruments is designed for measuring steady state fluorescence, fluorescence lifetime, and phosphorescence lifetime through UV-vis-NIR spectral ranges. According to the company, the spectrofluorometer provides sensitivity by single-photon counting.

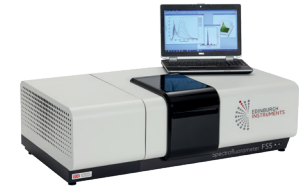

Edinburgh Instruments, Livingston, UK. www.edinst.com

Grating-based spectrometer

The C14384MA-01 compact grating-based spectrometer from Hamamatsu is designed for measuring sugar content in fruit. According to the company, the spectrometer has a spectral response range of 640 to 1050 nm, and a resolution of 17 to 20 nm (depending on the wavelength), and is suitable for pocket (consumer) spectrometers and handheld instruments.

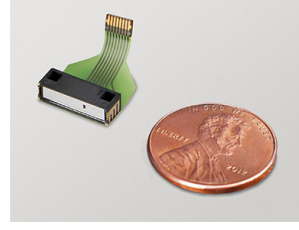

Hamamatsu Corporation, Bridgewater, NJ. www.hamamatsu.com

Diffraction database

The PDF-4+ 2019 database from ICDD is designed for phase identification and quantitative analysis. According to the company, the database includes 412,083 entries with digital patterns for use in total pattern analysis; 312,395 entries with I/Ic values for quantitative analysis by reference intensity ratio; and 311,225 entries with access to atomic coordinates sets for quantitative analysis by the Rietveld method.

International Centre for Diffraction Data, Newtown Square, PA. www.icdd.com

ULF Raman filters

BragGrate Raman filters from OptiGrate are designed to enable access to Stokes and anti-Stokes Raman bands in the ultralow terahertz frequency range down to 5 cm^{-1}. According to the company, laser line cleaning and light rejection notch filters are provided, and the filter production line is extended to cover many standard and custom laser wavelengths from 405 nm to 1550 nm.
OptiGrate, Oviedo, FL. www.optigrate.com

All-purpose diamond ATR accessory

The IRIS diamond attenuated total reflectance accessory from PIKE Technologies is designed for infrared sampling of powders, gels, liquids, solids, and more. According to the company, the accessory is suitable for research, QA/QC, and sample identification.
PIKE Technologies, Madison, WI. www.piketech.com

Microwave digestion

Milestone's UltraWAVE microwave digestion system uses the company's single reaction chamber technology for metals digestions. According to the company, the system uses a single pressurized vessel for all samples, allowing for simultaneous digestion of up to 22 samples. The system reportedly can accommodate a maximum temperature of 300 °C and pressure of 199 bar.
Milestone, Inc., Shelton, CT; www.milestonesci.com/ultrawave

UV-vis cuvettes and cells

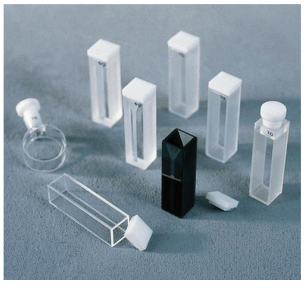

UV-vis-NIR cuvettes and cells, made from UV quartz, IR quartz, and glass materials, are available from REFLEX Analytical. According to the company, the accessories are available with fitted covers, plugs, screw caps, anaerobic screw caps, and graded seals.
REFLEX Analytical Corp., Ridgewood, NJ. www.reflexusa.com.

X-ray diffraction systems

Rigaku's sixth-generation Mini- Flex X-ray diffraction system is designed as a multipurpose analytical instrument that can determine phase identification and quantification, percent crystallinity, crystallite size and strain, lattice parameter refinement, Rietveld refinement, and molecular structure. According to the company, the system includes a HyPix-400 MF 2D hybrid pixel array detector, an available 600-W X-ray source, and an eight position automatic sample changer.
Rigaku Corporation, Tokyo, Japan. www.rigaku.com/en/products/xrd/miniflex

Automated electric fusion fluxer

The Katanax X-300 fluxer from Spex SamplePrep is designed to produce fused beads for X-ray fluorescence or inductively coupled plasma solutions for analysis. According to the company, the benefits of electric fluxers versus gas fluxers include safety, temperature control, low power consumption, and simple installation.
Spex SamplePrep, Metuchen, NJ. www.spexsampleprep.com/x300-fluxer

X-ray generator

The flex-Beam X-ray generator from XOS is designed as a polycapillary optic to provide a bright X-ray beam for advanced material analysis. According to the company, the generator enables the exchange of X-ray sources field alignment and consistent performance, and is available in several standard focused or collimated beam configurations and performance packages.
XOS, East Greenbush, NY. www.xos.com

Microwave digestion system

The CEM MARS 6 microwave digestion system is designed to digest challenging samples for trace metals analysis. According to the company, the system has hundreds of preprogrammed methods and vessel options for high throughput and difficult samples.
CEM Corporation, Matthews, NC. www.cem.com/mars6.

PITTCON PRODUCT SHOWCASE

Palm spectrometer

BaySpec's Breeze palm spectrometer was originally designed for 400 to 1700 nm with a one-button operation. According to the company, the spectrometer has now been upgraded to the 2500 nm range, enabling the device to operate at 1300 nm to 2500 nm.

BaySpec, Inc.,
San Jose, CA.
www.bayspec.com

Intensified image adapters

Photonis' Cricket intensified image adapter is designed to enable a camera to capture images across a broad spectral range, from 200 to 900 nm. According to the company, the image adapter is compatible with most charge-coupled device (CCD), complementary metal-oxide semiconductor (CMOS), EMCCD, and sCMOS cameras, and it is suitable for applications such as physics, fluorescence lifetime imaging microscopy (FLIM), plasma research, and corona detection.

Photonis Scientific,
Sturbridge, MA.
www.photonis.com

ICP-MS mass spectrometer

Advion's SOLATION spectrometer for inductively coupled plasma–mass spectrometry (ICP-MS) is designed for multielement analysis. According to the company, the spectrometer provides high sensitivity measurement of trace elements from a range of matrices, including complex samples such as urine, serum, plasma, whole blood and tissue, water, soil, food, beverage, and agricultural samples.

Advion, Inc.,
Ithaca, NY.
www.advion.com

Wire-grid polarizer

Moxtek polarizers are designed for broadband UV-vis-IR wavelengths. According to the company, the polarizers have uniform performance over wide cone angles, are made from heat-tolerant inorganic materials, and can be exposed to temperatures up to 300 °C.

Moxtek, Inc.,
Orem, UT.
moxtek.com/optics-products

SHORT COURSES

March 2020

1 An Introduction to Scanning Electron Microscopy (SEM) and Associated Energy Dispersive X-ray Spectroscopy (EDS)
Chicago, IL
www.pittcon.org/short-courses/short-courses-preview

1 Modern Portable Analytical Spectroscopy
Chicago, IL
www.pittcon.org/short-courses/short-courses-preview

1 Bioanalytical Detection using Mass Spectrometry
Chicago, IL
www.pittcon.org/short-courses/short-courses-preview

1 Advances in Raman Spectrometry
Chicago, IL
www.pittcon.org/short-courses/short-courses-preview

2 Elemental Analysis via Laser Induced Breakdown Spectroscopy and X-ray Fluorescence
Chicago, IL
www.pittcon.org/short-courses/short-courses-preview

2 Primer on XRF Spectrometry: Instrumentation
Chicago, IL
www.pittcon.org/short-courses/short-courses-preview

2 Frontiers in Vibrational Spectroscopy of Surfaces and Interfaces: Evolution, Revolution or Back to the Future
Chicago, IL
www.pittcon.org/short-courses/short-courses-preview

3 Introduction to Gas Chromatography/Infrared Spectroscopy Mass Spectrometry
Chicago, IL
www.pittcon.org/short-courses/short-courses-preview

3 Essentials of LC-MS
Chicago, IL
www.pittcon.org/short-courses/short-courses-preview

3 Introduction to Mass Spectrometry including Biomolecule Applications
Chicago, IL
www.pittcon.org/short-courses/short-courses-preview

3 Infrared (IR), Fluorescence and Luminescence Spectroscopy
Chicago, IL
www.pittcon.org/short-courses/short-courses-preview

5 Introduction to ICP-MS
Chicago, IL
www.pittcon.org/short-courses/short-courses-preview

5 GC/MS Fundamentals for Operators
Chicago, IL
www.pittcon.org/short-courses/short-courses-preview

Visit us at Pittcon to find out why "The Way We've Always Done It" should be...

- Costly
- Inconvenient
- High Pressure Gas Safety Concerns
- Operator Handling Required
- Unreliable Supply

"The Way We Do It Now"

Parker H_2, N_2 & Zero Air Gas Generators

H2PEMPD

NItroFlow Lab

Spectra 15

- Fast Payback
- Small Footprints & Under Bench Designs
- Low Cost of Ownership & Easy Maintenance
- Generate Gases On-site for Total Control and Proven Safety

Purge Gas Generators for FT-IR • TOC Gas Generators for TOC Analyzers • Instrument Air Systems for NMR
Hydrogen Generators for Fuel & Carrier Gas • Zero Air Generators for GC-FID • Nitrogen Generators for LCMS

PITTCON® 2020
CONFERENCE & EXPO

Visit us at Booth #2311

parker.com/igfg
1.800.343.4048

Parker

CALENDAR OF EVENTS

March 2020

1–5 Pittcon Conference & Expo 2020
Chicago, IL
https://pittcon.org

22–26 ACS Spring National Meeting & Exposition 2020
Philadelphia, PA
https://www.acs.org/content/acs/en/meetings.html

27–29 ACS Central Regional Meeting (CERM) 2020
Columbus, OH
https://www.acs.org/content/acs/en/meetings/regional/central.html

29–April 2 53rd Annual International Meeting of the ESR Spectroscopy Group of the Royal Society of Chemistry
Manchester, United Kingdom
https://www.esr-group.org/conferences/2020-conference-manchester

29–April 2 MSACL 2020
Palm Springs, CA
https://msacl.org/index.php?header=MSACL_2020_US

31–April 3 Analytica
Munich, Germany
https://www.analytica.de/index-2.html

April 2020

6-9 Spring SciX 2020
Liverpool, United Kingdom
https://springscix.org

13-17 Materials Research Society Spring Meeting 2020
Phoenix, AZ
https://www.mrs.org/spring2020

26–30 SPIE Defense + Commercial Sensing Expo 2020
Los Angeles, CA
http://spie.org/x6776.xml

28–30 Interphex 2020
New York, NY
https://www.interphex.com

May 2020

3–7 SETAC Europe 30th Annual Meeting
Dublin, Ireland
http://www.setac.org/

6–8 AKL '20: International Laser Technology Congress
Aachen, Germany
http://www.lasercongress.org/en/congress/structure/

10–15 CLEO 2020
San Jose, CA
https://www.cleoconference.org/home

26–30 Nontarget Analysis for Environmental Risk Assessment
Durhman, NC
https://www.setac.org/

31–June 4 ASMS 2020
Houston, TX
https://www.asms.org/conferences/annual-conference/annual-conference-homepage

June 2020

12 ACS Middle Atlantic Regional Meeting (MARM) 2020
New York, NY
https://www.acs.org/content/acs/en/meetings/regional/middle-atlantic.html

28-July 1 ACS Northwest Regional Meeting (NORM) 2020
Bellingham, WA
https://www.acs.org/content/acs/en/meetings/regional/northwest.html

July 2020

25–31 International Diffuse Reflectance Conference (IDRC)
Chambersburg, PA
https://cnirs.org/content.aspx?page_id=0&club_id=409746

26–29 North American Chemical Residue Workshop 2020
Fort Lauderdale, FL
https://nacrw.org/site

26–30 AACC 2020 Annual Meeting & Clinical Lab Expo
Chicago, IL
https://www.aacc.org

August 2020

3–7 National Environmental Monitoring Conference (NEMC)
Minneapolis, MN
http://www.nemc.us/

6–10 Denver X-ray Conference 2020
Rockville, MD
http://www.dxcicdd.com

18–20 ACS Northeast Regional Meeting (NERM) 2020
Rochester, NY
https://www.acs.org/content/acs/en/meetings/regional/northeast.html

23–27 SPIE Optics + Photonics
San Diego, CA
https://spie.org/conferences-and-exhibitions/optics-and-photonics

September 2020

6–10 11th SETAC 8th World Congress
Singapore
https://www.setac.org/

8–10 11th CIRP Conference on Photonic Technologies (LANE 2020)
Fürth, Germany
https://www.lane-conference.org/

30–October 2 SpectroExpo
Amsterdam, The Netherlands
http://www.spectroexpo.com

October 2020

11–16 SciX 2020 Conference
Reno-Sparks, NV
https://facss.org

12–15 American Council of Independent Laboratories
Long Beach, CA
http://www.acil.org

13–14 Gulf Coast Conference
Galveston, TX
https://www.gulfcoastconference.com

25–28 2020 AAPS PharmSci 360
New Orleans, LA
https://www.showsbee.com/fairs/AAPS-Annual-Meeting.html

November 2020

15–19 Society of Environmental Toxicology and Chemistry (SETAC) North America 41st Annual Meeting
Fort Worth, TX
http://www.setac.org/

16–18 Eastern Analytical Symposium and Exhibition
Princeton, NJ
http://easinc.org/wordpress/?p=2085

29–December 4 Materials Research Society Fall Meeting and Exhibit
Boston, MA
https://www.mrs.org/meetings-events/fall-meetings-exhibits

Photo Credit: adobestock.com/selensergen

> "COMING TOGETHER is a **BEGINNING**; **KEEPING** TOGETHER is **PROGRESS**; **WORKING** TOGETHER is **SUCCESS**"

CANNABIS SCIENCE CONFERENCE

- 100+ SPEAKERS
- EXCITING EXHIBITS
- CANNA BOOT CAMP
- PANEL DISCUSSIONS
- NETWORKING MIXERS
- CANNAQUARIUM EXPERIENCE

and much more!

BALTIMORE, MD

APRIL 6-8, 2020

BALTIMORE CONVENTION CENTER

THE WORLD'S LARGEST CANNABIS SCIENCE EVENT!

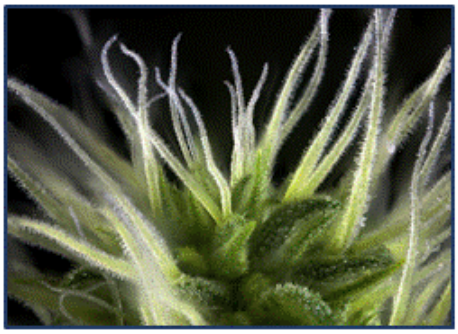

ANALYTICAL, MEDICAL, CULTIVATION & HEMP TRACKS!

Come grow with us!

"Cannabis Science Conference has proven to be among the most influential educational events in the movement. They assemble the brightest researchers in the world to teach patients & medical professionals sitting side-by-side, learning together. Cannabis Science Conference is helping to galvanize rigorous scientific data supporting cannabis as a medicine."

-**Sue Sisley, MD,** *President & Principal Investigator, Scottsdale Research Institute*

SAVE THE DATE *for our* **West Coast Event!**

PORTLAND, OREGON

8/31-9/2, 2020

OREGON CONVENTION CENTER

CannabisScienceConference.com

@CannabisScienceConference

@CannabisScienceConference

Sponsorship and exhibition opportunities are available.
Please contact Andrea at Andrea@CannabisScienceConference.com for more information.

• Continued from Page 40

(3) B. Busser, S. Moncayo, J.-L. Coll, L. Sancey, and V. Motto-Ros, *Coord. Chem. Rev.* **358**, 70–79 (2018).
(4) R. Gaudiuso et al., *Spectrochim. Acta Part B* **152**, 123–148 (2019).
(5) J.O. Cáceres, F. Pelascini, V. Motto-Ros, S. Moncayo, F. Trichard, G. Panczer, A. Marín-Roldán, J.A. Cruz, I. Coronado, and J. Martín-Chivelet, *Sci. Rep.* **7**, 5080 (2017).
(6) L. Sancey, V. Motto-Ros, B. Busser, S. Kotb, J.M. Benoit, A. Piednoir, F. Lux, O. Tillement, G. Panczer, and J. Yu, *Sci. Rep.* **4**, 6065 (2014).
(7) G. Alombert-Goget, F. Trichard, H. Li, C. Pezzani, M. Silvestre, N.s Barthalay, V. Motto-Ros, and K. Lebbou, *Optical Materials*, **65**, 28–32 (2016).
(8) F. Trichard, L. Sorbier, S. Moncayo, Y. Blouët, C.-P. Lienemann, and V. Motto-Ros, *Spectrochim. Act. B* **133**, 45–51 (2017).
(9) P. Veber et al., *CrystEngComm* **21**, 3844–3853 (2019).
(10) K. Janssens, W. de Nolf, G. van der Snickt, L. Vincze, B. Vekemans, R. Terzano, and F.E. Brenker, *Trends Anal. Chem.* **29**, 464–478 (2010).
(11) K.L. Moore, E. Lombi, F.-J. Zhao, and C.R.M. Grovenor, *Anal. Bioanal. Chem.* **402**, 3263–3273 (2012).
(12) D. Pozebon, G.L. Scheffler, V.L. Dressler, and M.A.G. Nunes, *J. Anal. At. Spectrom.* **29**, 2204–2228 (2014).
(13) M. Reich, R. Large, and P.A. Deditius, *Ore Geol. Rev.* **81**, 1215–1217 (2017).
(14) C. Fabre et al., *J. Anal. At. Spectrom.* **33**, 1345–1353 (2018).
(15) F. Trichard, F. Gaulier, J. Barbier, D. Espinat, B. Guichard, C.-P. Lienemann, L. Sorbier, P. Levitz, and V. Motto-Ros, *J. Catal.* **363**, 183–190 (2018).
(16) B. Busser et al., *Mod. Pathol.* **152**, 1–7 (2017).
(17) S. Kunjachan et al., *Nano Lett.* **15**, 7488 (2015).
(18) X. Le Guével et al., *Nanoscale* **10**, 18657–18664 (2018).
(19) V. Motto-Ros, E. Negre, P. Pelascini, G. Panczer, and J. Yu, *Spectrochim. Act. B* **92**, 60–69 (2014).
(20) V. Motto-Ros, S. Moncayo, F. Trichard, and F. Pelascini, *Spectrochim. Act. B* **155**, 127-133 (2019).
(21) J. Ian Fairchild et al., *Earth-Sci. Rev.* **75**, 105–153 (2016).
(22) D. Genty, A. Baker, and B. Vokal, *Chem. Geol.* **176**, 191–212 (2001).
(23) G. Munteanu, E. Kammenthaler, J. Mantenant, and C. Rico, *ArcheoSciences* **40**, 163–180 (2016).
(24) V. Motto-Ros, L. Sancey, Q. L. Ma, F. Lux, X. S. Bai, X. C. Wang, J. Yu, G. Panczer, and O. Tillement, *App. Phys. Lett.* **101**, 223702 (2012).
(25) Y. Gimenez et al., *Nature Sci. Rep.* **6,** 29936 (2016).
(26) L. Sancey et al., *ACS Nano* **9**, 2477 (2015).
(27) S. Moncayo, F. Trichard, B. Busser, M. Sabatier-Vincent, F. Pelascini, N. Pinel, I. Templier, J. Charles, L. Sancey, and V. Motto-Ros, *Spectrochim. Act. B* **133**, 40–44 (2017).
(28) S. Moncayo, L. Duponchel, N. Mousavipak, G. Panczer, F. Trichard, B. Bousquet, F. Pelascini, and V. Motto-Ros, *J. Anal. Atom. Spectrom.* **33**, 210–220 (2018).
(29) K. Rifai, F. Doucet, L. Özcan, and F. Vidal, *Spectrochim. Act. B* **150**, 43–48 (2018)

V. Motto-Ros, V. Gardette, and **M. Leprince** are with the Institut Lumière Matière at the Université de Lyon, in Villeurbanne, France. **Leprince, L. Sancey,** and **B. Busser** are with the Institute for Advanced Biosciences at the Univ. Grenoble Alpes, in Grenoble, France. **B. Busser** is also with Grenoble University Hospital, in Grenoble, France. **D. Genty** is with the Université de Bordeaux, in Pessac, France. **S. Roux** is with the Université de Franche-Comté, in Besançon, France. **F. Pelascini** is with Cetim Grand Est, in Illkirch-Graffenstaden, France. Direct correspondence to: vincent.motto-ros@univ-lyon1.fr •

AD INDEX

ADVERTISER	PG#
ABB	C4
Amptek	3
Analytik Jena	23
Avantes	35
B&W	68
Cannabis Science Conference	63
CEM Corporation	CVTIP
Coherent, Inc.	46
EDAX Inc.	37
Edinburgh	69
Elemission	39
Glass Expansion	42,43,70,71
Hamamatsu	49
Harrick Scientific Products, Inc.	51,72
Inorganic Ventures	45
International Centre for Diffraction Data	55
Kaiser	19
LightMachinery, Inc.	29
Metrohm USA	25
Milestone Inc.	7
Millipore	9
Ocean Insight	C2,73
OptiGrate Corporation	C3
Parker	61
PIKE Technologies, Inc.	5,66,78
REFLEX Analytical Corporation	52
Renishaw, Inc.	8,74,75
Rigaku GMG	54
Shimadzu Scientific Instruments	11
Specac	17
Spex SamplePrep	15
Starna Cells Inc.	21
Wasatch Photonics, Inc.	76
Witec GmbH	27,77
XOS	47

Photo Credit: adobestock.com/selensergen

Supplement to
Spectroscopy®
SOLUTIONS FOR MATERIALS ANALYSIS
FEBRUARY 2020
WWW.SPECTROSCOPYONLINE.COM

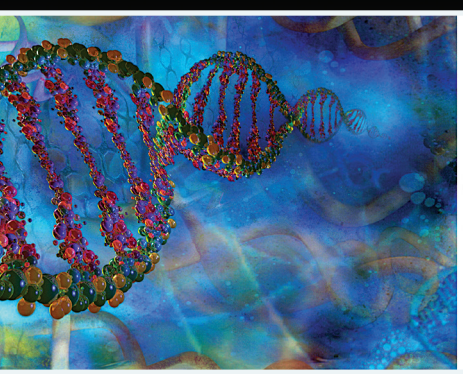

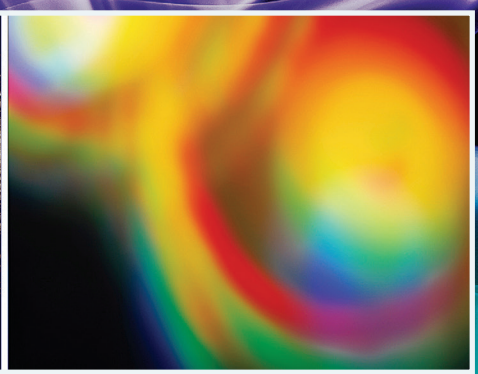

THE APPLICATION NOTEBOOK

PIKE TECHNOLOGIES

SPECTROSCOPIC CREATIVITY

Accessories for UV/Vis, Near-IR and Mid-IR measurements.

PIKE Technologies is a primary source for spectroscopy accessories worldwide. Products include attenuated total reflection (ATR), diffuse and specular reflection, integrating spheres, polarizers, transmission sampling accessories and more.

LONG-PATH GAS CELL

High-performance gas cells for analysis of air contaminants, pure gases and gas mixtures in the ppm to ppb range. Pathlengths range from 1 to 30 meters. Temperature-controlled configurations, heating up to 200 °C are available.

XY AUTOSAMPLER

Speed up productivity with this automated NIR and MIR diffuse reflection/transmission accessory. Microtiter plates are customizable up to 96 wells. Visit our website or contact us for details.

THE IRIS DIAMOND ATR

With IRIS, you can expect high-quality spectra covering a wide range of samples, including powders, gels, liquids, solids. Ideal for research, QA/QC and sample identification.

608.274.2721 | info@piketech.com | www.piketech.com | 6125 Cottonwood Dr. Madison, WI 53719, USA

THE APPLICATION NOTEBOOK

Atomic Spectroscopy

68 QTRam® for Content Uniformity Analysis of Low-Dose Pharmaceutical Tablets

Jun Zhao, PhD, Christopher Kautz*, and Andrés Román, PhD†, *B&W Tek, LLC, †Rutgers, the State University of New Jersey*

70 A Robust, High Performance, Fully Demountable ICP Torch

Ryan Brennan, Justin Masone, Terrance Hettipathirana and Glyn Russell, Glass Expansion, Inc.

Molecular Spectroscopy

69 Measuring the Carrier Lifetime of Perovskites Using Time-Resolved Photoluminescence

Edinburgh Instruments

72 A Corrosive Liquid Investigated by Diamond ATR Infrared Spectroscopy

Susan Berets and Bisirat Araya, Harrick Scientific Products, Inc.

73 Identifying Textiles with Extended-Range NIR Spectroscopy

Anne-Marie Dowgiallo, PhD, Ocean Insight

76 Bioreactor Fermentation Monitoring with Raman Spectroscopy

Dieter Bingemann, David Creasey, Wasatch Photonics Inc.

77 Gallium Nitride Quality and Stress Field Characterization with 3D Confocal Raman Imaging

WITec GmbH

78 Tracking Photocuring via ATR-FT-IR with Illumination through the ATR Element

Marshall J. Allen and Zachariah A. Page, Department of Chemistry, The University of Texas at Austin

B&W TEK
A Metrohm Group Company

QTRam® for Content Uniformity Analysis of Low-Dose Pharmaceutical Tablets

Jun Zhao, PhD*, Christopher Kautz*, and Andrés Román, PhD†, *B&W Tek, LLC, †Rutgers, the State University of New Jersey

Compressed tablet is the most common form of orally administered drug. The *United States Pharmacopeia (USP)* chapter <*905*> requires that dosage uniformity of such products containing less than 25 mg or less than 25% active pharmaceutical ingredients (API) by weight must be analyzed for content uniformity, which is based on the assay of each API in a number of individual dosage units. Traditional wet chemistry methods, such as titration or high performance liquid chromatography (HPLC), require complete dissolution of the tablets in suitable solvents, which destroy the samples, create waste, and can be labor intensive and time consuming. Vibrational spectroscopic techniques, notably near-infrared (NIR) absorption and Raman scattering, are nondestructive, fast, and require no consumables. Transmission Raman spectroscopy (TRS) is particularly promising, due to its ability to sample a large portion of the sample's volume.

QTRam is a compact transmission Raman analyzer designed specifically for content uniformity analysis of pharmaceuticals in solid dosage forms. In this note, we use a model drug, acetaminophen, to demonstrate the capability of QTRam to quantify low concentrations of API in compressed tablets.

Data Collection

QTRam is used to measure transmission Raman spectra of the uncoated tablets. The interrogated sample area is 4 mm in diameter as set by the excitation and collection apertures. BWAnalyst®, the 21 CFR pt 11 compliant software for QTRam, is used to collect all spectra. Each spectrum is an average of 10 scans, and each scan takes 3 s. Two or three spectra were acquired from each tablet sample.

Experimental and Results

Acetaminophen, also known as paracetamol and APAP, is chosen as a model API in this study, due to its availability and low toxicity. We target a hypothetical formulation of 1.5 mg API in a 300 mg tablet, for example, 0.5% APAP w/w. Nine blends were prepared, consisting of APAP, mannitol, silicified microcrystalline cellulose (MCC), croscarmellose, and magnesium stearate (MgSt). The blended powders are compressed into round tablets of 10 mm diameter and 3.0 mm thickness, each weighing roughly 300 mg.

Chemometrics

For quantification, partial least squares (PLS) regression models are built using B&W Tek's chemometric software BWIQ®. Assuming the API is distributed uniformly in the scale of the interrogated volume, we use the blend concentration as the reference for the individual tablets. Eight tablets are used from each blend, which should reduce the calibration error caused by unideal uniformity by way of averaging.

Conclusion

The QTRam is capable of fast and accurate analysis for content uniformity of low-dose pharmaceutical tablets.

B&W Tek
19 Shea Way, Newark, DE 19713
tel. (302) 368-7824
Website: www.bwtek.com

EDINBURGH INSTRUMENTS

Measuring the Carrier Lifetime of Perovskites Using Time-Resolved Photoluminescence

Edinburgh Instruments

The effect of annealing time on the charge carrier lifetime of three MAPI perovskite films is investigated using time-resolved photoluminescence spectroscopy.

Halide perovskite photovoltaic cells have attracted tremendous attention in recent years, due to the rapid rise of their solar cell efficiencies, which have increased from 9% in 2012 to over 25% by 2019, and are now competitive with crystalline silicon (1,2). In this application note, time-resolved photoluminescence spectroscopy is shown to be a powerful tool for investigating and optimizing the behavior of perovskites through the measurement of charge carrier lifetimes.

Experimental

Methyl ammonium lead iodide (MAPI) perovskite films were deposited on quartz discs, using the methylamine/acetonitrile route (3), followed by annealing at 100 °C. Photoluminescence lifetimes were measured using an Edinburgh Instruments FLS1000 photoluminescence spectrometer equipped with an EPL-405 pulsed diode laser, a PMT-900 detector, and time-correlated single photon counting (TCSPC) counting electronics.

Results

During the fabrication of perovskite solar cells, the perovskite layer is first deposited by spin-coating, and the layer is then annealed at a high temperature to complete the film formation process. The temperature and duration of this annealing step can have a dramatic impact on the microstructure of the perovskite layer and on the efficiency of the photovoltaic cell.

The photoluminescence decays of three MAPI films fabricated with different annealing times were measured using TCSPC and fit with stretched exponential decays using the Fluoracle® software of the FLS1000 (Figure 1). As the annealing time is increased from 15 to 60 min, the mean lifetime of the photoluminescence decay was found to increase from 28 to 44 ns.

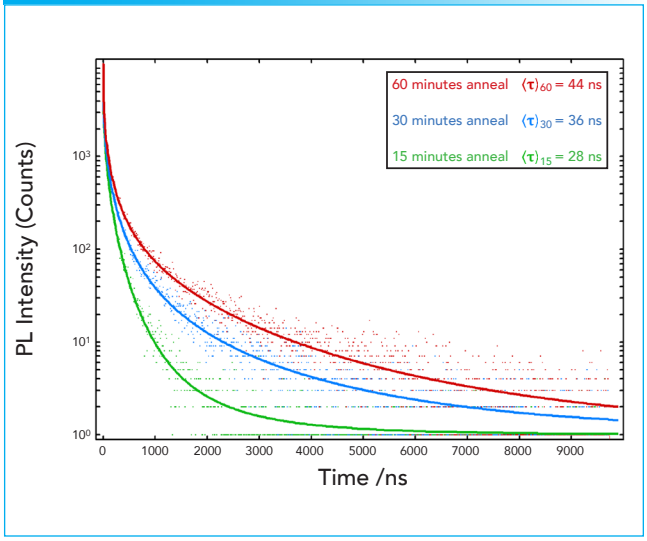

Figure 1: Photoluminescence decays of three MAPI perovskite thin films that were annealed for 15, 30, and 60 min. Excitation source = EPL-405 pulsed diode laser, Rep Rate = 100 kHz, λem = 780 nm, Δλem = 10 nm.

Conclusion

The mean lifetime of the MAPI films was measured using TCSPC with the FLS1000 photoluminescence spectrometer and was found to increase with annealing time, indicating that longer annealing extends the average charge carrier lifetime which may improve solar cell efficiency.

References

1 NREL Efficiency Chart, *Rev.* 11-05-2019

2 M. A. Green, Y. Hishikawa, E. D. Dunlop, D. H. Levi, J. Hohl-Ebinger, and A. W. Y. Ho-Baillie, *Prog. Photovolt. Res. Appl.* **26,** 3–12 (2018)

3 N. K. Noel, S. N. Habisreutinger, B. Wenger, M. T. Klug, M. T. Hörantner, M. B. Johnston, R. J. Nicholas, D. T. Moore and H.J. Snaith, *Energy Environ. Sci.* **10,** 145–152 (2017).

Edinburgh Instruments
2 Bain Square, Kirkton Campus, Livingston, EH54 7DQ, UK
tel. +44 1506 425 300
Website: www.edinst.com

GLASS EXPANSION
Quality By Design

A Robust, High Performance, Revolutionary Demountable ICP Torch

Ryan Brennan, Justin Masone, Terrance Hettipathirana and Glyn Russell, Glass Expansion, Inc.

Glass Expansion designed and patented the D-Torch, a revolutionary, demountable torch. The D-Torch uses high-precision engineering to provide the benefits of a demountable torch, such as lower running costs, chemical inertness, and configurable injector geometry, without compromising usability, performance, or durability. In this report, we discuss the effects of harsh matrices on torches, as well as the features, benefits, and improvements in analysis achieved with the D-Torch.

A single-piece inductively coupled plasma (ICP) torch can be a costly consumable item requiring regular maintenance and replacement, particularly with aggressive sample matrices, such as hydrofluoric acid (HF), organic solvents, and high total dissolved solids (TDS). Dealing with such samples is a common challenge with ICP spectrometry, and, generally, most "real samples" analyzed by ICP laboratories contain considerable concentrations of TDS, including soils, sludges, wastewater, brines, high acid digests, and fusions. Analyzing these types of samples can pose a number of challenges for the ICP analyst, including increased frequency of torch replacement due to shortened torch life.

The combination of high temperature from the plasma and salt deposits on the torch causes a quartz torch outer tube to devitrify. The disadvantage of a single-piece torch is that it is a relatively high-cost consumable item, and the entire torch must be replaced, when, in most cases, it is just the outer tube that suffers from devitrification. For this reason, many ICP manufacturers have moved away from the single-piece torch, and most now use a semi-demountable torch design.

The D-Torch (Figure 1) is a robust and higher-performing alternative to both a single-piece and a semi-demountable quartz torch. Compared to other demountable torches, the D-Torch is the only torch design that comes standard with a ceramic intermediate tube for greater robustness and a lower cost of ownership. With the D-Torch design, the analyst most often replaces only the outer tube, rather than replacing the entire torch or a quartz torch body. With demountable torch designs offered by other manufacturers, the intermediate tube is made of quartz and fused to the quartz outer tube, which is an additional consumable whose cost can quickly add up and negate the economic benefits of the torch itself. The D-Torch also features fully interchangeable injectors, allowing the analyst to install a specific injector (i.e., material and inner diameter) for each application, whether it be for aqueous, organics, high TDS, or HF.

Figure 1: Glass Expansion D-Torch for Agilent 5100/5110 and 5800/5900 ICP-OES instrument.

Another exclusivity of the Glass Expansion D-Torch is an optional ceramic outer tube, which is of particular benefit for the analysis of high-TDS sample matrices, as the Sialon material does not devitrify. In addition to providing durability, the ceramic outer tube on an ICP torch produces a hotter, more robust plasma, which reduces matrix effects and improves sensitivities and detection limits. Compared to a quartz outer tube, the ceramic outer tube has a much longer lifetime, greatly reducing maintenance, cleaning, and downtime due to torch failure. In some sample matrices, quartz outer tubes can degrade in hours, while the ceramic outer tube will last years under the same conditions.

The ceramic outer tube is ideal for:

- monitoring of wear metals in engine oils, as quartz outer tubes often suffer cracking and shortened lifetimes due to thermal shock
- analysis of fusion samples where the lithium salts rapidly attack quartz
- measuring high-TDS samples that will quickly devitrify the quartz outer tube.

Each Glass Expansion D-Torch design is a direct replacement for the standard torch, including ICP models that incorporate an easy-to-use, self-aligning torch installation. Each D-Torch model is designed with a base that provides the same self-aligning, turn-key installation for ICP models such as the Agilent 5800 and 5900, PerkinElmer Avio, Thermo iCAP, and Spectro Arcos MV. Compared to other demountable torches, the D-Torch also offers easier cleaning and maintenance with the ability to remove the injector and outer tube, with no O-rings to degrade and go brittle.

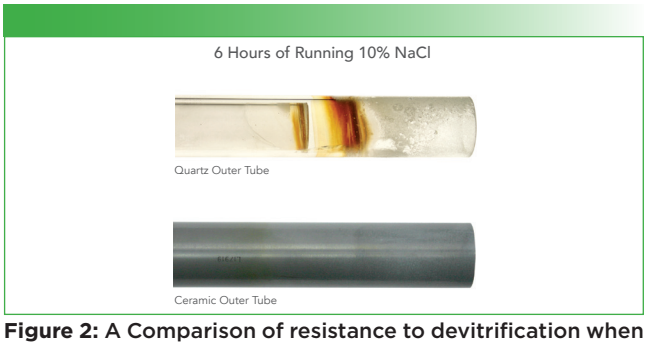

Figure 2: A Comparison of resistance to devitrification when exposed to high salt matrix.

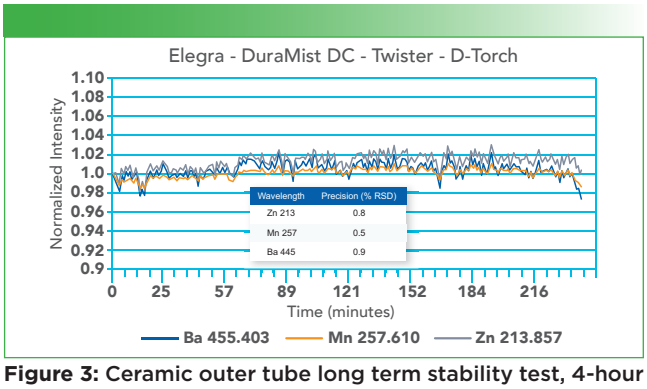

Figure 3: Ceramic outer tube long term stability test, 4-hour analysis of 1 ppm standard in 10% NaCl.

Results

Glass Expansion manufactures a D-Torch design for many of the most-popular ICP models; this particular study highlighted the performance of the fully ceramic D-Torch model designed for the Agilent 5100 and 5110 systems, and is also fully compatible with Agilent's recently released 5800 and 5900 ICP-OES instruments.

As mentioned previously, a combination of high temperature and salt deposits causes a quartz torch to devitrify. Higher concentrations of salt in the samples lead to more rapid devitrification. The quartz torch in Figure 2 was run for only 6 h with samples containing 10% NaCl and is already badly degraded. By contrast, the D-Torch ceramic outer tube in Figure 1 shows no degradation at all, and it was run for the same period and with the same samples as the quartz torch.

To further evaluate the performance of the ceramic outer tube in a high TDS matrix, a 1 ppm multi-element standard was prepared in a 10% NaCl matrix and aspirated at 1 mL/min for 4 h with no rinsing. The combination of the DuraMist DC nebulizer, Twister spray chamber, ceramic D-Torch, and Elegra argon humidifier provided exceptional stability (Figure 3). A measurement was taken approximately every minute over a period of 4 h, while a precision of less than 1% was maintained throughout the experiment.

Table I: Comparison of signal intensity with a ceramic and quartz outer tube obtained via axial viewing on an Agilent 5100 SDV ICP-OES

Analyte	Ceramic Outer Tube	Quartz Outer Tube	% Increase
As	134	117	15
As	173	148	17
Be	214773	180840	19
Cd	4259	3367	26
Co	1050	855	23
Cr	5490	4435	24
Cu	5258	4558	15
Fe	3408	2767	23
Mn	49529	40237	23
Mo	954	778	23
Ni	721	584	24
Pb	285	226	26
Sb	326	278	17
Se	102	90	13
Ti	12964	10820	20
Tl	185	146	27
V	4677	3815	23
Zn	4801	4113	17

In addition to providing ICP laboratories with a more robust torch option, the ceramic outer tube of the D-Torch can provide a higher average signal intensity compared to a standard quartz torch. Table I shows the average signal intensity, based on three separate measurements of 10 replicates using a 100 ppb multi-element standard. The overall average increase in signal intensity with the ceramic outer tube was 21%.

Conclusions

The Glass Expansion D-Torch is the most cost-effective torch over the lifetime of the instrument, compared to both single-piece quartz torches and semi-demountable quartz torches, as well as alternative fully demountable designs. The unique ceramic outer of the D-Torch provides the ICP laboratory with an ICP torch that does not devitrify due to high salts or fracture when exposed to organic solvents. The ceramic outer tube also provides a higher average signal intensity, providing laboratories with an additional boost in performance.

Glass Expansion
31 Jonathan Bourne Dr., Unit 7, Pocasset, MA 02559
tel. (508) 563-1800, (508) 563-1802 (Fax)
Website: www.geicp.com

HARRICK

A Corrosive Liquid Investigated by Diamond ATR Infrared Spectroscopy

Susan Berets and Bisirat Araya, Harrick Scientific Products, Inc.

Because of their corrosive properties, corrosive lipids are challenging to analyze by ATR-FT-IR. Repeated and prolonged analysis can damage many ATR crystals. Diamond ATR is a better choice for such applications than other ATR crystal materials like ZnSe and Ge. This application note examines a corrosive liquid as it becomes progressively more concentrated using diamond ATR.

Experimental

Infrared spectra were collected on an FT-IR spectrometer equipped with the Harrick DiaMaxATR™ single-reflection high-throughput diamond ATR accessory (see Figure 1). The system was purged to remove water vapor and CO_2. Spectra were collected at 4 cm^{-1} resolution and the signal was averaged over 16 scans. The spectra were referenced to the clean ATR crystal.

The sample used here was Easy-Off™ Heavy Duty Oven Cleaner (Reckitt Benckiser). Two drops of the oven cleaner were placed on the center of the ATR crystal and spectra were collected at 20 scans per s over a period of 60 min.

Results and Discussion

Figure 2 shows the series of FT-IR spectra acquired over the period of 60 min, showing water evaporating from the oven cleaner and concentrating the remaining ingredients. The MSDS for the oven cleaner indicates that it is composed of 2-(2-Butoxyethoxy)ethanol, 2-amino-ethanol, sodium hydroxide, and liquefied petroleum gases. As it dries, the OH stretching and bending vibrations around 3300 and 1645 cm^{-1} respectively decrease, showing the evaporation of water present with sodium hydroxide. The bands at 2958, 2930, 2862, and 2800 cm^{-1}, due to CH stretches, increase as the oven cleaner becomes more concentrated, as do the amine bands at 1658 and 1590 cm-$^{-1}$. Presumably the volatile petroleum components are also evaporating. But the decrease in the volatile organics is more difficult to discern, due to the increased concentration of the nonvolatile compounds. Note that the rate at which the oven cleaner concentrates could be measured by looking at peak areas, as demonstrated by the inset graph for the C=C transition at 1000 cm^{-1}

Conclusion

Because diamond is a more chemically durable material, it can be effectively used as an ATR crystal for some corrosive samples. This has been demonstrated here using the Harrick DiaMaxATR to measure the ATR spectra of oven cleaner, as it becomes increasingly concentrated due to evaporation of the solvent therein.

Figure 1: The DiaMaxATR Diamond ATR.

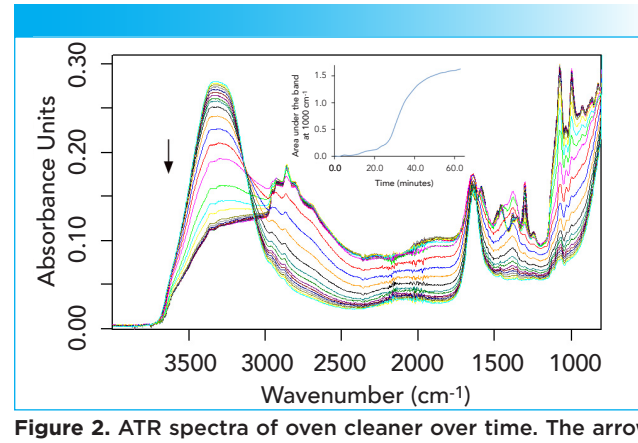

Figure 2. ATR spectra of oven cleaner over time. The arrow indicates increasing time, and the inset shows the change in concentration of C=C species with time.

Harrick Scientific Products, Inc.
141 Tompkins Ave., 2nd Floor, Pleasantville, NY 10570
tel. (800) 248-3847
Website: www.harricksci.com

Identifying Textiles with Extended-Range NIR Spectroscopy

Anne-Marie Dowgiallo, PhD, Ocean Insight

A compact, MEMS-based, single-photodetector NIR device, the NanoQuest, is used to distinguish different types of textiles.

NIR spectroscopy offers a simple tool to identify different types of textiles, with distinct spectral features observed at wavelengths >1700 nm. This approach may be useful for authentication of natural and synthetic consumer textile products.

Experimental Conditions

Reflectance from 100% cotton, nylon, and satin textile samples was measured across the extended NIR wavelength range (1350–2500 nm) using the Ocean Insight NanoQuest spectral sensor with a high-powered tungsten halogen light source (Ocean Insight model HL-2000-HP) and 600 µm visible-NIR reflection probe. Measurements were made with the probe oriented at 90 degrees relative to the fabric surface using a manual optical stage. All measurements were referenced to a WS-1 model PTFE (Teflon) diffuse reflection standard.

NanoQuest is based on Fourier–transform infrared (FT-IR) technology. Its patented micro-electro-mechanical systems (MEMS) technology allows for a continuous-wave Michelson interferometer to be created monolithically on a MEMS chip, enabling detection of all wavelengths simultaneously across the 1350–2500 nm range.

In the NanoQuest software, optical resolution was set to 8 nm (FWHM), and a custom gain setting was generated to optimize the signal to noise ratio for the measurement setup. Each sample was measured at five different locations with resulting spectral data pretreated by a second derivative with smoothing, and a standard normal variate (SNV) was applied. Principal component analysis (PCA) was applied to the dataset.

Results

The NIR spectra measured with the NanoQuest can easily discriminate among the different textile types. Figure 1 shows the reflectance spectra of the three textiles measured: cotton, nylon, and satin. Differences in the spectral profile for each sample can be seen readily, and the inset PCA plot shows distinct separation between the clusters for each textile sample.

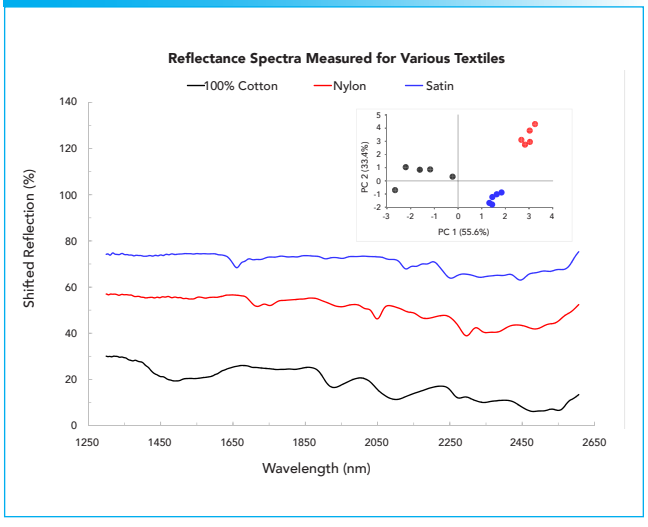

Figure 1: Comparison of the three textile samples measured with NIR reflectance. The inset PCA scatter plot shows results after pretreatment by second derivative and SNV.

Conclusions

The experiments clearly demonstrate that the NIR spectra measured with the NanoQuest exhibit unique features helpful to identify both natural and synthetic textiles. Application of PCA to the spectra further demonstrated the distinction among textile samples. Additional tests may include testing unknown textile samples to correctly identify them.

Ocean Insight
8060 Bryan Dairy Road, Largo, FL 33777
tel. (727) 733-2447
Website: www.OceanInsight.com

A Q&A

The Evolution of Raman: Adapting Instrument Design to the Needs of the Sample

Simon Nunn, Ph.D.
Business Manager
Raman Spectroscopy – Renishaw, Inc.

Raman spectroscopy is evolving. Diverse applications spanning life and materials science are driving growth of the technique and creating the need for innovative instrumental solutions. *Spectroscopy* recently spoke to Simon Nunn, Ph.D., Business Manager of Raman Spectroscopy at Renishaw, Inc., about the growing importance of the technique and how instrumentation is adapting to meet new challenges.

Spectroscopy: The applications for Raman spectroscopy are growing. What are some of the most exciting areas that you are seeing?

Nunn: Raman spectroscopy is applicable across a broad range of scientific disciplines, from biology to materials science. The technique can identify unknown compounds, differentiate between similar materials and perform spatial analysis. Perhaps the most exciting applications right now are those that have broad impact on the environment and human health. In environmental sciences, the technique is being used to study microplastics, both in drinking water and the marine environment. In the forensics community, Raman is used to identify fentanyl—a potent synthetic opioid that causes unintentional drug overdoses. In materials science, the technique characterizes the components of lithium-ion batteries used in the electrification of vehicles. In the pharmaceutical industry, Raman is routinely used to ensure the quality of drugs and understand the formulation process. Our challenge, as an instrument manufacturer, is to adapt our products to these growing applications and the diversity of samples they present.

Spectroscopy: Your company has been making research Raman systems for over 20 years. How has the product line evolved to meet the changing needs of scientists over that time?

Nunn: Raman instrumentation has evolved as the business of science has changed. In the early days of Raman, people studied the technique itself, often building their own instruments in the process. The advent of commercial instruments, such as Renishaw's RM microscope, obviated the need to build one's own spectrometer by providing an off-the-shelf solution that had the flexibility to adapt to a wide variety of research needs. Now, as the applications described above illustrate, Raman is widely used as an analytical tool, often by multidisciplinary teams investigating complex samples. This has driven the need for instrumentation that is designed around the needs of the sample and extracting the required information from that sample. The inVia™ confocal Raman microscope is a good example of a system that has evolved to meet these changing needs. On the sampling side, the addition of LiveTrack™ autofocus tracking technology enables 3D images to be created from uneven or curved surfaces.

> "The technique can identify unknown compounds, differentiate between similar materials and perform spatial analysis."

Many researchers are now combining techniques and to aid this, the new Correlate™ module in WiRE™ software enables Raman images to be correlated

with white light, SEM, EDS, or other imaging methods and to provide a comparison of complementary techniques, while Spectrum Search allows an unlimited number of components to be identified from a single spectrum of a mixture.

Spectroscopy: So, you're saying that adapting the instrument to the needs of the sample is a trend. Beyond the evolution of the research Raman microscope, what other developments support this assertion?

Nunn: A research Raman microscope must be a very flexible system to cover a diverse range of potential applications. However, if the type of sample is limited and well-defined, it is possible to further optimize the instrument to the needs of sample. The RA802 Pharmaceutical Analyser and RA816 Biological Analyser are good examples of instruments that are purpose-built for rapid imaging of solid dosage forms and biological samples, respectively. Designing an instrument to meet the specific requirements of an analysis ultimately speeds up that analysis and reduces variability from measurement to measurement. Dedicated systems are likely to increase in number as the applications for Raman continue to grow.

> "The use of fiber-optics allows flexible positioning of the sampling head, which in turn is capable of spatial resolution normally associated with research microscopes."

Spectroscopy: In the case of the Raman microscope and the dedicated analyzers you describe, the sample is brought to the instrument. Hand-held Raman systems show that it is possible to bring the spectrometer to the sample. Is there potential for research-style systems to do the same?

Nunn: You are correct. In a growing number of situations, it is preferable to bring the instrument to the sample. Handhelds are a good example of how this can be achieved. However, these systems work best when answering limited questions about a relatively small number of potential compounds, such as pass/fail identity of pharmaceutical excipients. There are other applications where broader questions are asked of more challenging samples, often on a microscopic scale. Examples include art conservation where non-destructive, *in-situ* analysis of an artifact is required, and battery research where air-sensitive materials are analyzed in a glovebox. In these cases, the performance attributes of a laboratory Raman system are required in a sample-centric form factor. The recently introduced Virsa™ Raman Analyser brings laboratory performance to the sample, whether in a gallery, glovebox, or mobile lab. The use of fiber-optics allows flexible positioning of the sampling head, which in turn is capable of spatial resolution normally associated with research microscopes. In this case, the microscope is brought to the sample rather than vice versa.

Raman instrumentation has evolved immensely since the first commercial microscopes were introduced. The expansion of the application space will necessitate further innovation, and we look forward to working with our customers to meet their changing needs.

Bioreactor Fermentation Monitoring with Raman Spectroscopy

Dieter Bingemann and David Creasey, Wasatch Photonics Inc.

Raman spectroscopy's high analytical selectivity and insensitivity to water is well suited for process monitoring in biotechnology. Here we explore the fermentation of glucose, a common feedstock, with a commonly used microorganism, yeast. Applying multivariate tools, we can monitor the main reactants and products with high sensitivity: glucose, ethanol, and carbon dioxide.

Biotechnology, the production of chemicals of choice using microorganisms, is an application very well suited to monitoring with Raman spectroscopy. Raman's high selectivity and low sensitivity to the solvent, water, can be employed using a simple immersion probe setup to monitor and more tightly control these processes.

Experimental

We used a Wasatch Photonics Raman spectrometer at 785 nm, fiber-coupled to an external laser and an immersion probe inserted into a stirred solution of 50 g/L glucose and 2 g/L yeast. The fermentation was observed over 14 h, with spectra collected every 2 min at 5 s integration time and an average of 20 scans.

We performed a separate multivariate calibration for glucose in the presence of yeast over the concentration range from 0 to 50 g/L glucose.

Results and Discussion

We correlated the glucose calibration spectra with the concentration using partial least squares (PLS) regression, yielding a prediction error of 0.7 g/L in the presence of yeast and about 0.1 g/L without yeast. The Raman spectra recorded during the fermentation are shown in Figure 1 together with the pure Raman spectra for the main reactant and product, glucose and ethanol.

Applying the PLS glucose model yielded the prediction of the glucose concentration, which showed a slow decrease with a noise level of below 1 g/L glucose.

Principal component analysis (PCA) identified the main spectral trends during the process. The first principal component expressed the remaining glucose level, while the second component captured the simultaneous decrease of glucose (spectrum negative in the corresponding loading) and increase of ethanol (positive spectrum in the loading). The corresponding PCA score therefore allowed the progress of the reaction to be summarized in a single coordinate, and to compare batch to batch.

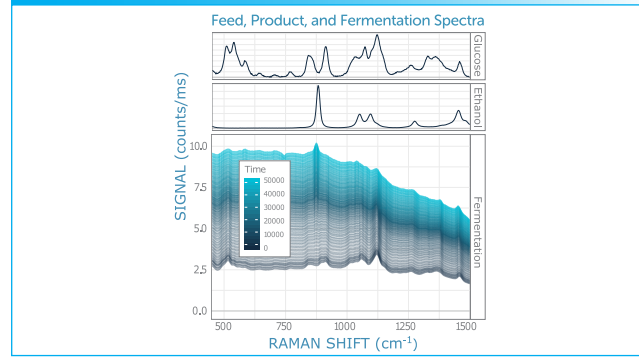

Figure 1: Raman spectra recorded during glucose fermentation over 14 h, with time (in seconds) indicated by the color, together with the reactant and product spectra. The glucose peaks around 1100 cm^{-1} decrease, while the ethanol peak at 900 cm^{-1} and the overall yeast background increase.

Additional reaction products could be discovered in the higher principal components; due to its specificity, Raman allows identification. For example, the fourth principle component for the fermentation spectra showed the production of dissolved carbon dioxide. Likewise, unwanted side-products could be discovered and identified during the fermentation.

Conclusion

Using an immersion probe and a Wasatch Photonics Raman spectrometer at 785 nm, we continuously monitor the fermentation of glucose with yeast. Despite the significant yeast background, multivariate regression yields the glucose concentration, while principal component analysis projects the spectra onto a reaction progress coordinate and allows deep insight into the details of the fermentation. The same approach could be used for other processes to harness the strength of Raman spectroscopy.

Wasatch Photonics
808 Aviation Parkway, Suite 1400, Morrisville, NC 27560
tel. (919) 544-7785
Website: www.wasatchphotonics.com

Gallium Nitride Quality and Stress Field Characterization with 3D Confocal Raman Imaging

WITec GmbH

The quality and stress field properties of gallium nitride (GaN) crystals must be investigated in order to refine production processes. 3D Confocal Raman microscopy is uniquely capable of the chemical c and visualizing strain in this material.

Experimental Conditions

A GaN sample grown on a sapphire substrate featuring hexagonal pits, courtesy of Dr. Eberhard Richter (Materials Technology Department of the Ferdinand Braun Institute, Berlin, Germany), was investigated, and stress fields were visualized. All measurements were carried out using a WITec alpha300 R confocal Raman microscope with an excitation wavelength of 532 nm and a UHTS 300 spectrometer.

Results and Conclusion

A 2D depth scan was performed and the resulting Raman image (Figure 1A) was color coded according to the measured spectra (Figure 1B). The red spectrum shows features typical of GaN and is dominant at the sample surface, showing that the crystal grown there was high in quality. The green spectrum shows enhanced fluorescence at low wavenumbers and is found only at the substrate pit walls. The blue spectrum measured above the pits is distinct from the red one (Figure 1B, inset). The A1(LO) peak is upshifted and broadened compared to the red spectrum, indicating a lower quality GaN crystal.

Next, a stack of 2D scans was performed at different focal planes. Figure 1C shows one layer from the stack. A 3D representation was generated from the image stack (Figure 1D). The fluorescence signal (green) forms rings at the walls of the pits, while the tops of the pits are dominated by the distorted GaN spectrum (blue). The topmost layers show an undistorted GaN spectrum (red).

In order to reveal stress fields in the GaN sample, a peak shift analysis was performed for the entire z-stack. The position of the E_2^{high} peak near 570 cm^{-1} was quantified for each spectrum by fitting a Lorentzian function. Figure 2 shows the same sample volume as in Figure 1D, but color coded according to the determined peak position. The stress fields propagate from the interface to the surface mainly in tube-like structures, which become narrower towards the surface, again indicating higher crystal quality. However, the overall differences in the peak positions were quite small (<1 cm^{-1}) and thus, the overall differences in the strain of the GaN crystal were also small. Nevertheless, the peak shift sensitivity was sufficient to measure and visualize them.

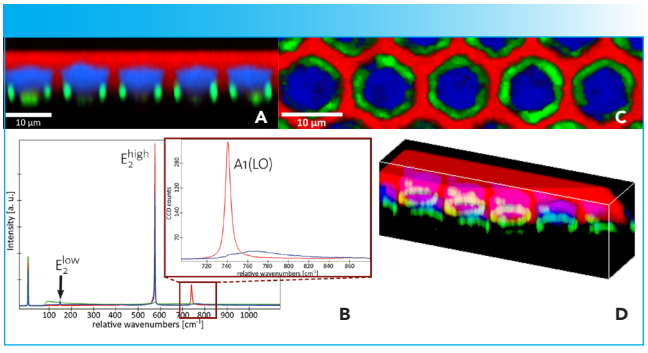

Figure 1: 3D Raman analysis of a GaN crystal grown on a patterned sapphire substrate. A: Depth scan (240 x 80 pixels on an area of 60 x 20µm^2) along the red line in Figure 1. B: Corresponding Raman spectra. In the inset, the green spectrum is omitted for clarity. C, D: 3D Raman image of the sample volume (180 x 45 x 20 pixels in a volume of 60 x 15 x 20µm^2). At the front right corner, a part of the structure is removed.

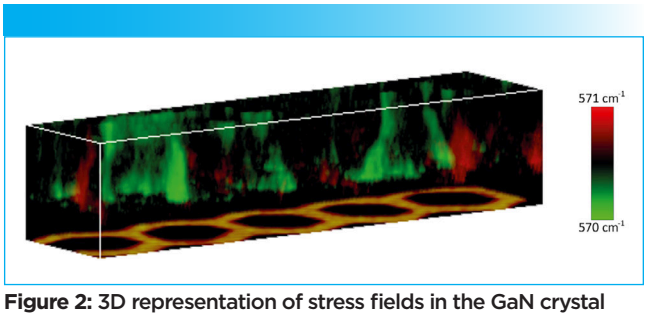

Figure 2: 3D representation of stress fields in the GaN crystal (the same sample volume as in Figure 2D). The position of the Raman peak near 570 cm^{-1} is color coded, revealing stress fields in the crystal.

WITec GmbH
Lise-Meitner-Str. 6, D-89081 Ulm, Germany
tel. +49 (0) 731 140 700; +49 (0) 731 140 70 200
Website: www.WITec.de

PIKE TECHNOLOGIES

Tracking Photocuring via ATR-FT-IR with Illumination through the ATR Element

Marshall J. Allen and Zachariah A. Page, Department of Chemistry, The University of Texas at Austin

The utility of the GladiATR diamond ATR, modified with an internal liquid light guide to illuminate the sample from underneath the ATR element, was explored to analyze the photo-polymerization of carbitol acrylate at 405 nm using 1 wt% TPO.

Photocuring, or the solidification of a liquid mixture (for example, resin) upon exposure to light, is a widely adopted method for dental coatings and sealants, medical adhesives, photoresists, and 3D printing. The ability to track this process in realtime enables resin optimization tailored for a particular application. Attenuated total reflectance-Fourier-transform infrared spectroscopy (ATR-FT-IR) is a facile way to monitor the solidification process through changes in chemical functionality and determine reaction kinetics and efficiency at the ATR crystal interface.

Conventional photochemical ATR setups irradiate samples from top-down while IR measurements presented are being taken from the bottom-up. This disparity results in a difference in light intensity throughout the depth of the sample due to absorption and sample thickness nonuniformity; limits the accuracy of analysis; and mitigates characterization of opaque resins. In this application, we overcome these challenges by illumination from beneath the sample through a diamond ATR prism, aligning the absorption cross section of the sample with the evanescent wave of the IR beam for characterization.

Experimental Conditions

PIKE Technologies' GladiATR diamond ATR (Figure 1) was modified to incorporate a liquid light guide and enable illumination from beneath the diamond. The use of a liquid light guide imparts modularity, as numerous light sources with variable wavelengths and intensities can be directly coupled for photocuring purposes.

To demonstrate the capabilities of the light-guide coupled GladiATR, photopolymerization of an acrylate-based resin using violet light (λ_{max} = 405 nm) was performed. The resin comprised carbitol acrylate and diphenyl(2,4,6-trimethylbenzoyl)phosphine oxide (TPO, 1 wt%). Approximately 20 µL of resin were placed on the ATR crystal and real-time tracking was initiated. After 19 s, the sample was irradiated with 405 nm light at an intensity of 36 mW/cm^2. The FT-IR instrument scan rate was 80 kHz while using an MCT detector, and 4 scans were co-added.

Figure 1: GladiATR ATR with internal UV-visible light guide for through-diamond illumination.

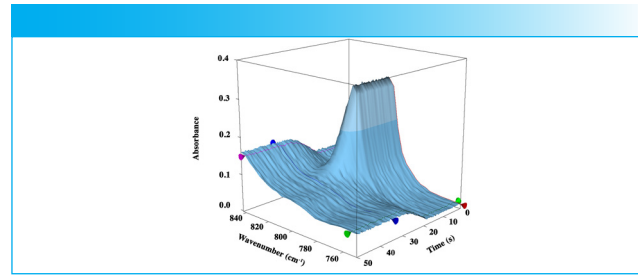

Figure 2: Acrylate photopolymerization using 405 nm light. Waterfall plot showing the band change over time. Irradiation began at 19 s.

Results

The polymerization was monitored by observing the disappearance of the C=C-H wag band at 810 cm^{-1} (Figure 2). Within 20 s of irradiation, the conversion was approximately 98%. A clear initiation was observed at time of irradiation, indicating no lag time between the light and measurement.

Conclusion

Monitoring UV curing via ATR-FT-IR by illuminating the sample from underneath offers a quantifiable sampling method to determine reaction kinetics. The modular capabilities of the ATR accessory allow for curing using any UV-visible wavelength.

PIKE Technologies, Inc.
6125 Cottonwood Drive, Madison, WI 53719
tel. (608) 274-2721, fax (608) 274-0103
Website: www.piketech.com

Ultra-Low Frequency Raman Spectroscopy

"Extend your Raman system into THz frequency range (5-200 cm^{-1})"

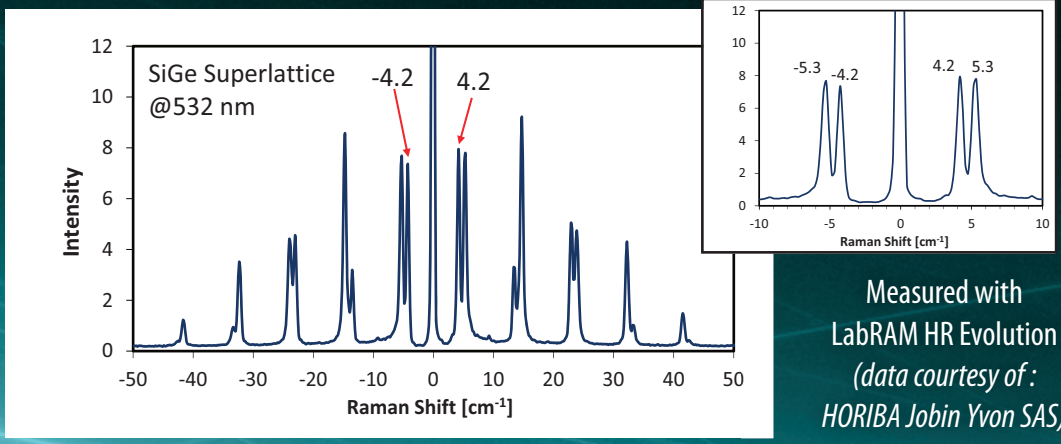

Measured with
LabRAM HR Evolution
(data courtesy of :
HORIBA Jobin Yvon SAS)

BragGrate™ Bandpass and Notch Filters

Spectral and spatial laser line cleaning filters and ultra-narrow line notch filters for low frequency Raman Spectroscopy

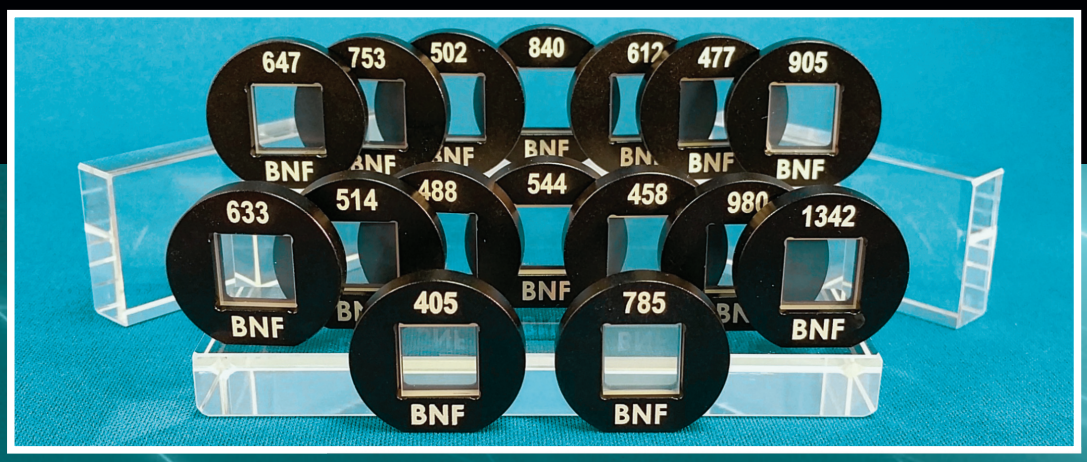

Wavelengths in Production (nm)
405, 442, 458, 473, 488, 491, 514, 532, 552, 561, 568, 588, 594, 632, 660, 785, 830, 980, 1064, 1550

- **Frequencies below 10 cm^{-1} with single stage spectrometer**
- **Angle tunable for precise wavelength adjustment**
- **Stokes and anti-Stokes Raman bands**
- **Unlimited optical life-time**
- **Custom wavelengths in range 400–2000 nm**

OptiGRATE
HIGH EFFICIENCY FOR HIGH POWER

+1 (407) 542-7704
info@optigrate.com
www.optigrate.com

MB3000-CH90 laboratory gas analyzer

Measurement made easy

The MB3000-CH90 gas analyzer provides fast and accurate FT-IR critical gas measurements down to ppb levels in a user-friendly environment. This high performance and maintenance-free spectrometer is used in R&D or QA/QC laboratories for checking gas purity, controlling gas mixing and composition or performing unknown components speciation. The heated gas cell can be easily swapped and replaced with other sampling accessories, making the MB3000-CH90 a flexible and versatile tool for any laboratory.
Measurement made easy.

Want to learn more? Visit **abb.com/analytical**
or contact us at **ftir@ca.abb.com**